The Pennsylvania State University

The Graduate School

The College of Earth and Mineral Sciences

COMPOSITIONAL FORMULATION AND POST-PROCESS HEAT TREATMENT OPTIMIZATION OF AN ADVANCED ALUMINUM ALLOY FOR ADDITIVE MANUFACTURING

A Thesis in

Materials Science and Engineering

by

Rebecca A. Sweny

Submitted in Partial Fulfillment
of the Requirements
for the Degree of

Master of Science

August 2018

The thesis of Rebecca A. Sweny was reviewed and approved* by the following:

Rich Martukanitz
Director of the Center for Innovative Materials Processing through Direct Digital Deposition
Thesis Advisor

Robert Voigt
Graduate Program Coordinator of Industrial & Manufacturing Engineering

Allison Beese
Assistant Professor of Material Science and Engineering and Mechanical Engineering

Jay Keist
Research Associate of Material Science and Engineering

Suzanne Mohney
Professor of Material Science and Engineering
Chair of the Intercollege Graduate Degree Program in Materials Science and Engineering

*Signatures are on file in the Graduate School

ABSTRACT

Traditional aluminum alloys for use in additive manufacturing have been developed from traditional foundry technologies. There is a need for the development of an aluminum alloy which takes full advantage of the benefits additive manufacturing offers, i.e. rapid solidification and cooling. Preliminary research conducted by the Center for Innovative Materials Processing through Direct Energy Deposition (CIMP-3D) in 2016 had shown that Al-Cu-Ag-Mg precipitation-hardenable alloys could achieve hardness exceeding 140 VHN after deposition and heat treatment, compared to the traditional aluminum alloy for additive manufacturing (Al-10Si-0.5Mg) which provided hardness near 100 VHN. A correlated improvement of strength was also seen with the advanced Al-Cu-Ag-Mg alloy, approaching 500 MPa, a typical yield strength for a 7075-T651 alloy. To better refine the target composition for commercialization, three metal powders were used to blend 9 characteristic Al-Cu-Ag-Mg compositions. Manufactured test specimens were printed by multiple deposition tracks using blended experimental powders. Specimen's surface appearance was examined for porosity, cracks, and lack of fusion. Samples were subjected to post processing precipitation hardening heat treatment cycles to study the effect of aging temperature and time on hardness of samples varying in composition. The peak-aged condition was determined to be 20 hours at 160°C for alloys with moderate Cu and Ag contents. The alloy demonstrating the most improved hardness was characterized and tested for mechanical properties. The relationships between composition, aging temperature and aging duration were analyzed to determine the optimal parameters for an advanced aluminum alloy.

TABLE OF CONTENTS

LIST OF FIGURES

LIST OF TABLES

ACKNOWLEDGEMENTS

I would like to thank the staff of CIMP-3D for all of their help, especially Dr. Rich Martukanitz, Jay Tressler, and Ed Good.

Chapter 1

INTRODUCTION

The motivation behind this research is to work towards finalizing an alloy design for a material that will provide significant performance improvements over the current aluminum alloy (Al-10Si-0.5Mg) primarily used for additive manufacturing. Preliminary research conducted at The Center for Innovative Materials Processing through Direct Digital Deposition (CIMP-3D) had shown that alloys representing the Al-Cu-Ag-Mg precipitation-hardenable system could achieve hardness exceeding 140 VHN after deposition and heat treatment.[1] In contrast, the conventional alloy for additive manufacturing (Al-10Si-0.5Mg) only provides a hardness of 100 VHN.[2] Improvement in hardness of the Al-Cu-Ag-Mg alloy tracks directly to improved strength, with the advanced alloy being capable of achieving tensile strengths exceeding 470 MPa (68 ksi).[1] To put this in perspective, the manufacturer of the Al-10Si-0.5Mg powder lists the potential tensile strength of that alloy to be 350 MPa (50 ksi).[2] The holy grail of aerospace alloys, 7075-T651, has a typical tensile strength of 572 MPa (83 ksi).[3] Significant interest has been expressed by the Navy and Air Force in the development of an improved aluminum alloy for additive manufacturing. Based on the prior research noted above, as well as research within the literature, it is believed that the proposed alloy system has the potential to meet the needs for an advanced aluminum alloy. Successful results could lead to an expansion of applications for additive manufacturing techniques for producing new designs or restoration of existing components.

The goal of this research is to utilize the previous work done by CIMP-3D to design a full factorial experiment for determining optimal chemistry and aging treatments for an advanced aluminum alloy. The objectives of this research and thesis are to:

- Discuss the additive manufacturing process and the conditions under which additive manufacturing is utilized for metallic systems.
- Discuss the alloys currently used for additive manufacturing, their applications, and the need for improvement.
- Discuss the aluminum alloy system, the methods by which aluminum is strengthened, and its sensitivity to solidification cracking.
- Discuss the Al-Cu-Ag-Mg system and its alloying elements, strengthening phases, heat treatment cycles for precipitation, and properties and applications of the system.
- Present previous research at CIMP-3D on the Al-Cu-Ag-Mg system.
- Design experiments of 9 compositions of Al-Cu-Ag-Mg that would be used to additively manufacture specimens to determine optimal chemistry for an advanced aluminum alloy.
- Perform aging experiments to determine heat treatment cycles for peak strengthening.

Chapter 2

BACKGROUND

2.1 Additive Manufacturing

Additive manufacturing (AM) is a layerwise building process which utilizes a heat source, such as laser energy, to consolidate micron-sized metallic powders to form a three-dimensional component. AM technology utilizes three dimensional Computer Aided Design (CAD), engineered to directly fabricate a component. Using CAD, the component is sliced into layers to control the build process. A generic design to application process for AM involves the following eight steps: [4]

1) CAD
2) STL convert
3) File transfer to machine
4) Machine set-up
5) Build
6) Remove
7) Post-process
8) Application

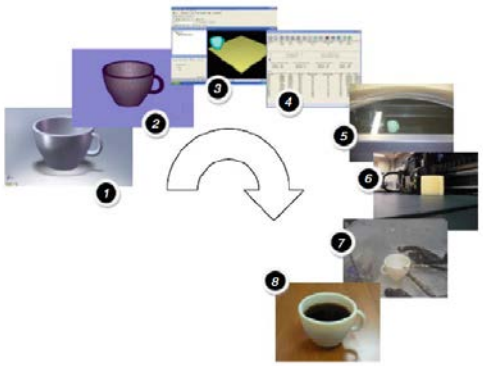

Figure 2-1: AM design to application process. [4]

While these steps are generic to most additive manufacturing processes, the building process can utilize various bonding methods which are determined by the type of AM technique. Each method uses a layer-based approach following the same generic

CAD to complete the build process, however, AM machines can differ in the materials they use, as well as how the layers are created and bonded. These differences effectively determine material characteristics, mechanical properties and surface finish of a component. In addition, the specific AM technique will also determine factors such as material requirements, processing time, post-processing requirements, size limitation, resolution, and operation cost.[4]

The two predominant types of AM processes for metals are directed energy deposition and powder bed fusion. While these two additive methods have many similarities when it comes to operation, the main difference lies in the method by which the layers are formed. The subsequent sections will describe each method in detail.

2.1.1 Powder Bed Fusion

The powder bed fusion (PBF) process generally consists of a laser energy source, an optics head, a processing chamber (consisting of a powder reservoir, recoating system, and build plate) and a control system, and is shown in Figure 2-2. [4] The powder bed fusion process utilizes laser energy, usually fiber delivered, to selectively melt and solidify material in a pre-deposited bed of metal powder. The building area is prepared for processing by spreading a uniform powder layer (20µm -80µm) over the build plate using a recoater blade. Once the laser selectively consolidates the layer, the build plate drops a step and the recoating system distributes a fresh layer of powder over the build

plate that is ready for processing. This process continues until all layers of the build are formed and the part has reached final dimensions.[5]

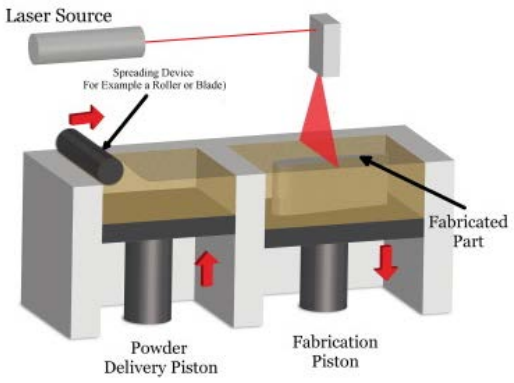

Figure 2-2. Powder bed fusion system schematic. [5]

While this process is more time consuming than directed energy processes, benefits are gained from providing improved dimensional accuracy compared to other AM techniques, as well as providing a high level of customization. Powder bed fusion can fabricate complex internal features with no additional support structure requirements. Post processing requirements are minimal, with the only requirement being removal of excess powder and minimal cleaning. Additional post-processing techniques, such as hot isostatic pressing (HIP), can be used to achieve high material quality with densities approaching 100%.[6]

2.1.2 Directed Energy Deposition

Directed energy deposition (DED) is a near net shaping process in which the heat source, such as a laser, is used to melt or solidify a powder or wire feedstock to build a

structure.[7] As the feedstock is fed into the path of the laser, either the build plate or the laser itself is digitally manipulated by a predetermined pattern to melt and consolidate layers. DED systems are comprised of a few base components: a laser energy source, an optical focus system, a powder feeding system, a motion system, a controlled environmental process chamber, and a control system for integration of all functions. Figure 2-3 shows a schematic of a standard directed energy deposition system.

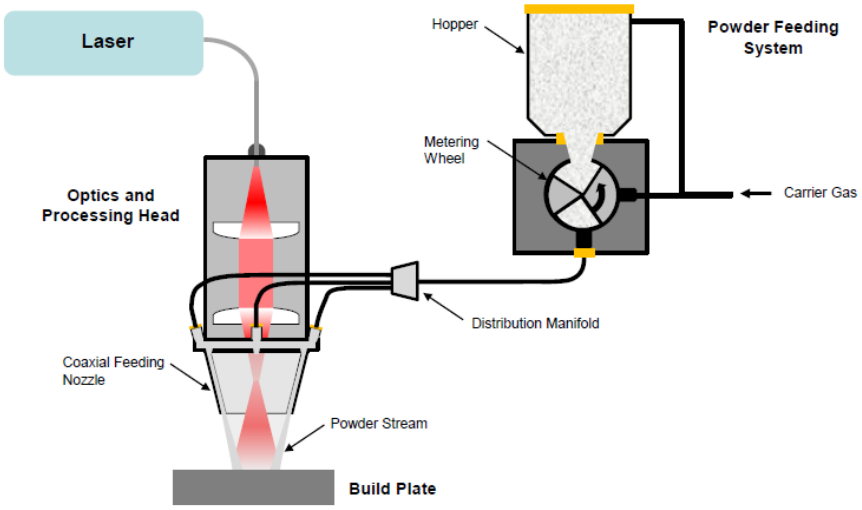

Figure 2-3: Directed energy deposition system schematic.[7]

Laser energy sources used for DED are typically lasers capable of fiber delivery. Hard optics in a DED machine would restrict movement of the nozzle, limiting the machine's capability. Fiber delivery requires collimation and focusing, which is done by the optical system. The powder feeding system consists of a powder reservoir, a powder feeder, and a powder nozzle. The powder feed system typically utilizes gas assistance to deposit material from the nozzle onto an existing surface. The motion system controls the

motion of the processing head (z-direction) and the build plate (x-y motion). The processing chamber is used to contain a purged inert gas, such as argon, to minimize oxidation of the melt pool. The control system then acts to integrate all functions of the systems to provide a smooth print.[8]

Directed energy deposition is capable of a high build rate and large build volumes by achieving a layer thickness between 40μm and 1mm. [9] The DED process balances the need for surface quality and speed, however, extra post-processing steps may be required to achieve the desired part, as this is a near net shaping process. This could include cutting off supports, machining to reach finish dimensions, or densification. Potential process defects can include lack of fusion, porosity, and cracking.[10]

2.1.3 Processing Conditions

Laser-based additive manufacturing utilizes a computer controlled laser energy source to melt metal powder. Laser based processing techniques involve complex non-equilibrium metallurgical processes. These processes often display multiple means of heat and mass transfer and can even involve chemical reactions.[11] Because of this complex interaction between laser and material, mechanical properties and microstructural features are difficult to control and standardize. Main contributing factors to the material-process interactions include powder characteristics such as composition, particle size and distribution, packing density, and flowability. Other contributing factors include processing parameters such as laser type, laser power, spot size, scan speed, line

spacing, and powder layer thickness. The capability of fabricating high performance components with specific mechanical properties and microstructural features varies depending on the AM process used. [11]

As described in the previous sections, laser melting can be performed utilizing a pre-spread powder bed or coaxial fed powder and directed energy laser metal deposition. For both processes, common lasers include ytterbium (doped) fiber lasers (λ=1070nm), Nd:YAG lasers (λ=1064nm), or direct diode lasers (λ=808nm).[8] However, beam-powder interaction in each of these processes is very different. In powder bed fusion processes, there is a thin layer of powder over the build area which acts as an insulator during cooling. In direct energy deposition processes, powder is fed directly onto the deposition surface. In this case, the component is surrounded by a gas environment and has the ability to cool quicker due to surface heat losses.

Solidification dynamics are extremely important to consider when laser processing metals. The application of a laser energy source to melt metal powder results in local solidification rates between 0.1 m/s and 5 m/s [12] and is also accompanied by high residual stresses. A material must be able to withstand these conditions in order to be deemed “weldable”. If a material is unweldable, it will demonstrate cracking that can extend through multiple build layers. Unweldable materials will not make suitable candidates for laser processed engineering components. Factors that can affect the weldability of the material include melting range, coherency during solidification, thermal conductivity, reactivity, and coefficient of thermal expansion.[13] Alloying elements have a significant role in controlling these properties and can be utilized to control weldability of the material.

Components that are laser processed are at risk for stress due to steep thermal gradients and shrinkage that occurs during liquid-solid transformation. Accumulation of stress is the primary factor responsible for distortion and delamination of additively manufactured components. It is imperative that the processing conditions and the material are chosen with the involved metallurgical processes in mind.

2.1.4 Alloys for Additive Manufacturing

Out of over 5,500 alloys used today in traditional manufacturing, the majority cannot be used to additively manufacture engineering components. The characteristic physical properties of aluminum alloys, such as their wide solidification temperature range, high thermal conductivity, high thermal expansion coefficient, and high solidification shrinkage dictate their weldability.[14] Because of the melting and solidification dynamics of additive manufacturing, unweldable metals lead to undesirable microstructures with columnar grains and cracks.[15] These properties must be considered when designing an alloy to be laser processed.

Additive manufacturing currently utilizes various metallic powder systems including titanium alloys, nickel-based alloys, aluminum alloys, stainless steel alloys, and cobalt-chromium alloys. Alloys $AlSi_{10}Mg$, TiAl6V4, CoCr, Inconel 718, and 316L are currently the only few commercial alloys that can be reliably printed.[16] Mechanical properties for these alloys are displayed in Table 2-1.

Table 2-1. Mechanical properties of alloys for AM.

Material	Tensile Strength (MPa)	Yield Strength (MPa)	Elongation (%)	Hardness (VHN)
Al-10Si-0.5Mg[17],[18]	350	230	11	98
Ti-6Al-4V[19],[20]	1100	1000	14.5	360
CoCr[21]	1097	683	21	400
In718[22]	1391	1202	17	488
316L[23],[24]	540	470	50	180

Note: table displays properties in the z-direction in the following conditions: Al-10Si-0.5Mg after stress relieved at 300°C for 2 hours. Ti-6Al-4V after HIP. CoCr after solution treated conditions: 1. Heat to 650 °C ±10 °C, hold for 15 min; 2. Heat to 1000 °C ±10 °C hold for 5 min; 3. Heat to 1050 °C ±10 °C hold for 2 hr; 4. Fast cool to < 60 °C ±10 °C using 2 bar argon quench. In718 after being solution treated at 980 °C ± 10 °C for 1 hr, aged at 720 °C ± 10 °C for 8 hr, and further aged at 620 °C ± 10 °C for 8 hr. 316L in the as-built condition.

The Al-10Si-0.5Mg alloy is commonly used for automotive and aerospace applications as well as consumer goods. It possesses a low density, beneficial for lightweight components while offering a relatively high strength to mass ratio. The Al-10Si-0.5Mg alloy has a high thermal and electrical conductivity needed for cooling of electronics.[17] This material is weldable, unlike most other aluminum alloys, making it an ideal candidate for laser processing. Additionally, the laser processing conditions used in additive manufacturing provide an as-built condition which is comparable to the precipitation strengthened (T6 temper) condition.[18]

The Ti-6Al-4V alloy is commonly used for applications requiring corrosion resistance and biocompatibility, such as service in seawater, aerospace, and biomechanical applications. It offers high strength to weight ratio, good fatigue resistance, and good high temperature performance. Conversely, Ti-6Al-4V has a low modulus of elasticity and a low thermal expansion.[19],[20]

The family of CoCr alloys are commonly used in engine components, gas turbines and orthopedic implants. They offer a very high specific strength, high resistance to corrosion, biocompatibility, and good mechanical properties comparable to steel. The

CoCr alloys have a high melting point, making them suitable for high temperature applications. However, CoCr is susceptible to fracture due to its low ductility.[21]

Inconnel 718 is a nickel-based alloy commonly used for applications requiring high strength in extreme temperatures. It offers excellent tensile and impact strength, as well as high corrosion resistance, making this material desirable for aerospace applications, such as jet engines and gas turbines. It possesses excellent weldability and crack resistance, making it a prime candidate for additive manufacturing.[22]

Stainless Steel 316L is a corrosion resistant iron-based alloy commonly used for applications requiring non-corroding material, such as in the automobile and aerospace industries. Stainless steel relies on the additions of chromium, nickel, and molybdenum to provide a non-reactive material that possesses moderate to good strength needed for engineering applications. [23]

While the materials available for additive manufacturing are limited, there is a wide range of applications in which additive manufacturing can be used. With the expansion of materials available for additive manufacturing, applications will also expand.

2.1.5 Applications

The additive process greatly simplifies the production of complex, three dimensional shapes. Today, AM technology offers efficient design to part production. Additive manufacturing is a vast and quickly developing technology, with the number of applications growing rapidly. AM was first used exclusively to create prototypes for

product development, but as the technology improved, more materials could be used, accuracy increased and overall product quality improved. New AM technology provides a limited need for tooling while the design complexity does not increase cost.[4]

New AM technology offers cost effective production of small lots, for example for special purpose tooling. Opportunities for part customization have increased, for example in personalized medical implants. Design flexibility allows complex structures to be optimized for functionality, all while consolidating component parts and conserving and recycling material. Today, AM technology is demanded to produce complex components for a wide variety of applications, some of which include aerospace, healthcare, electronics, and the automotive industries.[14] Laser processing in manufacturing is not only based on faster through-put, but also increased precision. Laser-based additive manufacturing provides flexibility and greater design freedom. [7] However, the limited number of materials available for additive manufacturing must be improved.

2.1.6 Need for Improvement

The inherent qualities additive manufacturing provide drives the use of the technology toward high value parts. These applications require demanding material properties, such as ultimate strength, yield strength, fracture toughness, fatigue strength, and corrosion resistance. However, the materials available for printing are limited. Laser processing results in an increased solidification rate (0.1 m/s to 0.5 m/s), constraining printable metals to alloys which are easily weldable.[12]

Aluminum is lightweight, a desirable attribute for the aerospace industry, however, many aluminum alloys display only moderate strength. Additionally, factors such as surface oxide scales, high thermal conductivity, and large solidification shrinkage, physical properties of aluminum are less repeatable and reliable. The traditional aluminum alloys used for additive manufacturing were developed from existing foundry technologies. There is a need for the development of a new aluminum alloy which takes full advantage of the benefits additive manufacturing has to offer, such as rapid solidification and cooling.

2.2 The Aluminum Systems

2.2.1 Aluminum Alloys

Aluminum is a lightweight metal offering a variety of applications from the food industry to the aerospace industry. Aluminum is a soft and malleable metal which offers good thermal and electrical conductivity compared to other AM materials. It offers a resistance to corrosion in air, making it a suitable candidate for applications needing corrosion resistance. While some applications may be suitable for unalloyed aluminum, engineering applications require a strengthened material. There are two primary classifications of aluminum alloys: casting alloys and wrought alloys. These two categories are then subdivided into heat-treatable and non heat-treatable alloys.[25] There are a variety of methods by which aluminum can be strengthened, such as solid solution strengthening alloying elements, cold-working, and heat treatment to develop

strengthening precipitates. Table 2-2 shows common aluminum alloys, the mechanisms by which they are strengthened, and their corresponding strength values.

Table 2-2. Aluminum alloys and their strengthening methods. [26]

Alloy Series	Alloying Elements	Methods for Increasing Strength	Yield Strength ksi (MPa)	Tensile Strength ksi (MPa)
1xxx	None	Cold-working	4-24 (30-165)	10-27 (70-185)
2xxx	Cu	Cold-working, precipitation	11-64 (75-440)	27-70 (185-485)
3xxx	Mn	Cold-working, solid solution, dispersion	6-36 (40-250)	16-41 (110-285)
4xxx	Si	Cold-working, dispersion	46 (315)	55 (380)
5xxx	Mg	Cold-working, solid solution	6-59 (40-405)	18-63 (125-435)
6xxx	Mg, Si	Cold-working, precipitation	7-55 (50-380)	13-58 (90-400)
7xxx	Zn, Mg, Cu	Cold-working, precipitation	15-78 (105-540)	33-88 (230-605)

For additive manufacturing applications, there is interest in aluminum alloys which are strengthened through post processing heat treatment to optimize mechanical properties. Common alloying additions and combinations for precipitation strengthening of aluminum include Cu, Cu+Mg, Cu+Li, Mg+Si, Zn+Mg, and Zn+Mg+Cu. Precipitation strengthened aluminum alloys provide some of the highest strength aluminum alloys available.

2.2.2 Strengthening Mechanisms

As discussed above, there are several mechanisms by which aluminum can be strengthened: the addition of alloying elements, solid solution strengthening, and precipitation strengthening. Alloying elements influence the mechanism by which the

alloy is strengthened. These strengthening mechanisms will be discussed in the next sections.

2.2.2.1 Alloying

The addition of alloying elements for primarily solid solution strengthening of aluminum is used to produce a material with increased mechanical properties, capable for use in engineering applications. In most instances, solid solution strengthening is used in combination with work hardening. Common alloy designations and their strengthening effect on aluminum are shown in Table 2-2. The additions of Mn (3xxx) and Mg (5xxx) allow the material to be strengthened through solid solution strengthening and work hardening. The additions of Cu (2xxx), Mg-Si (6xxx), and Zn-Mg-Cu (7xxx) enable the material to be precipitation strengthened through a heat treatment cycle.[27] Alloying additions also influence the melting and solidification dynamics of the material.[14] In this thesis, the primary focus is on the additions of Cu, Ag, and Mg. The effects of these individual element additions will be discussed in subsequent sections.

2.2.2.2 Solid Solution Strengthening

Solid solution strengthening is a mechanism of strengthening pure metal by dissolving alloying elements into the metal while in liquid form. Alloying elements cause nonuniformities in the lattice that impede dislocation motion, increasing strength. Alloying elements can increase the strength of aluminum up to 6 times that of pure

aluminum.[26] The extent to which the alloy is strengthened is dependent on the type and amount of alloying elements. There are two types of solid solutions that can be formed: substitutional solid solutions and interstitial solid solutions. In substitutional solid solutions, the alloying element replaces an atom of the metal in the lattice, interrupting dislocation motion, which is shown in Figure 2-4. In interstitial solid solutions, atoms are small enough to fit into spaces, or interstices, between the metal atoms in the lattice. These also interrupt dislocation movement, which is shown in Figure 2-5. In both instances, the dislocation then requires greater energy to continue around the impediment.

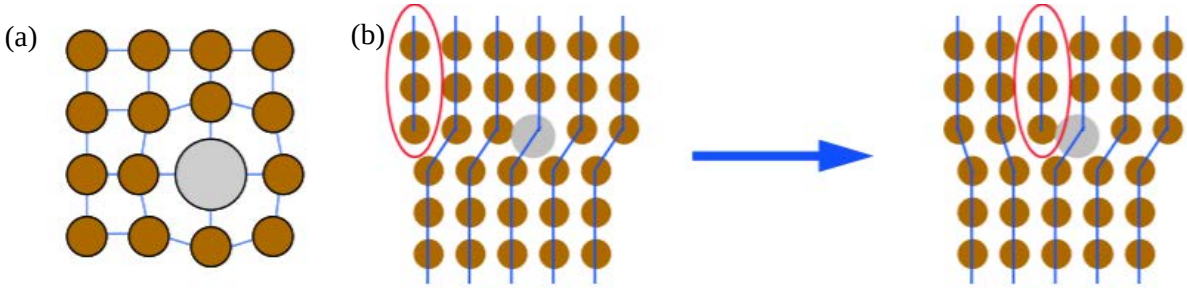

Figure 2-4. (a) substitutional solid solution (b) a substitutional atom stopping dislocation motion.[28]

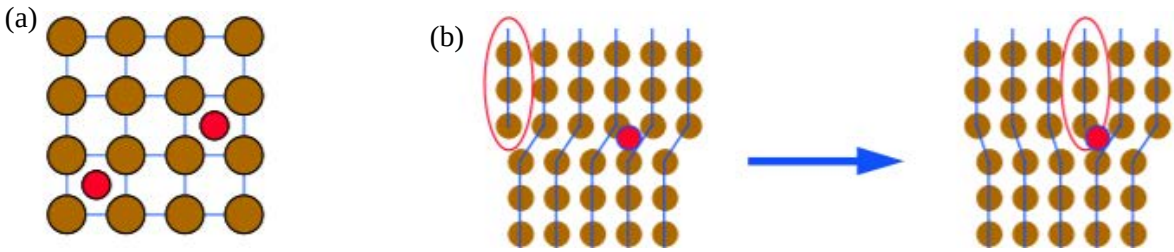

Figure 2-5. (a) interstitial solid solution (b) interstitial atom stopping dislocation motion.[28]

The effect of solid solution strengthening depends on a number of factors. The concentration of the solute atoms, the shear modulus of the solute atoms, and the size of the solute atoms all contribute to the strengthening of the material. If alloying elements

are added beyond their solubility limit, the material matrix can no longer accommodate all of the solute. In this case, a different mechanism of strengthening is employed; the precipitation of intermetallic compounds.[29]

2.2.2.3 Precipitation Strengthening

Precipitation strengthening is a heat treatment technique which utilizes the addition of second-phase particles, or precipitates, to strengthen a material. Each alloying element has a solubility limit in the material to which it is added. Alloying beyond the solubility limit allows the material to form a second phase which strengthens via precipitation. To form a precipitate, there must be a solid solution between the metal and the alloy which has a decreasing solid solubility with decreasing temperature.[30] This relationship is demonstrated in Figure 2-6 by the highlighted solvus line between α and α+θ in the Al-Cu diagram.

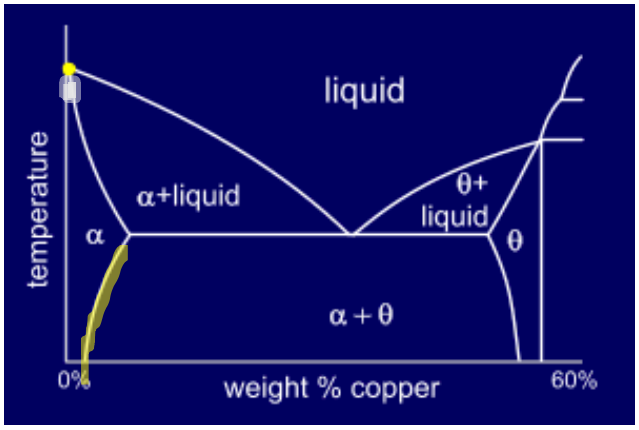

Figure 2-6. Al-Cu phase diagram highlighting the decreasing solubility with temperature required for precipitation.[31]

Due to this requirement, only certain Al alloys can be precipitation strengthened. These include the 2xxx series alloys through the formation of Al-Cu precipitates, 6xxx series alloys through the formation of Mg-Si precipitates, and 7xxx alloys through the formation of Al-Cu-Mg-Zn precipitates.[26]

Precipitates strengthen of the material by impeding dislocation movement, may be used to increase strength up to 5-15 times that of unalloyed aluminum.[26] Achievable strength depends on conditions such as the alloying elements and heat treatment conditions. There are three steps involved in the precipitation hardening process: solution treatment, quench, and age. A solution treatment involves heating the material to a temperature at which it will homogenize until a solid solution is formed. Quenching involves rapidly cooling of the material to obtain a single phase, supersaturated, solid solution. Aging involves heating the material to an intermediate temperature below the solvus temperature, allowing the formation of small, dispersed, second phase precipitates.[32] This process is illustrated in Figure 2-7.

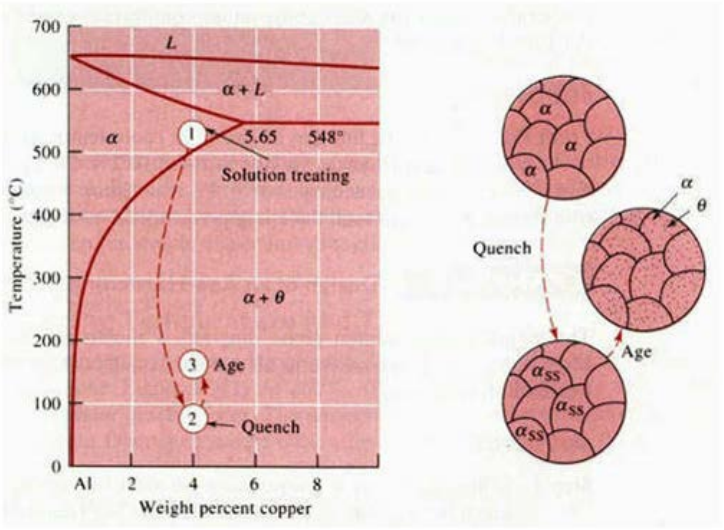

Figure 2-7. Al-Cu phase diagram highlighting the steps involved in precipitation hardening heat treatment and the resulting microstructures.[33]

The temperature and duration of the aging process will determine the condition to which the material is aged. There are three conditions of aging: under-aged, peak-aged, and over-aged. Each condition has a specific type, size, and distribution of precipitates which contribute uniquely to the resultant mechanical properties. During plastic deformation, stress must be increased to move the dislocation through the distribution of precipitates. Based on the aged condition, the dislocation and precipitate will interact accordingly. [32]

In the under-aged condition, precipitates are small and not substantially hard. These precipitates can be sheared by the dislocation through the Friedel effect, forming an antiphase boundary shown in Figure 2-8 (a).

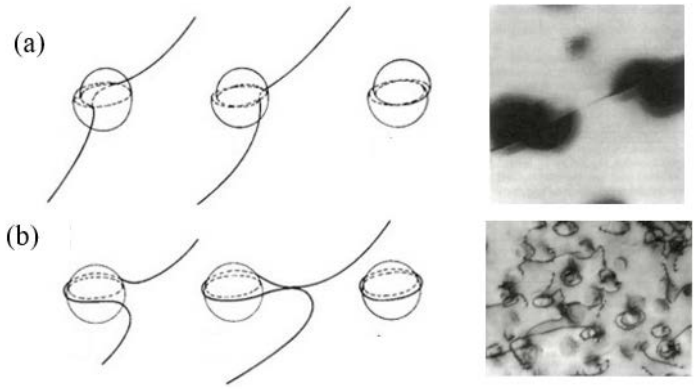

Figure 2-8. a) Representation of shearing precipitates by the Freidel effect. b) bow-out by precipitates by the Orowan mechanism.[34]

Conversely, in the over-aged condition precipitates are large and hard. These precipitates are bypassed by the dislocation through the Orowan Mechanism. The dislocation bends around the particle until it is completely enclosed and the dislocation can continue on, leaving a dislocation ring around the precipitate. This mechanism is shown in Figure 2-8 (b). These particles are incoherent with the matrix making it difficult for a dislocation to

overcome the phase boundary of the precipitate.[34] In each of these conditions, dislocations are still able to move through or around a precipitate. This is in contrast to the peak-aged condition, which due to the size, distribution, and hardness of the precipitate, impedes easy motion of the dislocation around the precipitate.

2.2.3 Solidification Crack Sensitivity

Out of thousands of alloys used in manufacturing and engineering today, most cannot be used in additive manufacturing due to the inherent melting and solidification dynamics of alloys. [35] The application of a laser energy source to melt metal powders results in local solidification rates between 0.1 m/s and 5 m/s.[12] As a result, the class of metal materials suitable for additive manufacturing are limited to those that are easily weldable. To be deemed weldable, material properties including melting point, thermal conductivity, thermal expansion, reactivity, and electrical resistance must be considered. The melting point of the material must be low enough to be melted by the energy source. Additionally, materials with high thermal conductivity and expansion, high reactivity, and high electrical resistance are all difficult to weld. Materials that are deemed unweldable cannot withstand the solidification conditions and therefore crack through many successive print layers.

For unweldable materials, the primary equilibrium phase starts to solidify first, at a composition different from the bulk liquid composition. As a result, the liquid becomes solute enriched near the solidification interface. This changes the equilibrium liquidus temperature, creating an undercooled condition. [36] The undercooled condition leads to

the formation of cellular or dendritic grains, allowing interdendritic liquid networks to be trapped inside solidified sections. As the material cools, solidification shrinkage and thermal contraction leave cavities in the interdendritic regions or grain boundaries where cracks can propagate.[37]

Current printable aluminum alloys for AM are designed around the Al-Si system, however, most alloys used in engineering applications are based on elements such as Cu, Mg, Zn, and Si to produce strengthening phases. To be used in additive manufacturing, these alloys must have inherent weldable properties. Materials that are deemed unweldable are extremely susceptible to solidification cracking. Solidification cracking or hot tears originate within the liquid pool due to solidification shrinkage strains and thermally induced stresses, causing tearing of the solidifying network. Solidification cracking of aluminum alloys can be generally explained by the continuous development of the coherent network during solidification, being acted upon by the thermal stresses and solidification shrinkage strains. It has been found that the phenomena is roughly linked to the range of solidification temperatures, which for binary alloys is maximum at the solid solubility limit. Based on this introductory description, solidification crack susceptibility would be at a maximum for binary alloys at an intermediate solute concentration less than the solid solubility, and prior research has shown this to be the case.[96] Although multiple alloy additions increase the complexity of this description, the primary alloying addition tends to dominate the influence of solidification cracking.

A material's susceptibility to solidification cracking can be identified by their solidification curves, which have been empirically developed to assess solidification cracking based on composition. Figure 2-9 shows a crack sensitivity map for

solidification cracking in ternary Al-Cu-Mg system, with contour lines showing total crack length. As shown in the figure, alloys containing relatively high levels of Cu and low levels of Mg have been shown to be fairly insensitive to solidification cracking, and hence, are of interest in the present study.

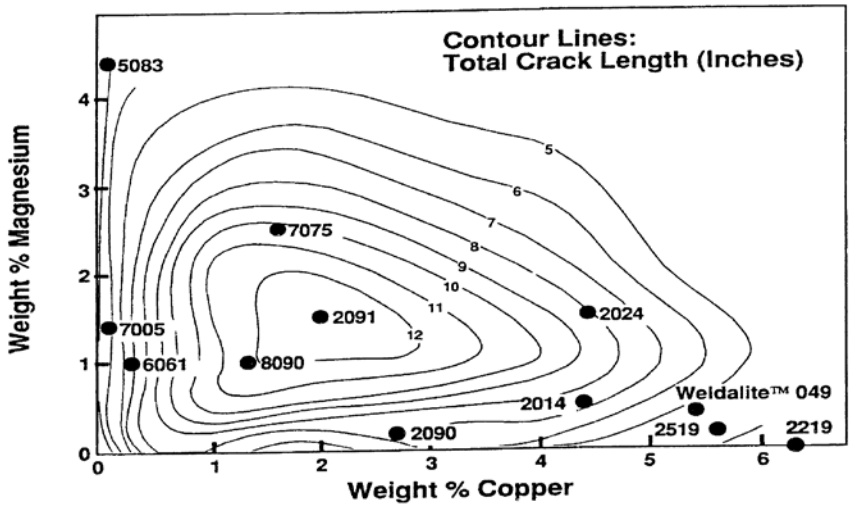

Figure 2-9. Solidification cracking of the Al-Cu-Mg system.[39]

Alloying content plays a major role in the solidification of materials. There is a critical content of solute that exists in each alloy system that corresponds to a thin liquid film formation. This thin liquid film becomes trapped in interdendritic regions and provides conditions for cracking upon solidification. Alloys with solute concentration in this thin liquid film formation range are deemed unweldable and not applicable to additive manufacturing. **[14], [38]**

In Al-Cu alloys, cracking sensitivity increases with increasing Cu content up to 3 wt% Cu, but decreases to a relatively low level of crack sensitivity in alloys with higher Cu content. In Al-Cu-Mg alloys, such as 2219 and 2519, additions above 6 wt% Cu are found to be outside of the crack sensitivity range. Research by Taminger and Hafley of NASA Langley Research Center shows microstructures of electron-beam freeform

fabricated 2219 possessing no cracking, complete layer fusion, and very little porosity. **[14], [38], [40]**

Processing parameters can also be taken into account to avoid solidification cracking. Zhang et al. found that in alloys with a wide solidification temperature range, reducing the scanning speed from 20 m/min to 8 m/min during SLM of Al-4.24Cu-1.97Mg-0.56Mn eliminated imperfections and microcracks. **[41]** A slow scanning speed allows the metal to stay in the liquid form for a longer duration, allowing more fluidity for the backfill of dendrite shrinkages. If the rate of crack backfilling is not greater than the rate of induced strains the material will contain cracks. **[42]**

2.3 Al-Cu-Ag-Mg System

The Al-Cu-Ag-Mg alloy system represents a precipitation hardenable material. The combination of alloying elements, added in the right quantities, promotes the formation of precipitates. When aged, the precipitates grow and subsequently improve the strength of the material by blocking dislocation motion. In addition to promoting precipitate formation, alloy additions to aluminum should not negatively impact the material during processing. In laser processing applications, precautions must be taken to limit additions that have high sensitivity to solidification cracking, porosity, or feature definition and surface quality. Elements that form oxides that readily hydrate, such as Mg, are prone to porosity. Alloying additions that dramatically alter liquid metal properties or have a high vapor pressure should be reduced**.** The following sections

describe the role of each alloying element in aluminum and provides rationale for the amounts chosen for the subsequent experiments.

2.3.1 Alloying Elements

Copper

Copper is used as an alloying element in aluminum to provide an increase in strength by facilitating precipitation hardening. Alloys typically contain between 2 and 10 wt% Cu, with most commercial aluminum alloys not exceeding 6 wt% Cu. Up to 5.7 wt% Cu is soluble in aluminum. Copper is a precipitation strengthener in aluminum based on the Cu rich precipitate phase, $CuAl_2$ and its precursors.[43] $CuAl_2$, or θ, has a precipitation sequence as follows:

$$\alpha_{SSSS} \rightarrow \text{GP zones} \rightarrow \theta'' \text{ (GP II zones)} \rightarrow \theta' \rightarrow \theta \quad [44],[45]$$

From the alpha aluminum phase, GP zones form first. The GP zones are small discs, less than 0.1μm in diameter, of atoms that form as a coherent single layer of pure Cu on the $\{001\}_\alpha$ plane of the fcc Al-Cu solid solution. The θ" phase, also called GP II zones, are coherent, intermediate precipitates consisting of two or more {001} layers of Cu atoms that are separated by three Al layers. The θ' phase is the primary strengthening phase in Al-Cu. These precipitates are disc-shaped platelets of several atomic layers with a body centered tetragonal crystal structure on the {100} planes in aluminum. They incorporate some Al atoms and are semi coherent to the matrix. The θ phase is a full,

three dimensional precipitate of equilibrium $CuAl_2$, which is incoherent with the matrix and has a body centered tetragonal crystal structure.[44], [46], [47]

Figure 2-10 displays the precipitation sequence for Al-Cu shown on the phase diagram. Point 1 marks the temperature for solution heat treating, around 550°C. Point 2 marks the temperature after quenching in a supersaturated solid solution. Point 3 marks the temperature at which the material is aged to precipitate θ. Figure 2-11 displays the structure at each stage of precipitation upon aging.

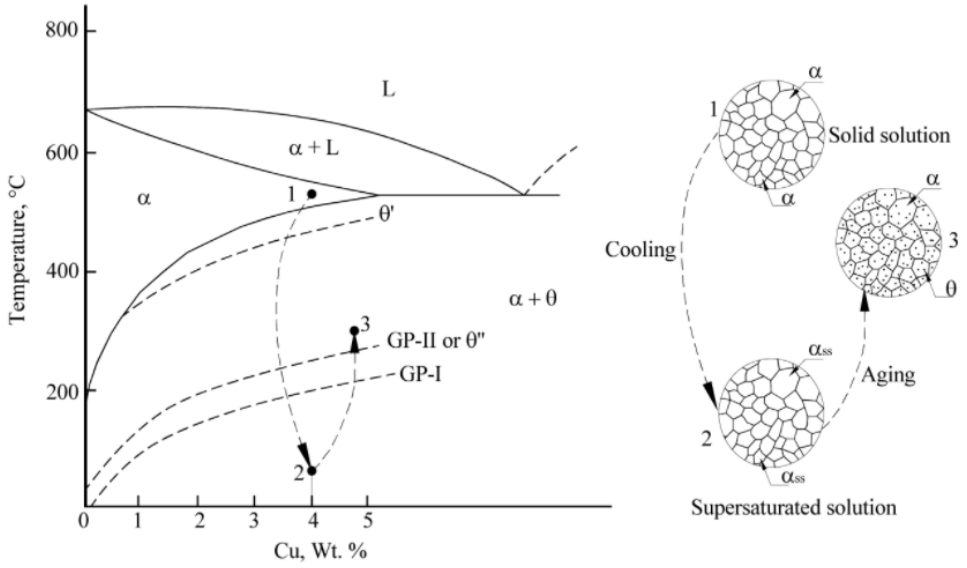

Figure 2-10. Precipitation hardening process of Al-Cu and the precipitate phases formed.[48]

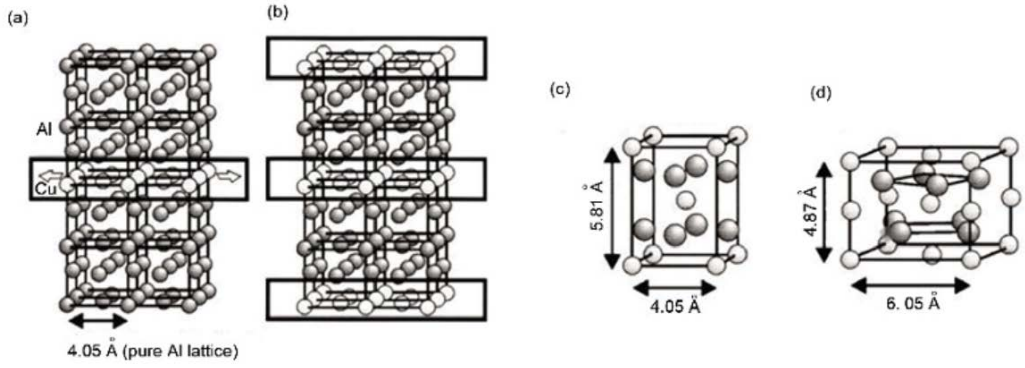

Figure 2-11. Al-Cu precipitation sequence (a) GP zones (b) θ" (GP II zones) (c) θ' (d) θ.[49]

The amount of Cu in the alloy determines how much θ is precipitated. Consequently, increasing Cu content improves strength and hardness of the alloy, providing for some of the highest strength heat treatable aluminum alloys.[43], [50] However, high additions of Cu can reduce ductility and corrosion resistance of the alloy.[51] Additions of Cu can also impact solidification cracking, but additions above 6 wt% Cu are outside of the crack sensitivity range.[14], [40] In addition to the strength benefits, Cu is a good alloying candidate for an additive manufacturing material because it does not alter surface tension of Al-Cu in the liquid state. This attribute is advantageous for a small molten pool which may translate to good surface finish and high feature resolution.[1],[10]

The Al-Cu system provides a backbone for understanding the larger Al-Cu-Mg-Ag system. For this thesis, Cu additions of 6, 7, and 8 wt% Cu are considered for increasing strength, reducing solidification crack sensitivity, and improving liquid metal characteristics in Al-Cu-Mg-Ag alloys.

Magnesium

Magnesium is a solid solution strengthener when added to aluminum, and is one of the lightest engineering materials available, being even significantly lighter than aluminum.[51] Magnesium is typically added to aluminum in amounts up to 10 wt%, and Al-Mg alloys are moderate strength materials which improve strain hardening without significantly reducing ductility or corrosion resistance. These alloys are non heat-treatable and are seldom used as the sole alloying element for aluminum engineering

materials.[52] When used in combination with other alloying elements such as Cu, Mg provides an improvement in hardness and tensile strength through the formation of an intermetallic compound, Al_2CuMg, which forms upon aging.[53] The Al_2CuMg phase, designated S, has the precipitation sequences as follows:

$$\alpha_{SSSS} \rightarrow \text{co-clusters/GP zones} \rightarrow \text{GP II/S''} \rightarrow \text{S'/S}$$ [54]

There has been a lot of discrepancy in past research regarding the precipitation sequence of S. Silcock et al. suggested that GP zones in Al-Cu-Mg alloys are small rod-like particles rich in Mg and Cu that form on {100} in aluminum.[55] However, Wang and Starink concluded that the evidence which shows Cu and Mg rich GP zone possessing a distinct shape and internal order is weak and therefore cannot be distinguished from Cu-Mg co-clusters. The GPII/S" intermediate precipitate is a fully coherent phase that has a plate-like morphology, yet there is currently no agreed upon structure for S".[54], [56] The S' precipitate is a form of Al_2CuMg that forms as platelets on {210} aluminum planes and are elongated along the <100> direction. It forms the same orthorhombic crystal structure and orientation as equilibrium S, with only small differences in lattice parameters. Because of this almost identical crystal structure, a separate designation is unwarranted.[54]

Because this material will be used in laser processing applications, the formation of MgO during melting must be considered. Higher levels of Mg tend to promote the formation of MgO, which could lead to undesirable hydrogen porosity.[57] Girisha et al. concluded that Al-Cu-Mg alloys containing 1 wt% Mg have the most favorable improvements to hardness and tensile strength through precipitation.[53] However, the

level of Mg additions should be limited in order to avoid solidification cracking during laser processing. Magnesium additions of less than 0.5 wt% are considered in this research for minimizing solidification cracks, increasing strength, while also minimizing vaporization loss and formation of hygroscopic MgO.

Silver

Silver is used as an alloying element in aluminum to improve heat resistant properties, tensile stregnth, and creep resistance.[58] Silver is a precipitation strengthener in aluminum based on the formation of Al_2Ag and its precursors. The Al_2Ag phase has a precipitation sequence as follows:

$$\alpha_{SSSS}\ (fcc) \rightarrow \text{GP zones} \rightarrow \Upsilon' \rightarrow \Upsilon \quad [59]$$

In Al-Ag alloys, GP zones are spherical clusters of high silver concentration with a tetrahedral structure. The γ'phase forms as thin, hexagonal plates on the {111} plane in aluminum. These precipitates are metastable, with the broad face of the precipitate being coherent to the matrix and the edge of the precipitate being semi coherent. The γ (Al_2Ag) phase, is the full, three dimensional equilibrium phase precipitate having an hcp crystal structure. [47], [60], [61]

In addition to promoting thermal stability and improving mechanical properties, silver additions do not lower surface tension in the liquid state. Silver compositions of 2, 3, and 4 wt% were chosen for this research based on maximizing the potential for precipitate strengthening.

Trace Elements

Additions of Ti and Zr are added to aluminum for the purposes of forming high temperature intermetallic phases that may result in grain refinement. Intermetallic phases affect dispersion hardening and as a result contribute to an increase in high temperature strength.[62] Grain refinement reduces grain size, effectively increasing strength and ductility. Minor additions of Zr (0.15 wt%) can also significantly improve hardness of aluminum alloys.[63] Trace additions of Ti can increase yield and tensile strength in Al-Cu-Mg-Ag alloys. [64]

2.3.2 Strengthening Phases in Al-Cu-Ag-Mg

When using three primary alloying elements, the relationship between compositions varies with the combinations of each element. Finding the amounts at which these elements provide the most advantages is necessary in strengthening aluminum to its highest potential. The Al-Cu-Mg system provides a well-known basis for understanding the Al-Cu-Ag-Mg system. Figure 2-12 shows the aluminum rich corner of the Al-Cu-Mg phase diagram, indicating the precipitate phases that form as a function of composition after long term aging at 190°C. The precipitates that can exist in these alloys include θ (Al_2Cu), S (Al_2CuMg), and T (Al_6CuMg_4). [65], [66], [67]

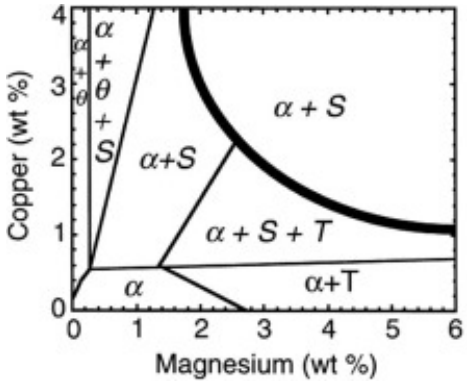

Figure 2-12. Aluminum rich corner of the Al-Cu-Mg phase diagram, demonstrating the phases present at each composition after aging long term at 190°C. [68]

When added to Al-Cu-Mg, Ag has shown to accelerate aging as well as stimulate an increased age hardening reaction. [61], [69] V.V. Teleshov stated that the effect of Ag on precipitation in Al-Cu-Mg is connected with the changes in the mechanism of decomposition of the solid solution during artificial aging.[70] The addition of Ag then promotes a new formation of each precipitate. In the Al-Cu-Mg alloy, the primary strengthening precipitate relies on the Cu/Mg ratio.[61], [71], [72]

The θ (Al_2Cu) phase is an equilibrium precipitate that forms in materials with a high Cu:Mg ratio.[73] It possesses a body centered tetragonal structure on the {100} planes in the aluminum matrix, but with the addition of Ag, Al_2Cu takes on a different form designated Ω. The Ω (Al_2Cu) phase precipitates as thin hexagonal plates which grow on the {111} planes in the aluminum matrix.[50], [74] The S (Al_2CuMg) phase is an equilibrium precipitate that forms in alloys with a moderate Cu:Mg ratio.[73] The S phase precipitates as orthorhombic laths on {210} planes and are elongated along the <100> direction in aluminum. [75], [76] With the additions of Ag, (Al_2CuMg) takes on a new form, X', which precipitates as a close packed hexagonal phase. The T(Al_6CuMg_4) phase is an

equilibrium precipitate that forms in alloys with a low Cu:Mg ratio.[73] It possesses a complex body-centered structure, but with the additions of Ag, this phase takes on a new face-centered cubic form, designated Z.[75] There is little commercial interest in Al-Cu-Mg alloys that possess a low Cu:Mg ratio (high Mg content) and reside in the α + S + T region of the phase diagram. This thesis focuses on alloys with very high Cu:Mg ratios that precipitate Ω. The precipitation sequence in an Al-Cu-Ag-Mg alloy with a high Cu:Mg ratio is:

α_{SSSS} → Mg-Ag co-clusters → Ω phase + θ' phase → θ + Mg, Ag, Cu enriched phases

[58], [67], [77], [78], [79]

The Mg-Ag precursor for precipitation is seen to form as little as 15s after aging at 180°C.[43] During this formation Ag traps Mg atoms creating clusters. The Mg-Ag co-clusters then act as heterogeneous nucleation sites for Ω.[80] The Ω precipitation is achieved by the diffusion of Cu atoms. There is a high binding energy between Cu and vacancies in Al-Cu-Ag-Mg, which after quenching, promotes diffusion of Cu to Mg-Ag co-clusters.[50] The Cu atoms diffuse to these Mg-Ag clusters and grow into platelets until the concentration of Cu reaches that of Ω (Al_2Cu).[72] The diffusion of Cu to Mg-Ag co-clusters is seen as soon as 30s after aging at 180°C.[43] After full precipitation of Ω, Mg and Ag are still detected at the matrix/precipitate interface.[81]

Although the chemistry and crystal structure of Ω is very similar to equilibrium θ, the Ω (Al_2Cu) precipitates are thin hexagonal plates which grow on the {111} planes in the aluminum matrix, as opposed to θ which grow on the {100} planes.[50], [74] These

precipitates are a variation of θ that result from the collaboration between Mg and Ag.[43] Figure 2-11 displays a TEM micrograph of Ω and θ and their respective orientations.

The Ω precipitates are found to occur on aging above 100°C and are stable and coherent up to an aging temperature of about 250°C.[73], [76], [81] Under conditions of prolonged aging (>250°C), Ω precipitates can be considered metastable.[66],[82] Because they are coherent**,** Ω precipitates provide coherency strain hardening, resulting from the interaction between dislocations and strain fields around precipitates. The precipitates block dislocation movement, effectively strengthening the material. Additionally, finely dispersed Ω precipitates have shown to enhance high temperature performance and mechanical properties, providing a source of high thermal stability.[81]

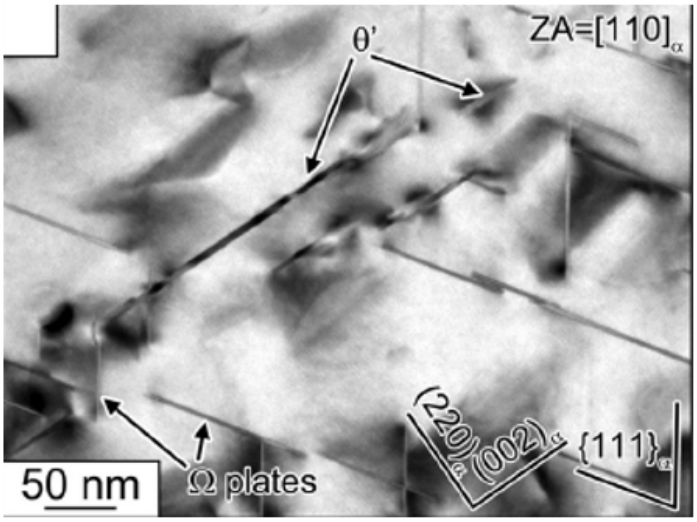

Figure 2-13. TEM micrograph of Al-5.6Cu-0.72Mg-0.5Ag after aging at 200°C.[67]

The θ' precipitates form concurrently with Ω during aging.[67] This precipitate phase is more stable at higher temperatures (300°C) than the Ω phase.[78] However, Ω precipitation is sensitive to S (Al_2CuMg) formation. As S coarsens, Mg and Ag are consumed from neighboring Ω.[66]

While Ag is required to precipitate Ω, Al-Obaisi et al found that additions of Ag to Al-Cu without Mg does not precipitate Ω.[43] The cooperation of Mg and Ag is essential to the formation of the Ω precipitate.[83] The Al-Cu-Ag-Mg system showed increased mechanical properties compared to Al-Cu-Mg with no Ag or Al-Cu-Ag with no Mg.[84] The additions of Ag to Al-Cu-Mg alloys can enhance the thermal stability of **Ω** precipitates**.**[85] Increasing the amount of Ag and Cu lead to more growth of the Ω phase, resulting in improvements in strength.[50], [80] Because Ω are able to withstand shearing by dislocation, it is a very efficient strengthening agent if uniformly distributed to form a network of precipitates. This is achievable through peak aging.

2.3.3 Precipitation Hardening Heat Treatment for Al-Cu-Ag-Mg

The precipitation hardening heat treatment cycle for an Al-Cu-Ag-Mg alloy consists of three steps: solution treating, quenching, and aging. Temperature and duration will determine the result of the heat treatment cycle. Solution treating involves heating the material to a temperature below the solidus line. At this temperature, the material will be homogenized and a solid solution will form. This temperature is chosen by estimating the solidus temperature for the quaternary alloy. Because quaternary systems are complex and the Al-Cu-Ag-Mg system is a relatively new research interest, concrete phase and processing diagrams are not readily available. However, a solution treatment temperature can be derived from a combination of understanding the foundation of the system (Al-Cu and Al-Cu-Mg) and a review of previous research on precipitation hardening heat treatment cycles for Al-Cu-Ag-Mg alloys.

A solution treatment temperature must be chosen carefully as to not allow the material to begin melting. For an Al-Cu alloy with 6 wt% Cu, this temperature must be below the eutectic temperature of 548°C to avoid melting. Figure 2-14 displays the phase diagram for Al-Cu.

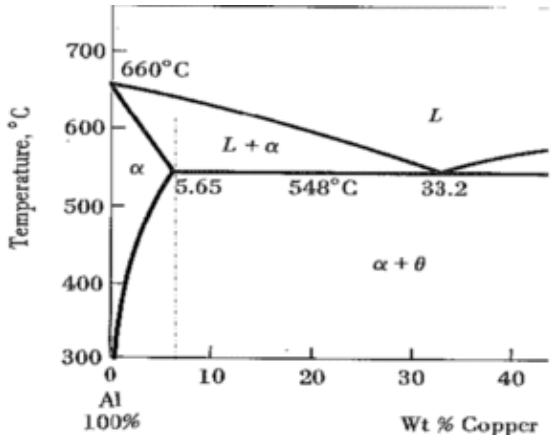

Figure 2-14. The Al-Cu phase diagram displaying temperatures for phase transformations.[32]

In work by Teleshov's et.al. on temperature ranges and phase transformations of alloys of the Al-Cu-Mg-Ag system, a solution treatment temperature of 540°C was used for an Al-5.4Cu-0.45Mg-0.61 Ag alloy.[70] Additionally, Hono et.al. used a solution treatment temperature of 540°C for 15 minutes for an Al-4.3Cu-0.7Ag -0.3Mg alloy.[77] In DeGeuser's work on the early stages of Ω phase precipitation in Al-Cu-Ag-Mg alloys, a solution treatment temperature of 520°C for 30 minutes was used for an Al-4Cu-0.3Mg-0.4Ag alloy.[82] Similarly, in research by Macchi et.al. on aging processes in Al-Cu-Mg alloys, a solution treatment temperature of 520°C was used for an Al-4Cu-0.3Mg.

After homogenizing, the material must be quenched immediately, in a quenching medium such as water, in order to freeze in a super saturated solid solution. When

quenching, the material cools at such a rapid rate that it does not allow time for diffusion that would occur upon natural cooling. Aging involves heating the material to an intermediate temperature in the two phase region, allowing the formation of small, second phase precipitates. At this temperature, diffusion rates become appreciable and small second phase particles form as finely dispersed precipitates. The aging temperature and time will determine the size and amount of these precipitates.

An aging temperature of 190°C is typical for aluminum alloys of the Al-Cu-Mg system.[70] However, researchers have used various aging temperatures for Al-Cu-Mg alloys ranging from 150°C to 220°C.[43],[45],[70],[75],[77],[78] In Al-Obaisi's work on precipitation hardening and statistical modeling of aging parameters and alloy compositions in Al-Cu-Mg-Ag alloys, the effect of changing alloying element amounts, aging time, and aging temperature on hardness was studied. Alloys of the Al-Cu-Ag-Mg system with alloying contents of Cu from 3 to 5.5 wt%, Mg from 0.45 to 1 wt%, and Ag from 0.3 to 0.6 wt% were aged at temperatures 160°C, 190°C, and 220°C for durations from 10 minutes to 64 hours. Their experiments showed that a low aging temperature of 160°C needed extended amounts of time (16-32 hours) to attain peak age condition, an aging time of 190°C demonstrated good values of hardness with aging times fitting industry needs, and a high aging temperature of 220°C resulted in the peak age condition being reached too rapidly and over-aging occurred quickly. They concluded that the optimum aging process for an Al-5Cu-1Mg-0.6Ag alloy is a temperature of 160°C for 22.75 hours to attain a peak hardness of 178.22 VHN.[43]

2.3.4 Properties and Application

The Al-Cu-Ag-Mg alloys have shown promising material properties for use in advance applications because of their high strength to density ratio, good heat resistance, good durability and corrosion resistance, good machinability and formability, low cost, and ready availability.[53],[58] The Al-Cu-Ag-Mg alloys **s**trengthened by the dispersion of Ω phase precipitates provide a combination of high strength, good fracture toughness, and improved creep resistance over Al-Cu-Mg alloys.[67] The Al-Cu-Ag-Mg alloys exhibit increased strengthening and mechanical properties up to temperatures of 200°C.[86]

Alloys based on the Al-Cu-Ag-Mg system present properties which are promising for applications which require a high service temperature while also offering an attractive ambient temperature strength and toughness. These materials are highly desirable in the aerospace industry, with several programs already researching Al-Cu-Mg-Ag alloys for wrought products for use in new-generation supersonic passenger airplanes.[70]

While this material has been studied for use as a wrought or casting material, developing its use in additive manufacturing will significantly expand its applications. Metals available for additive manufacturing are limited to AlSi10Mg, CoCr, Inconnel, Stainless Steel, and Ti64, with AlSi10Mg being the only material suitable for lightweight aerospace parts, hence there is a need for a material that can offer higher strength yet still be suitable for lightweight aerospace parts.

Chapter 3

PREVIOUS ARL RESEARCH

3.1 Initial Alloy Formulation

Initial experiments on an Al-Cu-Ag-Mg alloy for additive manufacturing were conducted by researchers at the Center for Innovative Materials Processing through Direct Digital Deposition that revealed promising results for an advanced aluminum alloy. In their preliminary research, three experimental alloys (Al-4Cu-2Ag, Al-8Cu-2Ag, and Al-8Cu-4Ag) were blended using pure aluminum, pure copper, and pure silver powders. Laser deposition was used to produce deposits for evaluation from these three experimental alloys, as well as three commercial alloys. The hardness of these alloys were then compared with commercial alloys 7090, 2219, and EOS AlSi10Mg. Table 3-1 displays the materials used in their initial experiments.

Table 3-1. Alloy compositions for initial experiment.

Specimen	Alloy	Commercial Alloy	Form	Powder Size (mm)	Solution HT Temperature
1	Al-8Zn-2.5Mg-1.0Cu-1.5Co	7090	Pre-Alloyed		466°C
2	Al-4Cu-2Ag	Experimental	Blended*	50 - 150	527°C
3	Al-8Cu-2Ag	Experimental	Blended*	50 - 150	516°C
4	Al-8Cu-4Ag	Experimental	Blended*	50 - 150	510°C
5	Al-6.3Cu	2219	Blended*	50 - 150	535°C
6	Al-10Si-0.5Mg	EOS AlSi10Mg	Pre-Alloyed	20 - 50	527°C
Base	Al-2.5Mg	5052	Plate		

*Blended using: 99.5% purity aluminum powder (50-125 mm), 99.0% purity copper powder (50-150 mm), and 99.9% purity silver powder (50-150 mm)

In addition to the six alloys listed in Table 3.1, each alloy was diluted at the substrate to contain a small amount of Mg. During deposition at the substrate, the alloy and base plate both melt, allowing the base material to dilute the alloy. The base plate used was commercial alloy 5052 (Al-2.5Mg). As a result, the composition of each of these alloys at the deposit-substrate interface was altered to contain approximately 0.5 wt% Mg. The substrate samples were designated as (+Mg). Figure 3.1 displays a specimen diagram showing the diluted substrate region and the bulk material region.

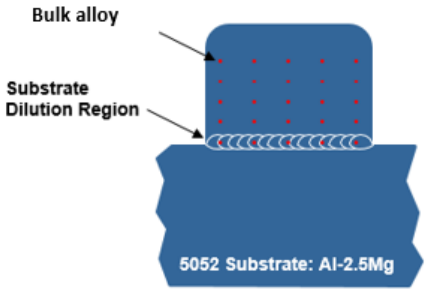

Figure 3-1. Specimen diagram showing hardness measurement locations.

3.2 Processing Test Specimens

Experiments were conducted using an Optomec LENS system for directed energy deposition. Table 3-2 shows the processing parameters used for printing the experimental builds. After processing, samples were sectioned for macrostructure and micro-hardness.

Table 3-2. Processing parameters for experimental builds.

Processing Parameters	
Laser Power:	450 W
Travel Speed:	0.3 – 0.6 cm/s
Powder Flow Rate:	2 g/min
Atmosphere:	Argon
# Passes:	15
# Layers:	25-50
Width:	6 mm
Height:	5 mm
Length:	60 mm

3.3 Aging and Mechanical Properties

After deposition, hardness values of each sample were taken in the as-built condition. Samples were then solution heat treated according to their composition, as shown in Table 3-3.

Table 3-3. Solution heat treatment temperatures of specimens according to composition.

Specimen	Alloy	Solution Heat Treatment Temp
5	Al-Cu	535°C
6	Al-Si-Mg	527°C
2, 3, 4	Al-Cu-Ag	510 °C
2+, 3+, 4+	Al-Cu-Ag-Mg	510°C

After solution heat treatment, samples were artificially aged for 2 hours at 93°C, 2 hours at 300°C, and 8 hours at 107°C. This provided a basis for choosing an aging temperature of 150°C to age samples for 4, 8, 12, and 16 hours. It was found that aging at 93°C for 2 hours left the material underaged, having no significant impact on hardness and aging at 300°C for 2 hours resulted in overaged material, showing no increase in

hardness after aging. Aging for 8 hours at 107°C showed slight increases in hardness in samples containing Mg. Hardness values for this preliminary aging experiment are shown in Table 3-4.

Table 3-4. Vickers hardness number at 50 gf for each alloy at bulk and substrate region.

Sample ID	**Alloy**	**As Built**	**AA for 2 hours at 93°C**	**AA for 8 hours at 107°C**	**AA for 2 hours at 300°C**
1	**7090**	68	74	73	58
1+ Mg	**7090 + 0.5Mg**	60	66	86	57
2	**Al-4Cu-2Ag**	63	63	64	59
2+Mg	**Al-4Cu-2Ag-0.5Mg**	68	64	74	60
3	**Al-8Cu-2Ag**	81	80	81	71
3+Mg	**Al-8Cu-2Ag-0.5Mg**	93	80	112	73
4	**Al-8Cu-4Ag**	88	84	86	76
4+Mg	**Al-8Cu-4Ag-0.5Mg**	104	80	100	77
5	**Al-6.3Cu**	67	68	70	60
5+Mg	**Al-6.3-0.5Mg**	77	98	103	67
6	**Al-10Si-0.5Mg**	101	104	108	71
6+Mg	**Al-10Si-1.0Mg**	90	108	126	65

Extended aging experiments were performed on samples 3, 4, 5, and 6. Vickers hardness measurements were taken from the bulk material deposit region, as well as at the interface region where samples contained Mg. Hardness was measured after aging for 4, 8, 12, and 16 hours. Figure 3-2 displays the hardness measurements of the bulk material region versus the interface region containing Mg for Sample 3 (Al-8Cu-2Ag). Figure 3-3 displays hardness measurements of the bulk material region versus interface region containing Mg for Sample 4 (Al-8Cu-4Ag). Table 3-5 displays these hardnesses for comparison.

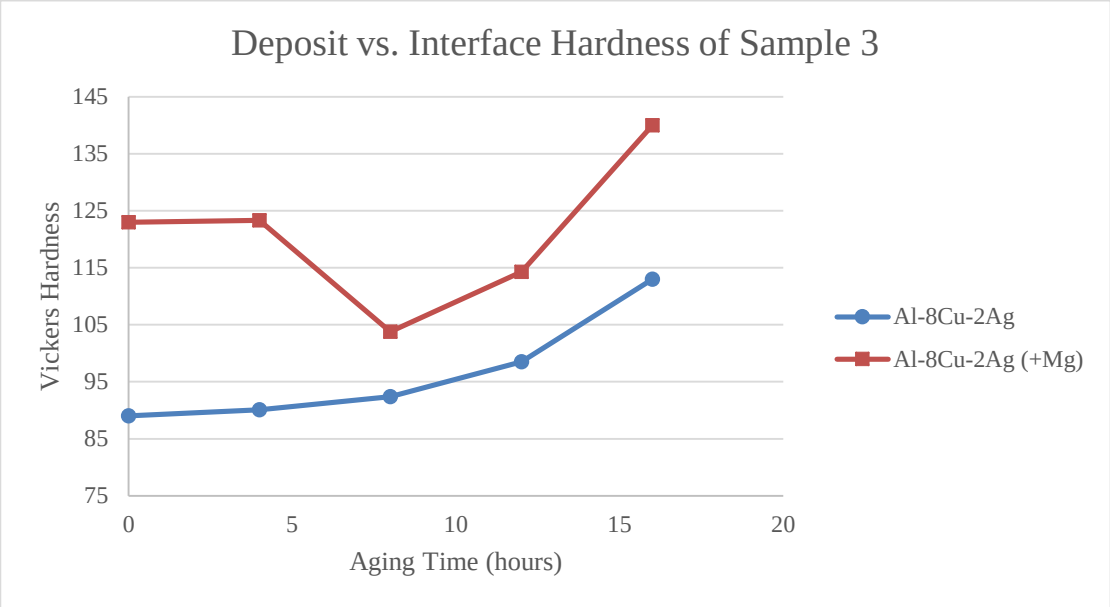

Figure 3-2. Deposit vs interface hardness of Sample 3 after aging 4, 8, 12, and 16 hours at 150°C.

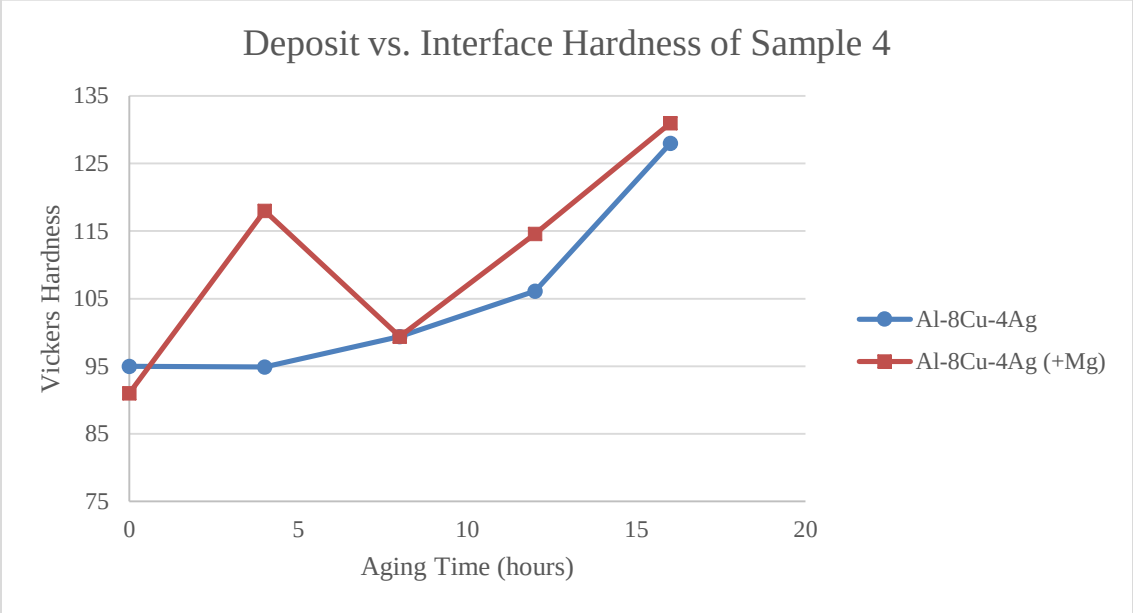

Figure 3-3. Deposit vs. interface hardness of Sample 4 after aging 4, 8, 12, and 16 hours at 150°C.

Table 3-5. Average Vickers hardness values after aging for 4, 8, 12, and 16 hours at 150°C.

Sample ID	**Alloy**	**As built**	**As solution treated**	**Aged 4h**	**Aged 8h**	**Aged 12 h**	**Aged 16h**
3	**Al-8Cu-2Ag**	81	88	90	92	99	113
3+Mg	**Al-8Cu-2Ag-0.5Mg**	93	124	123	104	114	140
4	**Al-8Cu-4Ag**	88	96	945	99	106	128
4+Mg	**Al-8Cu-4Ag-0.5Mg**	104	92	118	99	115	131
5	**Al-6.3Cu**	67	81	80	82	95	-
5+Mg	**Al-6.3-0.5Mg**	77	95	113	112	106	-
6	**Al-10Si-0.5Mg**	101	74	90	88	103	-
6+Mg	**Al-10Si-1.0Mg**	90	90	90	97	105	-

From the hardness data it is seen that adding Mg to Al-Cu-Ag alloys improves hardness. Additionally, aging these materials for extended periods of time increased hardness. Alloys 3 and 4 both show increasing hardness up to 16 hours after aging at 150°C; however, the aging curve did not appear to achieve the peak aged condition. Hardness is expected to continue to increase until peak age, followed by some decrease in hardness associated with the overaged condition. This complete aging curve was not observed. It appeared from the data that aging times would need to be extended, which is not surprising since some aluminum alloys require aging upwards of 25 hours before attaining peak aged condition.

A decrease in hardness is also displayed in both aging curves after an aging time of about 8 hours. This reversion may be attributed to the transition between precipitate phases. Research by Zuiko and Kaibyshev states that the precipitation of a low volume fraction of Ω promotes the dissolution of GP zones and precedes the formation of θ'.[95]

This effect can be seen in the aging curve displayed in Figure 3-4, showing a peak hardness after 3 hours, followed by a decrease in hardness and an additional peak after 12 hours.

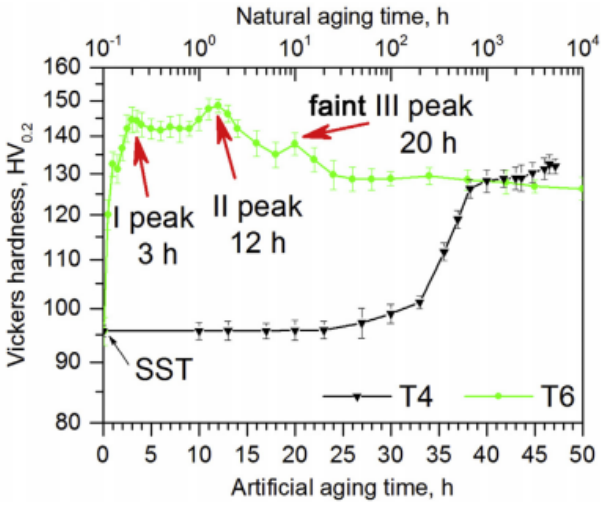

Figure 3-4. Age hardening response of Alloy 2519 after aging at 190°C.[95]

The highest achievable hardness was found to be the Al-8Cu-2Ag-0.5Mg alloy after aging for 16 hours. The tensile strength of this alloy was calculated using a conversion from hardness to tensile strength with the equation:

$$\sigma = \frac{H}{2.9}[1 - (m-2)\left[\frac{12.5\,(m-2}{1-(m-2)}\right]^{(m-2)} \qquad \textbf{Equation 1}$$

where H is the Vicker's hardness number and m is the Meyers Hardness Coefficient (m = n + 2).[87] From this equation, the ultimate tensile strength of the experimental Al-8Cu-2Ag-0.5Mg was calculated to be 489 MPa and did not achieve the peak aged strength. Based on this result, it was believed that the strength of a peak aged alloy would approach that of 7075-T651 material, 590 MPa. Figure 3-5 displays the ultimate tensile strength of the experimental Al-8Cu-2Ag-0.5Mg alloy in comparison with two alloys used for additive manufacturing, a recently developed Scalmalloy alloy and the currently

used AlSi10Mg alloy, as well as a common Al-Cu-Mg-Zn alloy used in aerospace applications, 7075-T651.

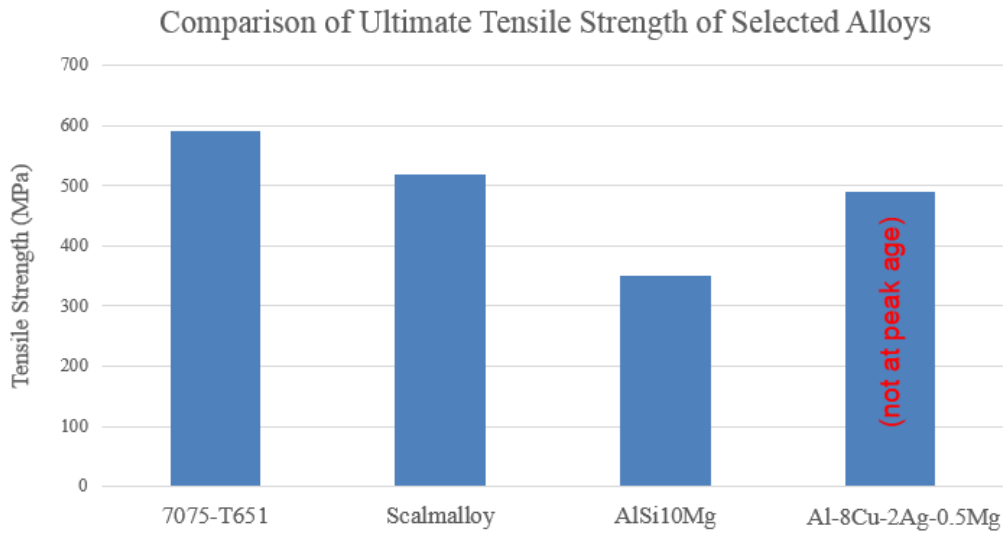

Figure 3-5. Ultimate tensile strength of experimental Al-Cu-Ag-Mg alloy and other aluminum alloys.[88],[89],[90]

From these preliminary results for the Al-8Cu-2Ag-0.5Mg and Al-8Cu-4Ag alloys, a compositional formulation and heat treatment experiment to optimize the strength of the alloy during directed energy deposition was devised. The next chapter will discuss materials selection and the methodology for the experiment to determine optimum chemistry and aging parameters for establishing an advanced aluminum alloy for additive manufacturing.

Chapter 4

ALLOY METHODOLOGY AND MATERIAL PREPARATION

4.1 Materials Selection

The alloys of interest are represented in the Al-Cu-Ag-Mg system, with the following compositions:

- Al: balance
- Cu: 6, 7, 8 wt%
- Ag: 2, 3, 4, wt%
- Mg: < 0.5 wt%
- Small amounts of Ti and Zr (< 0.3 wt%)

A full factorial design was used to develop an experimental plan. The full factorial design consists of 3 variables at 3 levels yielding 27 compositions:

$$x = levels^{variables} = 3^3 = 27$$

Table 3-1 lists these 27 possible composition combinations. Of these 27 compositions, 9 characteristic compositions could be achieved by blending using a pre-alloyed Al-Mg-Zn-Ti powder with additions of pure Ag powder and pure Cu powder. These 9 compositions are highlighted in Table 4-1, which essentially represents a 2 variable (Cu and Ag) experiment at 3 levels; Mg was kept constant at 0.30 wt%.

Table 4-1. Full factorial design for alloy composition combinations.

#	Cu	Ag	Mg
1	6	2	0.2
2	6	2	0.3
3	6	2	0.4
4	6	3	0.2
5	6	3	0.3
6	6	3	0.4
7	6	4	0.2
8	6	4	0.3
9	6	4	0.4

#	Cu	Ag	Mg
10	7	2	0.2
11	7	2	0.3
12	7	2	0.4
13	7	3	0.2
14	7	3	0.3
15	7	3	0.4
16	7	4	0.2
17	7	4	0.3
18	7	4	0.4

#	Cu	Ag	Mg
19	8	2	0.2
20	8	2	0.3
21	8	2	0.4
22	8	3	0.2
23	8	3	0.3
24	8	3	0.4
25	8	4	0.2
26	8	4	0.3
27	8	4	0.4

The Al-Mg powder composition, also having small amounts of titanium and zirconium for grain refinement, was chosen as the master alloy for mixing. Information for the master alloy is shown in Table 4-2. A composition of Al-0.35Mg-0.30Ti-0.30Zr was chosen to mix with pure Cu and pure Ag to achieve a final composition of the desired Ag and Cu content with an Mg content of about 0.30 wt%. A powder sieve size of -150/+325 (d_{10}=50 µm, d_{50}=75 µm, d_{90}=100 µm) was chosen to accommodate powder requirements for directed energy deposition.

Table 4-2. Al-Mg-Ti-Zr powder desired composition and size distribution.

Al-0.35Mg-0.30Ti-0.30Zr	**Nominal Composition**	**Composition Range**	**Size Distribution**
Mg	0.34	0.30-0.38	-150/+325 d_{10}=50 µm d_{50}=75 µm d_{90}=100 µm
Ti	0.28	0.22-0.30	
Zr	0.28	0.22-0.30	
All others: Si, Mn, Cr, Ni, Fe, Zn, Pb, S, P, B, K, Ca, Na	No more than 0.15% total others with each other no more than 0.05%		

While the desired composition and size distribution of the Al-Mg-Ti-Zr blending alloy is shown in Table 4-2, there were some variations and compromise in the final chemistry and size of this blending constituent due to the complexity of the atomization process. The characteristics of each blending constituent will be discussed in the next section.

4.2 Blending Constituents Characterization

Using the correct compositions and powder size is essential to the integrity of blend when mixing. Before mixing, powders must be characterized to confirm that their size distribution is suitable for mixing. Table 4-3 displays the composition of each blending constituent.

Table 4-3. Composition of blending constituents.

Blending Constituent	Al	Mg	Cu	Ag	Ti	Zr	Fe	Si	Zn	Mn, Cr, Ni, Pb, S, P, B, K, Ca, Na
Pure Ag	-	-	-	99.98	-	-	-	-	-	-
Pure Cu	-	-	99.9	-	-	-	-	-	-	-
Al-Mg-Ti-Zr	Balance	0.31	0.05	-	0.30	0.22	0.19	0.04	0.04	<0.005

Each of the three powder constituents for blending were characterized for size distribution using the Malvern Mastersizer 3000. Figure 4-1 displays the size distribution curves of the pure Cu powder, the pure Ag powder, and the custom Al-Mg-Ti-Zr powder. Table 4-3 displays the distribution values for these powders.

a).

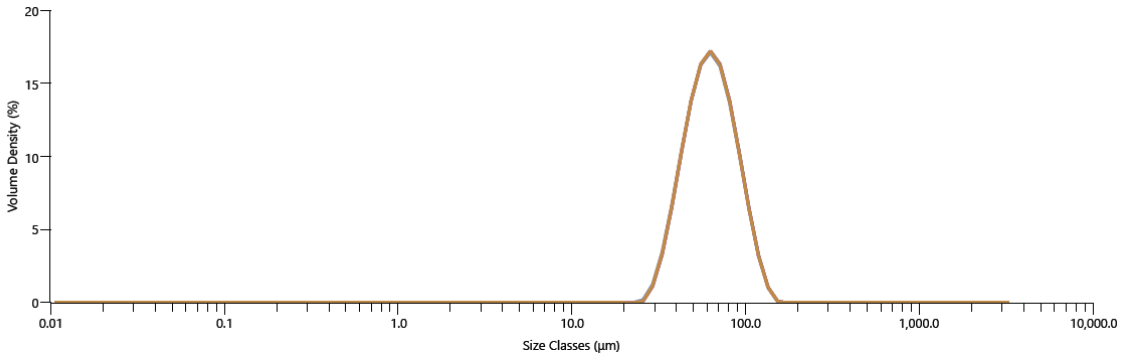

b).

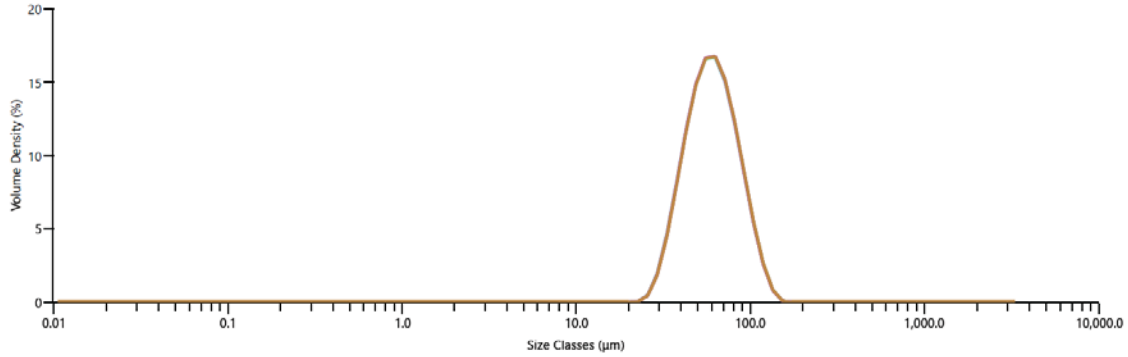

c).

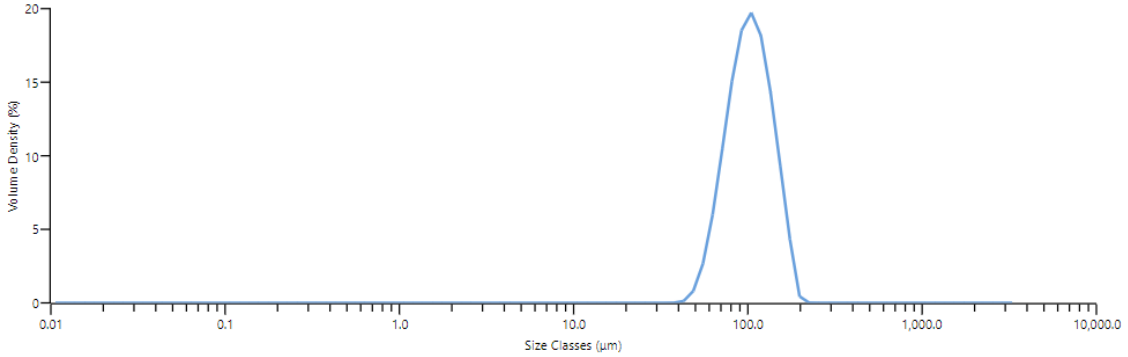

Figure 4-1. a). powder size distribution of pure Ag. b). powder size distribution of pure Cu. c). powder size distribution of Al-0.31Mg-0.30Ti-0.22Zr alloy.

Table 4-4. Size distribution values of each blending constituent.

	Pure Ag	**Pure Cu**	**Al-Mg-Ti-Zr**
D_{10}	40.5 µm	38.3 µm	69.2 µm
D_{50}	62.4 µm	59.5 µm	102 µm
D_{90}	96.2 µm	93.1 µm	147 µm

The powder size distribution for pure Ag and pure Cu show sizes that are smaller than that of the main blending constituent, Al-Mg-Ti-Zr. Because small additions of Cu and Ag were blended with larger amounts of Al-Mg-Ti-Zr, it is likely to blend better if Cu and Ag particles are somewhat smaller than the Al-Mg-Ti-Zr particles.

4.3 Mixing

To achieve the 9 characteristic compositions, pure Cu and pure Ag were mixed with an Al-0.31Mg-0.30Ti-0.22Zr alloy powder. The characteristic alloys are renumbered 1-9 for the experimental procedure. Table 4-5 displays these 9 alloys, the additions made per 100g of Al-Mg powder, and the final target composition after mixing. The additions are calculated by weight additions of Cu and Ag to 100g of Al-0.31Mg-0.30Ti-0.22Zr powder.

Table 4-5. Characteristic compositions, alloying element additions, and the final blend composition of the experimental alloys.

#	Target Composition			Additions to 100 g Al-0.31 Mg-0.3Ti-0.2Zr	Final Blend Composition
	Cu	Ag	Mg		
1	6	2	0.3	6.6 Cu + 2.2 Ag	6.1 Cu – 2.0 Ag – 0.28 Mg-0.28Ti-0.20Zr
2	6	3	0.3	6.7 Cu + 3.4 Ag	6.1 Cu – 3.1 Ag – 0.28 Mg-0.28Ti-0.20Zr
3	6	4	0.3	6.7 Cu + 4.5 Ag	6.0 Cu – 4.0 Ag – 0.28 Mg-0.28Ti-0.20Zr
4	7	2	0.3	7.8 Cu + 2.3 Ag	7.1 Cu – 2.1 Ag – 0.28 Mg-0.28Ti-0.20Zr
5	7	3	0.3	7.9 Cu + 3.4 Ag	7.1 Cu – 3.1 Ag – 0.28 Mg-0.28Ti-0.20Zr
6	7	4	0.3	7.9 Cu + 4.6 Ag	7.0 Cu – 4.1 Ag – 0.28 Mg-0.28Ti-0.20Zr
7	8	2	0.3	9.0 Cu + 2.3 Ag	8.1 Cu – 2.1 Ag – 0.28 Mg-0.28Ti-0.20Zr
8	8	3	0.3	9.0 Cu + 3.4 Ag	8.0 Cu – 3.0 Ag – 0.28 Mg-0.28Ti-0.20Zr
9	8	4	0.3	9.1 Cu + 4.6 Ag	8.0 Cu – 4.0 Ag-0.27 Mg-0.26Ti-0.19Zr

Appropriate additions of Cu and Ag were made to each of the nine containers holding 1.5kg of the Al-Mg-Ti-Zr powder. Each container was then blended on mechanical rollers for 1 hour. To test the quality of mixing, 3 random samples were chosen for characterization: Alloy 2, Alloy 4, and Alloy 9.

4.3.1 Blended Powder Particle Size

Three alloys were characterized for size distribution after blending using the Malvern Mastersizer 3000. Figure 4-2 displays the size distribution curves of Alloy 2, Alloy 4, and Alloy 9. Table 4-6 displays the distribution values for these alloys.

a).

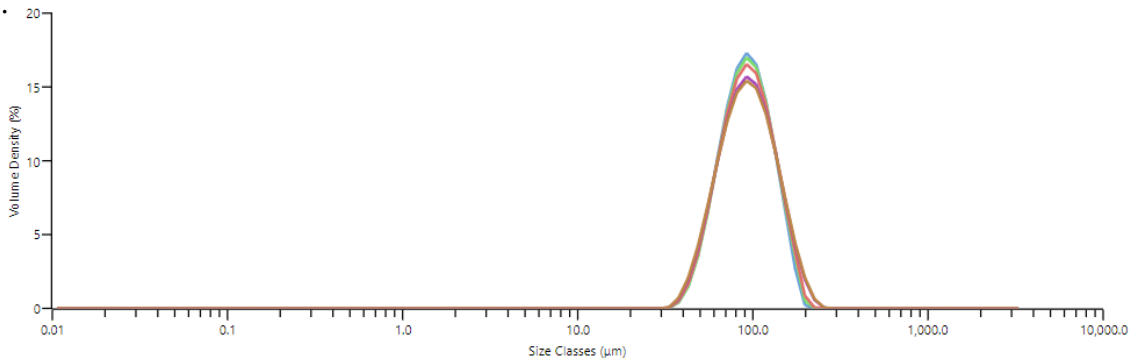

b).

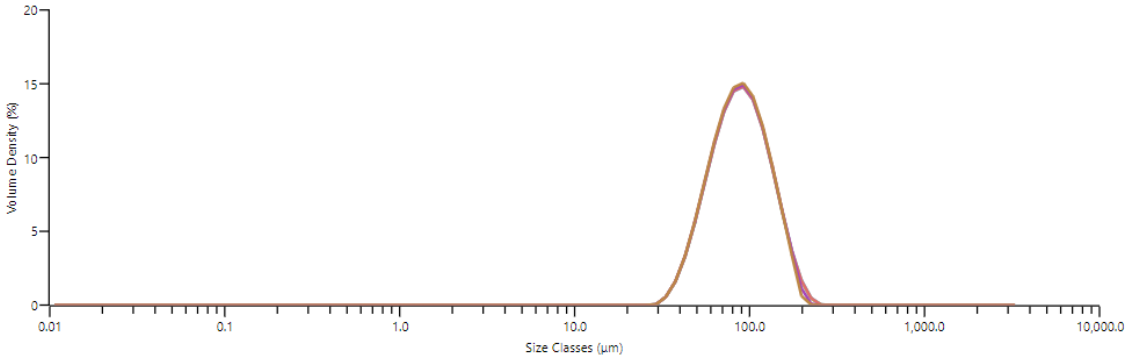

c).

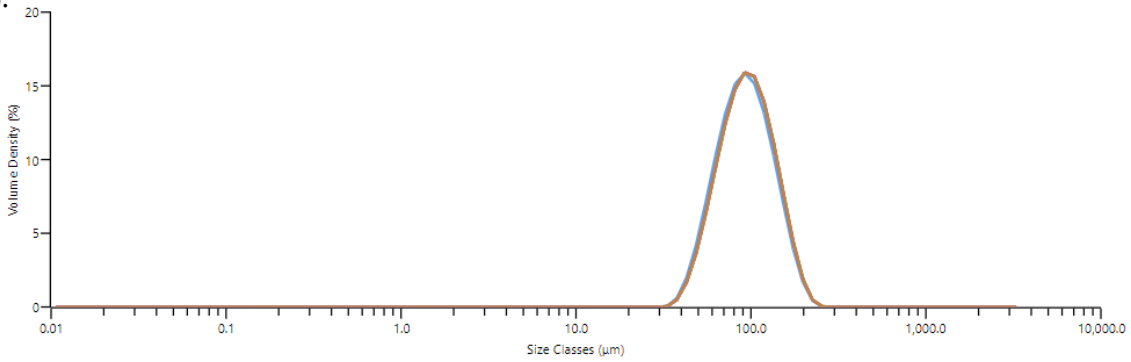

Figure 4-2. a) size distribution of Alloy 2. b) size distribution of Alloy 4. c) size distribution of Alloy 9.

Table 4-6. Size distribution values of randomly selected blended compositions.

	Alloy 2	Alloy 4	Alloy 9
D_{10}	59.0	52.8	57.1
D_{50}	91.5	88.1	91.8
D_{90}	139	144	146

4.4 Manufacturing Test Specimens

Deposits representing 7 of the experimental alloys were printed on 6061 aluminum plates for producing material for testing. The composition of the 6061 plate is displayed in Table 4-7.

Table 4-7. Composition of 6061 aluminum

	Al	Cr	Cu	Fe	Mg	Mn	Si	Ti	Zn
wt %	95.8 – 98.6	0.04 – 0.35	0.15 – 0.4	Max 0.7	0.8 – 1.2	Max 0.15	0.4 – 0.8	Max 0.15	Max 0.25

Experimental builds were manufactured using a High Power High Deposition (HPHD) laser deposition system at the Center for Innovative Materials Processing through Direct Digital Deposition, and are displayed in Figure 4-3. Argon assist gas was used for powder delivery.

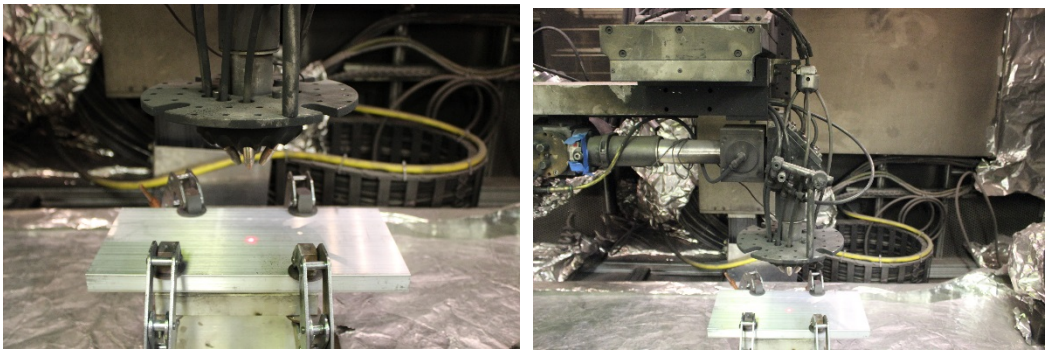

Figure 4-3. HPHD set up with 6010 base plate.

A test run of a six deposition track wide by two deposition track high was made to examine the deposit to confirm parameters to minimize lack of fusion defects. The result of this initial experiment is shown in Figure 4-4(a). Processing parameters for this run are displayed in Table 4-8.

Table 4-8. Processing parameters for HPHD machine test run using experimental alloy 1.

Run #	Powder Feeder Voltage Setting	Powder Feed Vibrate	Powder Feed Flow Rate (mm)	Nozzle Diameter (mm)	Spot Size (mm)	Focus Head Standoff (mm)	Step Over (in.)	Oxygen level	Notes
1	5	90	15	2	~ 3.5	10	0.1	10,000	1 pass
2	5	90	15	2	~ 3.5	10	0.1	10,000	1 pass
3	5	90	15	2	~ 3.5	10	0.1	10,000	6 pass, 2 layers

The test deposit was sectioned, polished, and etched to view the deposit and confirmed compatibility of the base plate material with the experimental material, as well as defined the hatch spacing of the deposition tracks. The multiple deposits were shown to be sufficiently overlapped and fully fused, which is illustrated in Figure 4-4(b).

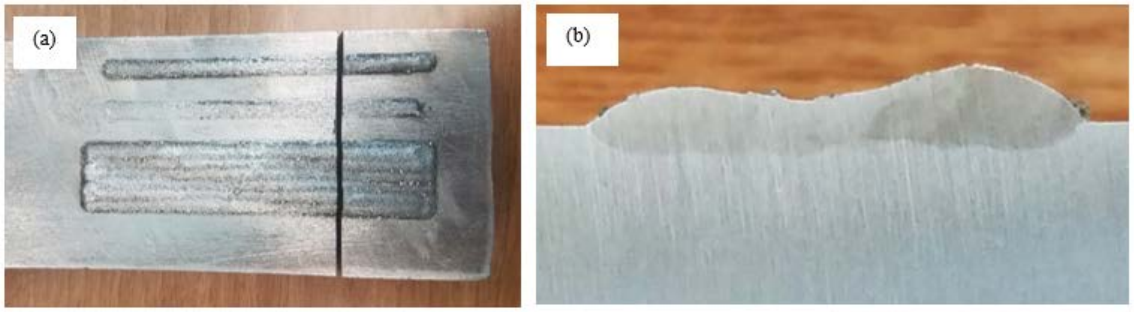

Figure 4-4. (a) test run deposition tracks (b) weld pool fusion.

Experimental material was used to build a 100mm by 100mm by 19mm wall from each alloy, displayed in Figure 4-5. The processing parameters used to produce deposition material, as well as comments are displayed in Table 4-9. Alloys 1 through 7 were printed successfully, however alloys 8 and 9 were excluded due to ruined powder. With the HPHD machine being located in a lab with no temperature control, humid weather conditions caused powder to clump and subsequently clog the powder feeder and cause porosity in the builds.

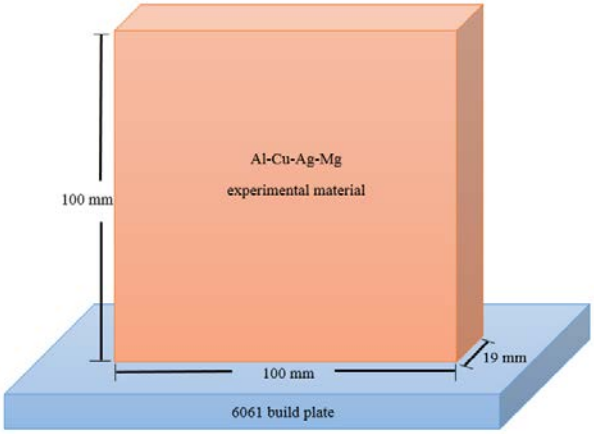

Figure 4-5. Dimensions of experimental builds.

Table 4-9. Processing parameters for HPHD machine for each experimental alloy build.

Alloy #	Powder Feeder Voltage Setting	Powder Feed Vibrate	Powder Feed Flow Rate (mm)	Nozzle Diameter (mm)	Spot Size (mm)	Focus Head Standoff (mm)	Step Over (mm)	Oxygen level (ppm)
1	5	90	15	2	~ 3.5	10	2.54	1,000
	Comments:	6 pass, after 6 layers raised power to 3000 watts, build to 4" H.						
2	5	90	15	2	~ 3.5	10	2.54	1,000
	Comments:	6 pass, stop at .6" H, feeder getting plugged up, increase powder feeder voltage and powder feed flow rate.						
	7	90	30	2	~ 3.5	10	2.54	1,000
	Comments:	Finish build to 4" H.						

3	7	90	50	2	~ 3.5	10	2.54	1,000
Comments:		6 pass, build to 4" H.						
4	7	90	50	2	~ 3.5	10	2.54	1,000
Comments:		6 pass, build to 4" H.						
5	7	90	50	2	~ 3.5	10	2.54	1,000
Comments:		6 pass, build to 4" H.						
6	7	90	50	2	~ 3.5	10	2.54	1,000
Comments:		6 pass. stopped at .41" H to grind surface flat, dirty mirror cleaned, finished building to 4" H						
7	7	90	50	2	~ 3.5	10	2.54	1,000
Comments:		6 pass, build to 4" H. stopped powder keeps plugging up.						

Each experimental build was then sectioned in half. Side A was utilized for heat treatment specimens and chemistry specimens. Side A was further sectioned to produce four slices: Slice 2 was allocated for as-built aging and Slice 3 was allocated for solution heat treatment and aging. Slices 1 and 4 were set aside as extras. Side B was retained for mechanical properties and metallography.

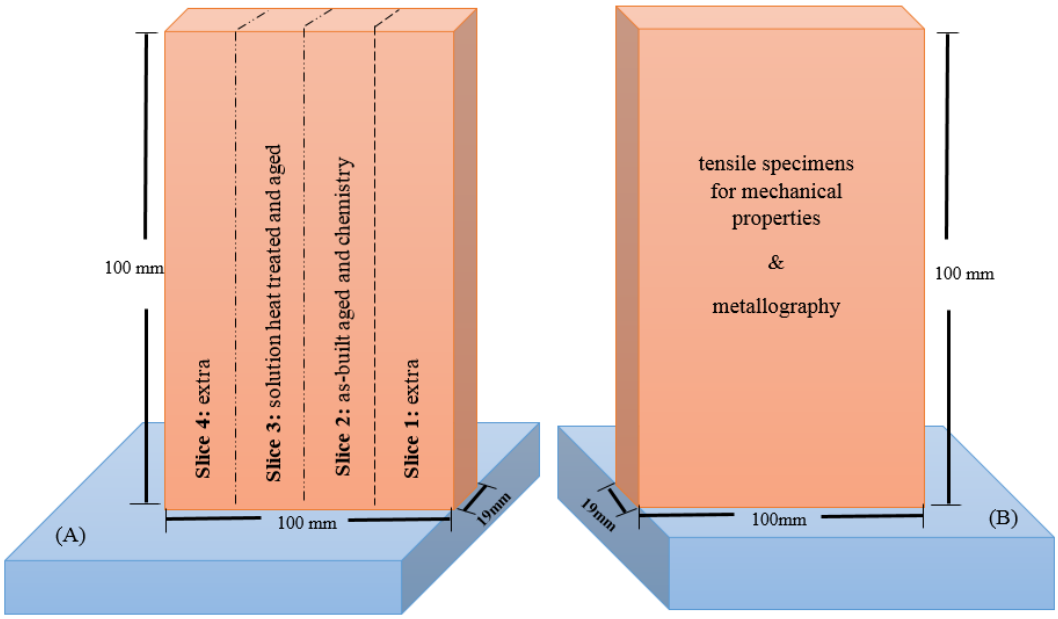

Figure 4-6. Build sectioning and allocation for aging specimens and tensile specimens.

4.5 Aging

Samples for aging were drilled for inserting a stainless steel wire for fixturing within the furnace, as shown in Figure 4-7. One set of samples from each build were aged from the as-built condition and another set of samples from each build were solution treated and aged. Figure 4-8 displays the set-up for solution heat treatment of Slice 3 from each build.

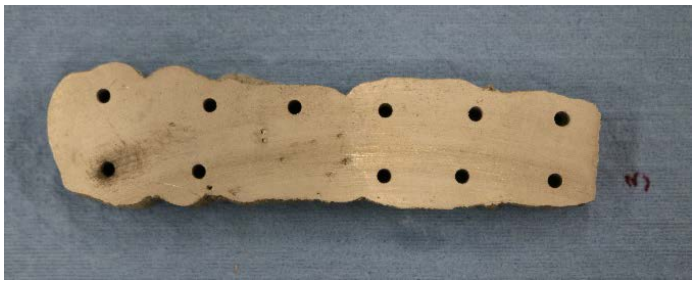

Figure 4-7. Holes drilled in samples for holding during heat treatment.

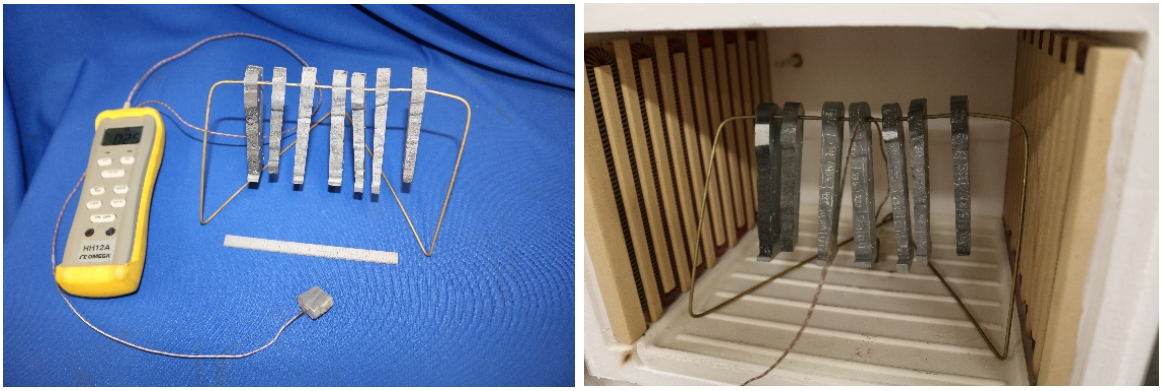

Figure 4-8. Experimental set-up for solution heat treatment of Slice 3 of each alloy.

Samples were sectioned for aging experiments as shown in Figure 4-9. Samples were randomly selected for aging duration from locations 1 through 12, excluding location 5 in all cases. Sample 5 from Slice 2 of each build was used to determine build composition. Table 4-10 displays the sample designations of randomly chosen samples

for each aging duration. Each sample was labeled with a 3-digit designation, with the first number representing the alloy, the second number representing the slice number, and the third number representing the piece number. Figure 4-10 shows the set-up for aging experiments.

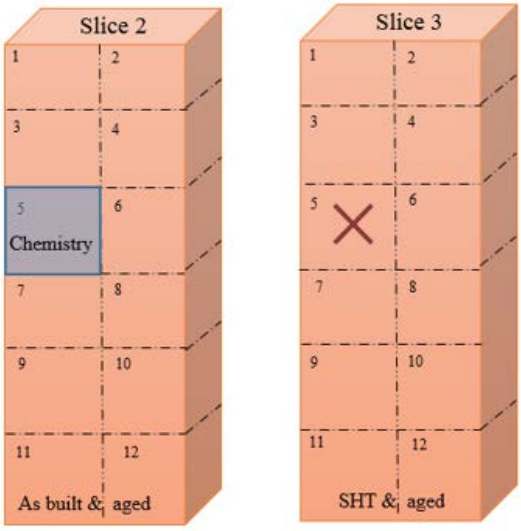

Figure 4-9. Aging sample sectioning and labeling.

Table 4-10. Aging sample designations.

As Built Sample Designation							
hours	**Alloy 1**	**Alloy 2**	**Alloy 3**	**Alloy 4**	**Alloy 5**	**Alloy 6**	**Alloy 7**
0	128	229	323	421	529	626	724
2	124	226	328	423	521	629	726
4	1210	2210	3211	4212	5210	6212	7210
8	127	2211	324	427	527	628	728
12	129	227	326	4210	524	6211	722
16	122	221	3212	4211	523	6210	727
20	123	224	3210	422	528	621	729
24	126	228	327	426	522	623	7212
28	1212	223	329	424	526	624	7211

Solution Heat Treated Sample Designation							
hours	**Alloy 1**	**Alloy 2**	**Alloy 3**	**Alloy 4**	**Alloy 5**	**Alloy 6**	**Alloy 7**
0	133	238	336	437	531	6311	732
2	139	2312	334	439	537	631	734
4	1310	2311	3312	433	536	637	739
8	131	2310	3311	438	539	6312	7310
12	132	237	3310	436	5312	632	7311
16	1311	231	337	4312	532	634	7312
20	134	233	333	434	533	6310	737
24	1312	232	338	4310	538	639	736
28	138	239	331	4311	5311	638	731

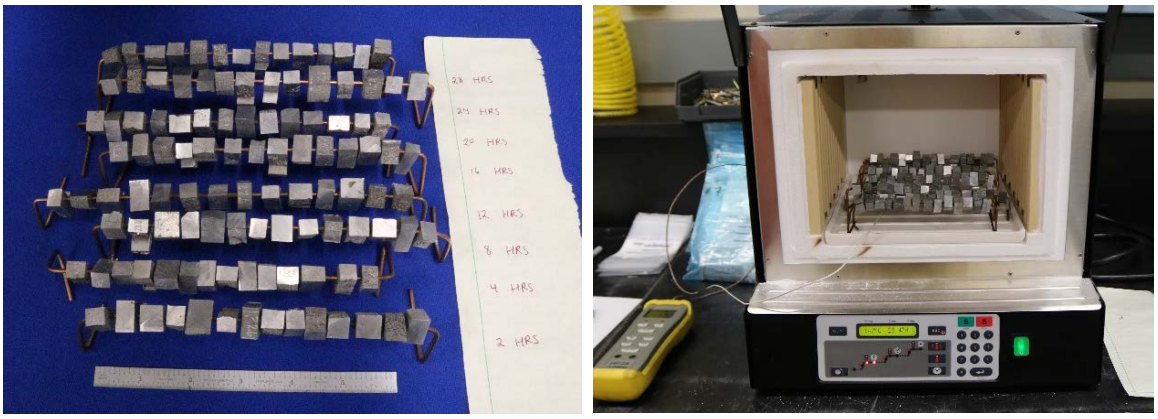

Figure 4-10. Experimental set-up for aging experiments.

Samples were solution treated at 510°C for 1 hour and 15 minutes and immediately quenched in cold water. Samples were then aged at 160°C for durations of 2, 4, 8, 12, 16, 20, 24, and 28 hours. Figure 4-11 displays the solution heat treatment heating curve and Figure 4-12 displays the aging heating curve.

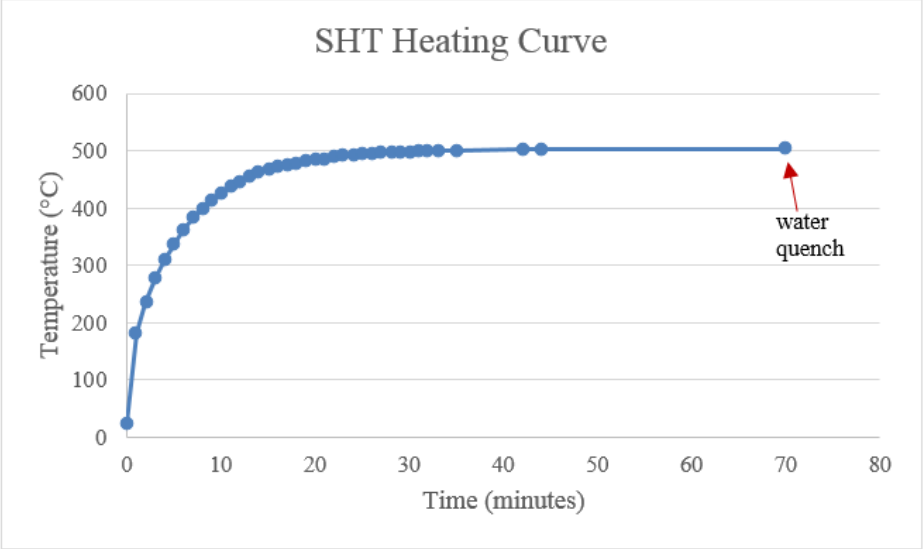

Figure 4-11. Solution heat treatment heating curve.

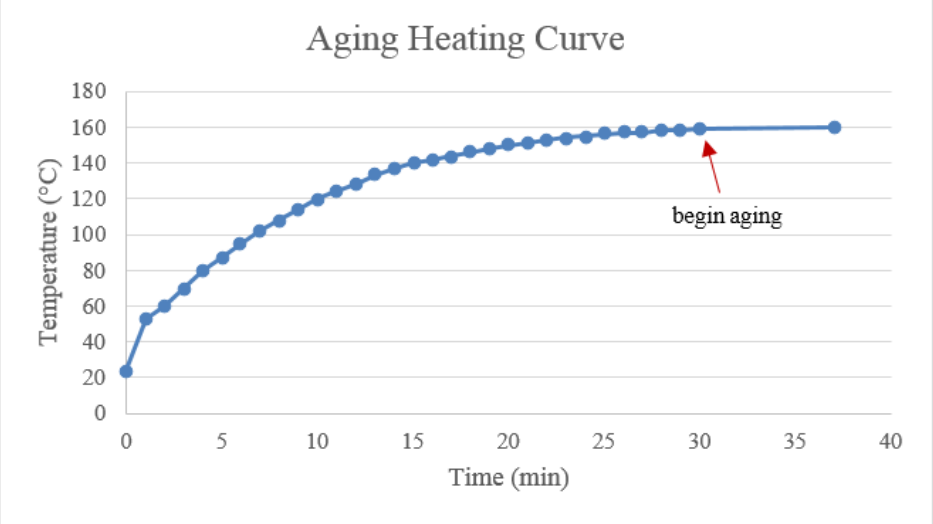

Figure 4-12. Aging heating curve.

4.6 Hardness and Mechanical Properties

Vickers hardness measurements were taken on a LECO hardness indenter. Each sample was tested for hardness 10 times. From this data, an alloy composition was identified for further testing of mechanical properties at the peak age condition. The alloy showing the highest hardness values after solution heat treatment and aging with the most consistent aging curve was chosen for mechanical testing, which was identified as Alloy 1. After choosing Alloy 1 for extensive characterization, specimens were sectioned as shown in Figure 4-13 for x-direction tensile bars, z-direction tensile bars, and metallography.

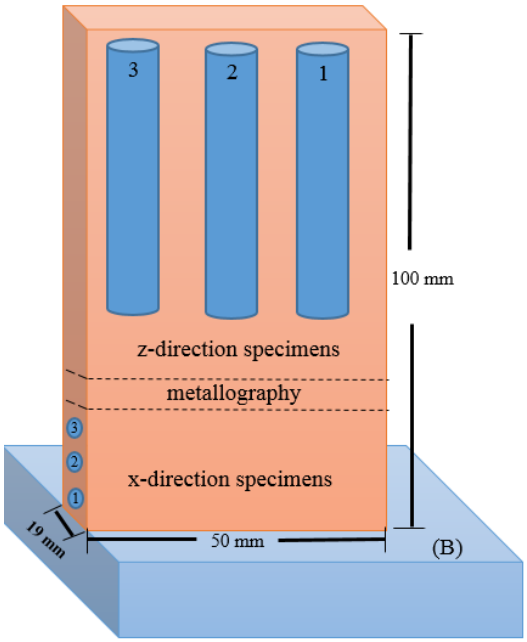

Figure 4-13. Tensile specimen designations.

Specimens were solution heat treated at 510°C, water quenched, and aged at 160°C for 20 hours, the peak age condition for alloy 1. Figures 4-14 and 4-15 display the heating curves for this solution treatment and age.

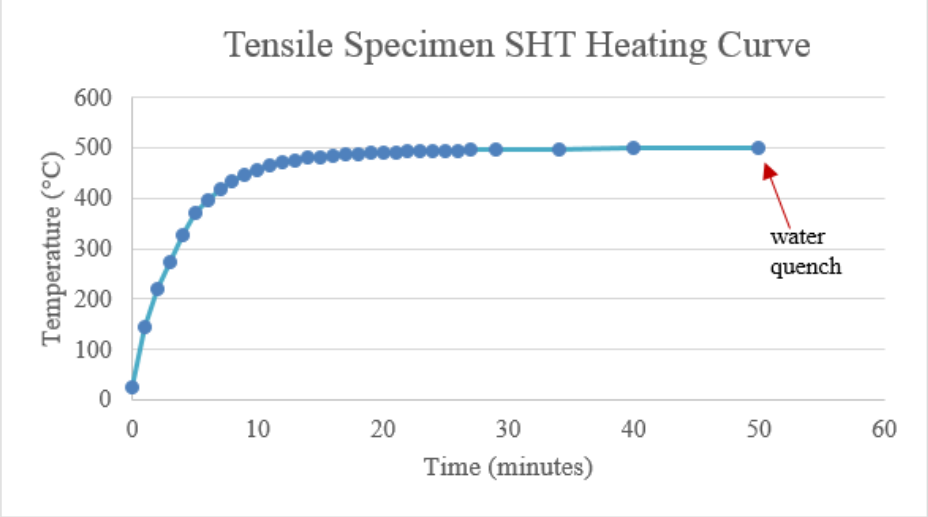

Figure 4-14. Tensile specimen solution heat treatment heating curve.

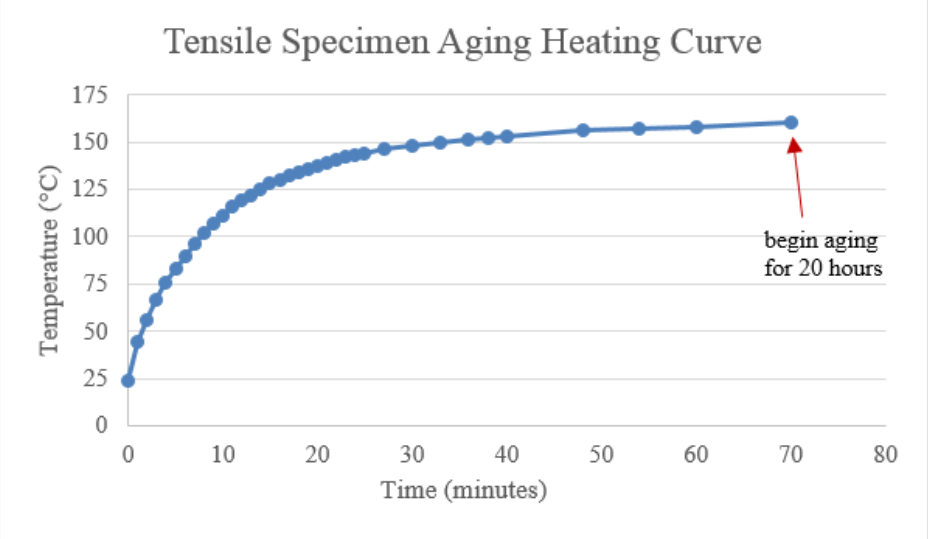

Figure 4-15. Tensile specimen aging heating curve.

Sections for tensile specimens were then forwarded to Westmoreland Mechanical Testing for mechanical properties testing using the ASTM E8 standard for tension testing of metallic materials. The exact specimen dimensions represented a gauge length of 16.0mm ± 0.1mm and a diameter within the gauge length of 4.0mm ± 0.1mm. These

dimensions are defined in ASTM E8 as a sub-size, round specimen where the gauge length is four times the diameter.

4.7 Metallography

Samples of Alloy 1 at the peak-age condition (solution treated and aged 20 hours) were cold mounted to avoid any additional heating. Samples were etched in Keller's reagent and viewed using optical microscopy. These samples were then coated in iridium and imaged using scanning electron microscopy. An additional sample of Alloy 1 at the peak age condition was fabricated for transmission electron microscopy using a focused ion beam. Optical micrographs were taken on a Nikon Epiphot inverted metallurgical microscope. SEM images were taken on the Quanta 250 SEM, and TEM images were taken using a FEI Talos F2000x.

Chapter 5

RESULTS AND DISCUSSION

5.1 Build Integrity

To understand the effect of alloy composition on the producibility of the additive manufacturing process, chemistry and build characteristics were analyzed.

5.1.1 Chemistry

Chemistry samples were sent to Westmoreland Mechanical Testing for chemical analysis by inductively coupled plasma (ICP) testing and were tested for Cu, Ag, Mg, Zr, and Ti content. The contents of each alloy are displayed in Table 5-1.

Table 5-1. Chemical analysis of each blended experimental alloy.

Alloy #	Target Compositions	Tested Compositions (wt %)				
		Cu	Ag	Mg	Zr	Ti
Alloy 1	Al-6Cu-2Ag-0.28Mg-0.28Ti-0.20Zr	4.91	1.39	0.20	0.20	0.29
Alloy 2	Al-6Cu-3Ag-0.28Mg-0.28Ti-0.20Zr	4.87	2.34	0.19	0.21	0.28
Alloy 3	Al-6Cu-4Ag-0.28Mg-0.28Ti-0.20Zr	4.44	2.64	0.21	0.21	0.28
Alloy 4	Al-7Cu-2Ag-0.28Mg-0.28Ti-0.20Zr	5.43	1.48	0.23	0.22	0.29
Alloy 5	Al-7Cu-3Ag-0.28Mg-0.28Ti-0.20Zr	5.46	2.19	0.19	0.21	0.28
Alloy 6	Al-7Cu-4Ag-0.28Mg-0.28Ti-0.20Zr	6.64	3.40	0.21	0.20	0.26
Alloy 7	Al-8Cu-2Ag-0.27Mg-0.26Ti-0.19Zr	7.74	1.87	0.21	0.22	0.29

Because these alloys were blended from elemental powders, it is possible that uneven composition distributions and local compositions could exist within the builds. While Alloys 1, 2, and 3 were all designed to contain a copper content of 6 wt% Cu, they all

exhibited lower amounts, with Alloy 1 possessing 4.91 wt% Cu, Alloy 2 possessing 4.87 wt% Cu, and Alloy 3 possessing 4.44 wt% Cu. The silver content for Alloys 1, 2, and 3 also tested low, with expected contents being 2 wt% Ag, 3 wt% Ag, and 4 wt% Ag, respectively, and tested contents being 1.39 wt% Ag, 2.34 wt% Ag, and 2.64 wt% Ag, respectively. The amount of Mg, Zr, and Ti for Alloys 1, 2, and 3 are fairly close to the expected values and are relatively consistent for all seven alloys.

In Alloys 4, 5, and 6, a copper content of 7 wt% Cu was expected. These alloys also tested low, with Alloy 4 containing 5.43 wt% Cu, Alloy 5 containing 5.46 wt% Cu, and Alloy 6 containing 6.64 wt% Cu. While Alloys 4 and 5 contain similar content of about 5.5 wt% Cu, Alloy 6 contains closer to 6.5 wt% Cu. In Alloys 4, 5, and 6 a silver content of 2 wt% Ag, 3 wt% Ag, and 4 wt% Ag, respectively, was expected. These contents tested to be 1.48 wt% Ag for Alloy 4, 2.19 wt% Ag for Alloy 5, and 3.40 wt% Ag for Alloy 6. The Mg, Zr, and Ti contents for these alloys were found to be fairly close to expected. Alloy 7 was anticipated to possess a copper content of 8 wt% Cu and 2 wt% Ag. This alloy tested to contain 7.74 wt% Cu and 1.87 wt% Ag, also with expected amounts of Mg, Ti, and Zr. This alloy composition proved to be fairly close to the desired composition. Because the levels of Mg, Zr, and Ti were relatively close to expected values for all compositions, and provided by the master alloy powder, it is speculated that the variance in Cu and Ag were due to non-uniform powder mixing.

5.1.2 Surface Quality and Cracking Observations

The High Power High Deposition (HPHD) is a laser-based directed energy deposition process that produces a near-net shape. This process typically requires post-process machining to reach final dimensions. While the surface quality of the parts produced from HPHD is not crucial to the integrity of the build, it can provide information about the quality of the material and its reaction to laser processing. Figures 5-1 through 5-7 show the front, back, and side vide of each experimental build, as well as the deposit-baseplate interface and a cross-section of the build.

In Alloy 1 (Al-4.91Cu-1.39Ag-0.20Mg-0.20Zr-0.29Ti, based on chemical analysis of the build), small, circular powder balls were formed on the surface of the deposit during the first few layers. On the middle layers, agglomeration stopped and a moderately smooth finish was seen, although it contained loose, dusty powder on the surface. As the build reached a higher height, it began to sag and melt over the edges due to the amount of heat being transferred to the material. This can be seen in Figures 5-1(a), 5-1(b), and 5-1(c). Figure 5-1(d) shows the deposit-baseplate interface. A fully fused deposit is seen with no cracking at the baseplate. A fully fused material is also seen in Figure 5-1(e) where the deposit meets the baseplate. A single pore was observed on the cross-section of the build, circled in red in Figure 5-1(e).

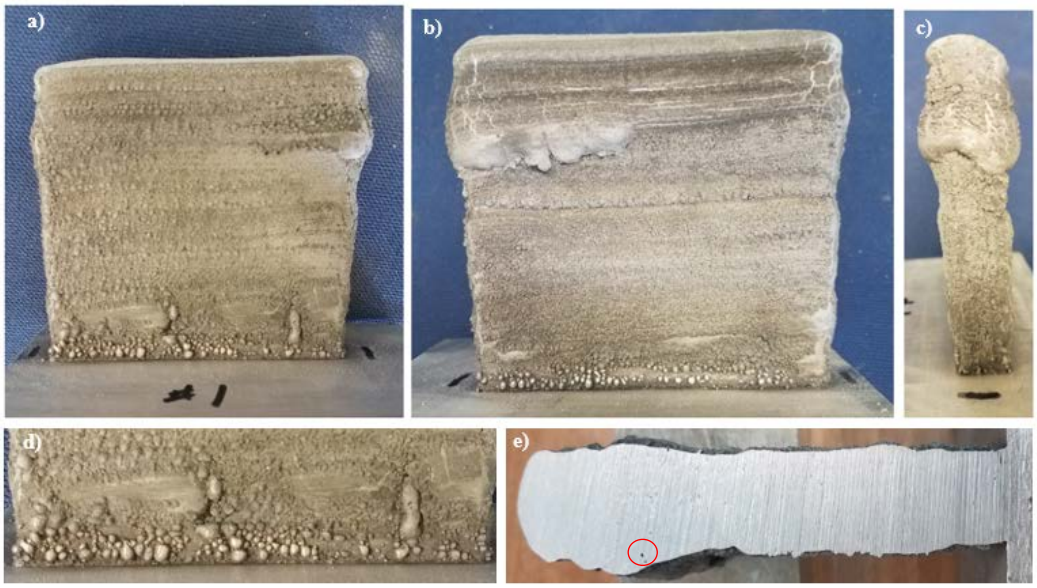

Figure 5-1. Alloy 1 surface finish from: a) front view. b) back view. c) side view. d) build-baseplate interface. e) cross-section.

In Alloy 2 (Al-4.87Cu-2.34Ag-0.19Mg-0.21Zr-0.28Ti), the deposit-baseplate interface formed large, agglomerated powder particles on the first 25mm of deposit layers, as also seen in build 1. After the first 25mm, agglomerating stopped and the surface appeared smooth, although it contained dusty powder on the surface. This alloy displayed a minimal amount of sagging in the top layers, as seen in Figure 5-2(a), (b), and (c). Cracks were observed at the corners of the deposit on the baseplate and are shown circled in red in Figure 5-2(d). A fully fused material was observed in the cross-section of the deposit-baseplate interface, shown in Figure 5-2(e); however, this alloy cracked off the baseplate during sectioning. Small, scattered pores were observed in the cross-section, displayed and circled in red in Figure 5-2(e).

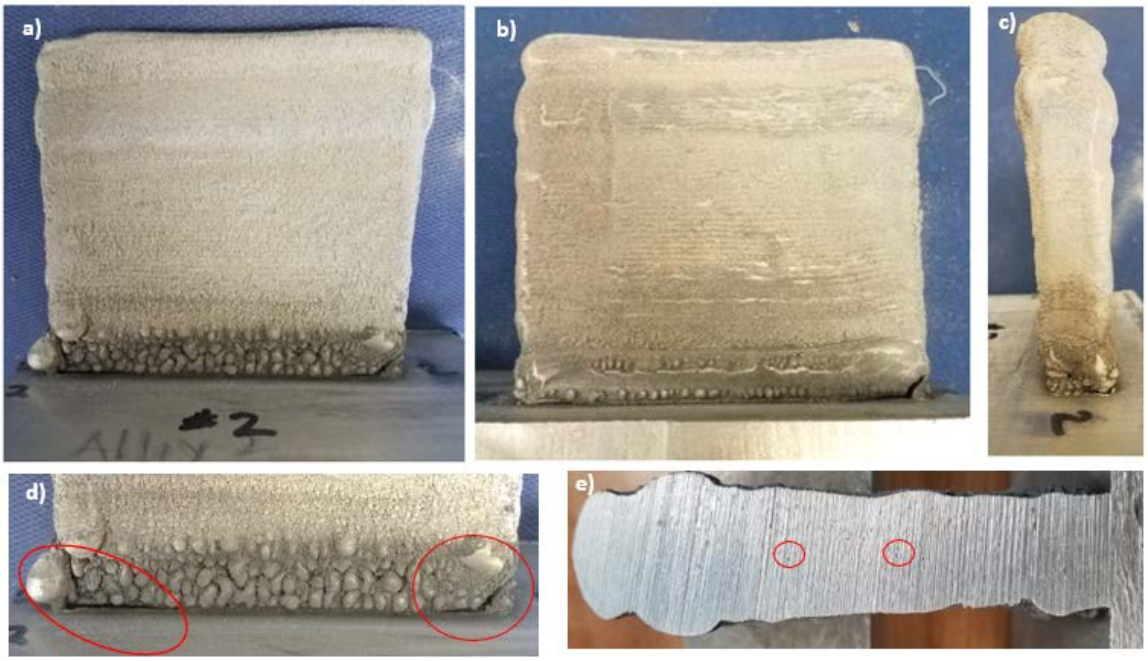

Figure 5-2. Alloy 2 surface finish from: a) front view. b) back view. c) side view. d) build-baseplate interface. e) cross-section.

In Alloy 3 (4.44Cu-2.64Ag-0.21Mg-0.21Zr-0.28Ti), minimum power agglomeration was observed in initial layers. Additionally, the surface finish was observed to be much smoother than Alloys 1 and 2, while it also contained less dusty powder on the surface. This build displayed some sagging throughout the build, but it also displays crevices in the build direction (z-direction), shown in Figure 5-3(a). This alloy also displayed cracking at the baseplate, seen in Figure 5-3(d). Like alloy 2, this alloy broke off the baseplate during sectioning. This alloy contained more pores, large and small, than the first two build and can be seen circled in red in Figure 5-3 (e).

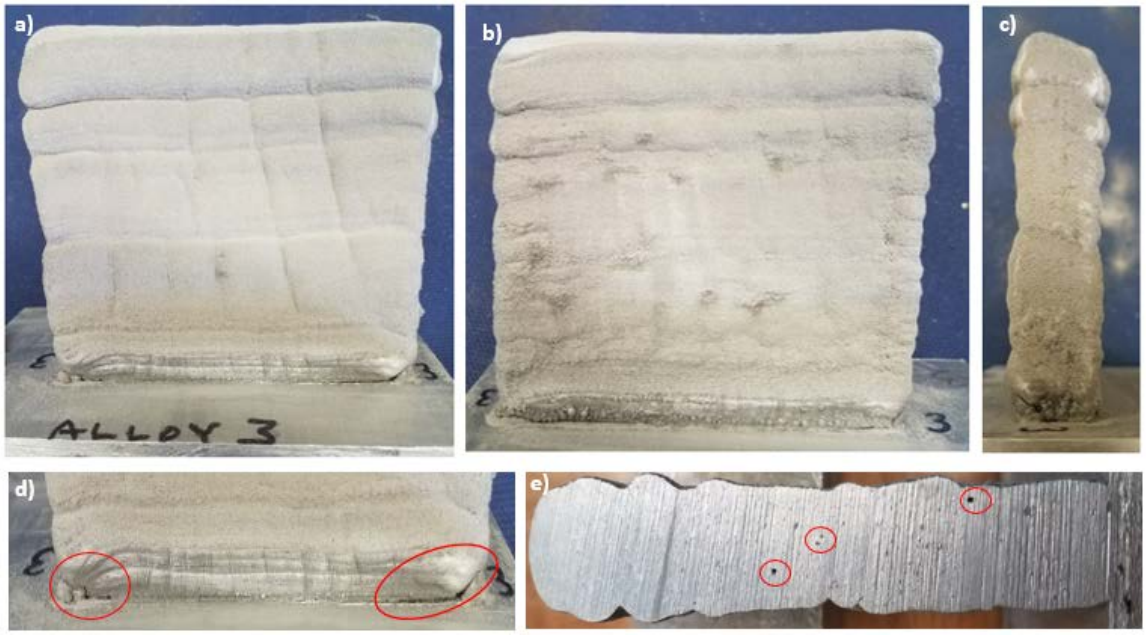

Figure 5-3. Alloy 3 surface finish from: a) front view. b) back view. c) side view. d) build-baseplate interface. e) cross-section.

In Alloy 4 (Al-5.43Cu-1.48Ag-0.23Mg-0.22Zr-0.29Ti), a small amount of material agglomeration was seen at the deposit-baseplate interface. This alloy possessed a smooth surface finish along with minimal sagging and crevices, which can be seen in Figures 5-4(a), (b) and (c). This alloy showed a small crack at the baseplate, shown in Figure 5-4(d). It should be noted that this material contains more Mg than any other alloy, which may provide a reason for cracking. It also displays even more pores than the first three builds, seen in Figure 5-4(e), but that may be expected since prior to processing the powder was stored in a laboratory under relatively humid conditions. This long resident time prior to processing was longer than the previous builds.

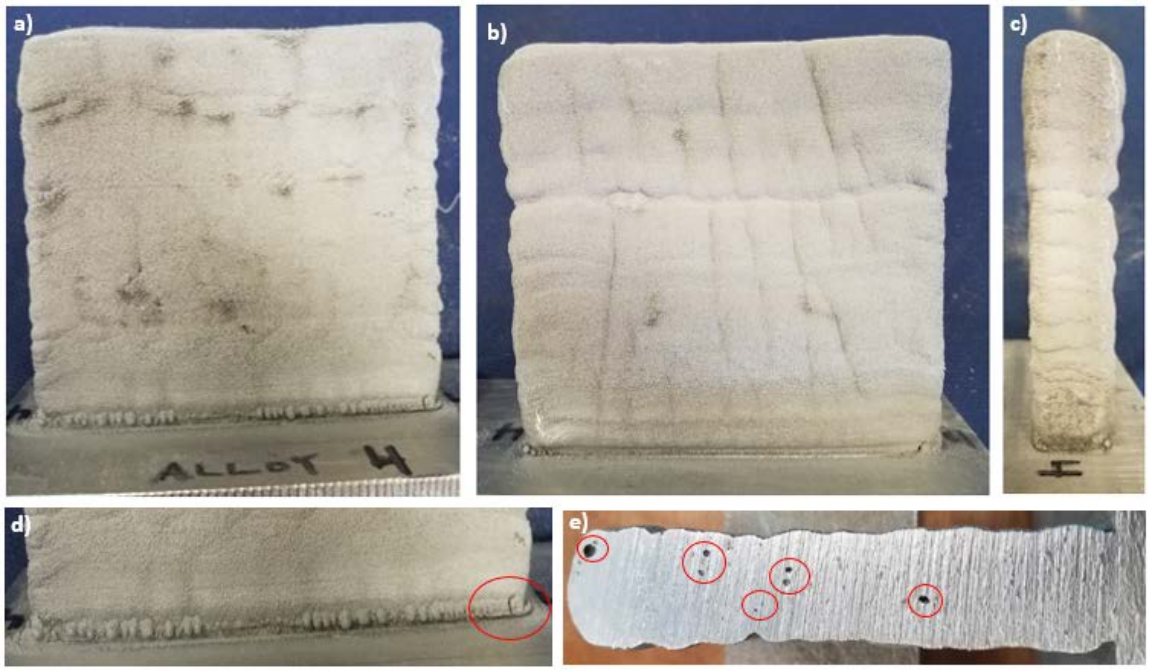

Figure 5-4. Alloy 4 surface finish from: a) front view. b) back view. c) side view. d) build-baseplate interface. e) cross-section.

In Alloy 5 (Al-5.46Cu-2.19Ag-0.19Mg-0.21Zr-0.28Ti), the deposit-baseplate interface is observed to be clean of any powder globbing or buildup, along with no cracking. This material possesses the lowest magnesium content of 0.19 wt% Mg. This alloy possesses a smooth surface finish, but it also shows sagging and vertical crevices, shown in Figures 5-5(a), (b), and (c). It maintains a fairly even thickness throughout the build. Pores were seen in the cross-section as expected.

In Alloy 6 (Al-6.64Cu-3.40Ag-0.21Mg-0.20Zr-0.26Ti), no significant clumping material or cracking was seen at the deposit-baseplate interface. The surface finish of this alloy was observed to be smooth; however, the vertical crevices appeared deep and the top of the deposit started to sag and widen, seen in Figures 5-6(a), (b), and (c). Similarly to all other builds, pores were found scattered throughout the cross-section, shown in Figure 5-6(e).

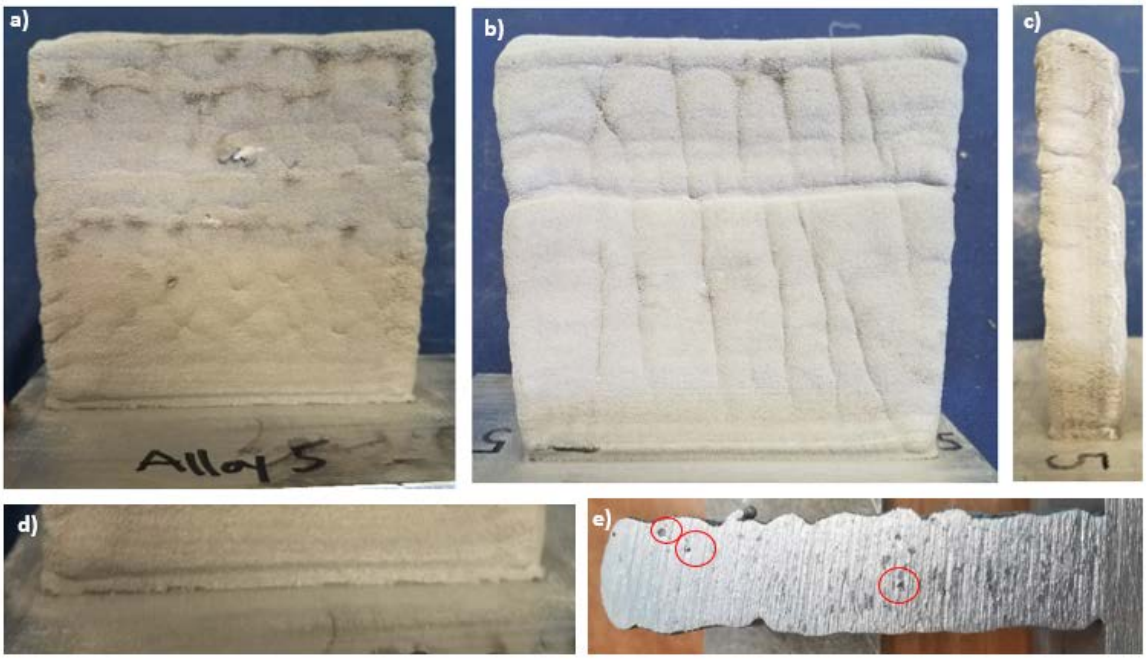

Figure 5-5. Alloy 5 surface finish from: a) front view. b) back view. c) side view. d) build-baseplate interface. e) cross-section.

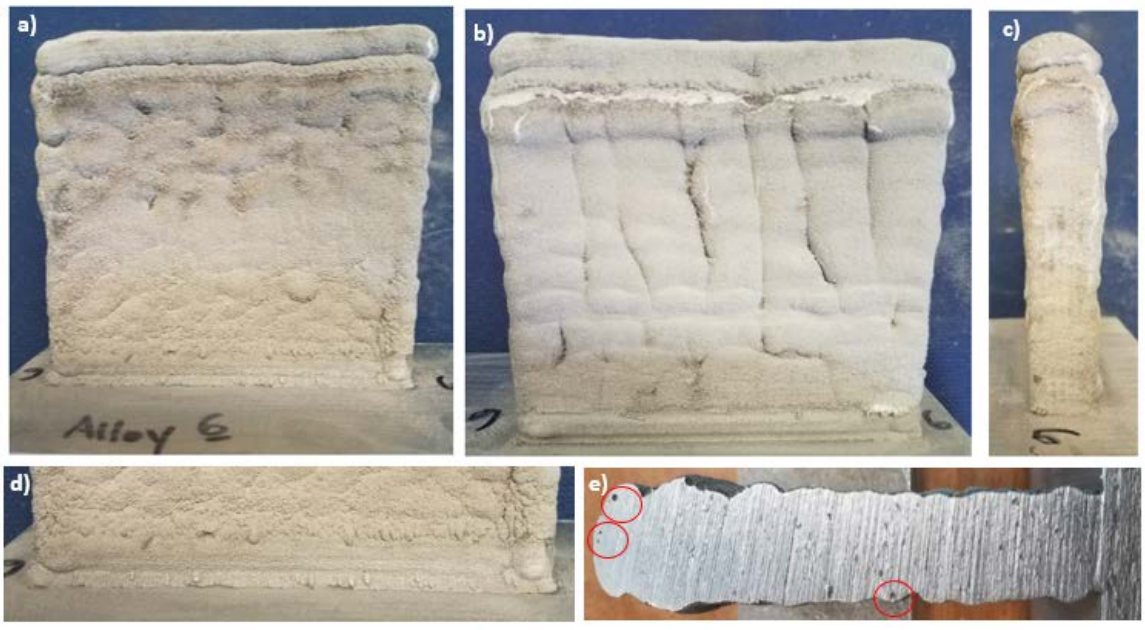

Figure 5-6. Alloy 6 surface finish from: a) front view. b) back view. c) side view. d) build-baseplate interface. e) cross-section.

In Alloy 7 (Al-7.74Cu-1.87Ag-0.21Mg-0.22Zr-0.29Ti), the deposit-baseplate interface appeared to be very smooth with no indication of cracks, shown in Figure 5-7(d). The surface appearance of the build was smooth while containing minimal crevices and sagging in the width, but there was a steep sag on the top of the build, as seen in Figure 5-7 (a), (b), and (c). A fully fuse cross-section is seen in Figure 5-7(e), as well as a few pores.

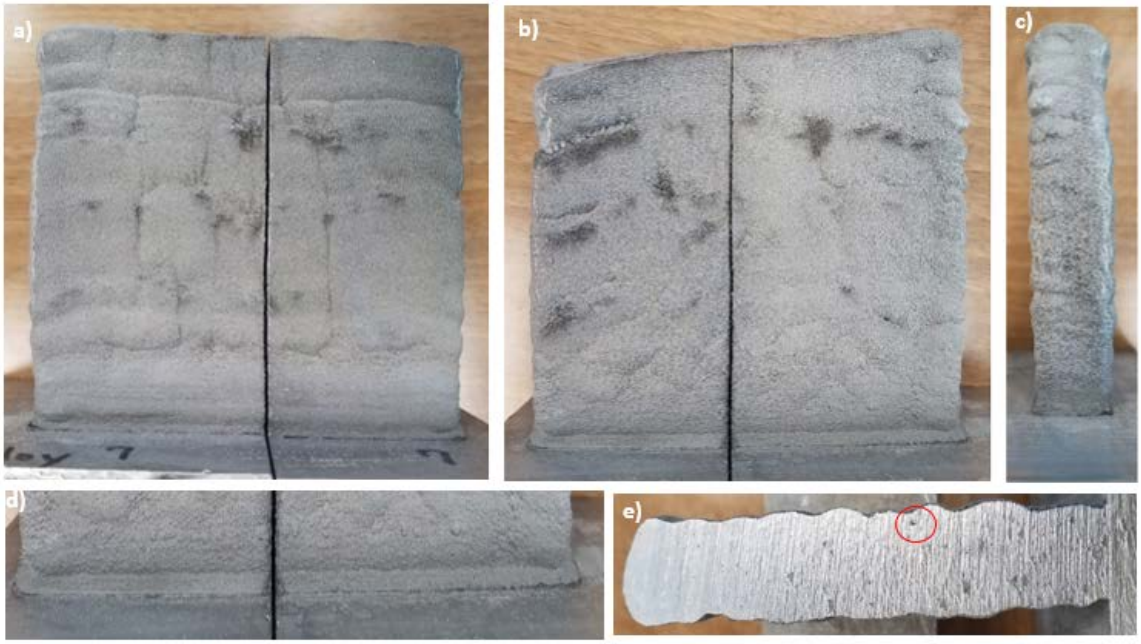

Figure 5-7. Alloy 7 surface finish from: a) front view. b) back view. c) side view. d) build-baseplate interface. e) cross-section.

5.2 Mechanical Properties

5.2.1 Vickers Hardness

Vickers hardness measurements of each alloy were taken after aging in the as-built condition as well as in the solution heat treated condition. Hardness was tested after aging for durations of 2 hours, 4 hours, 8 hours, 12 hours, 16 hours, 20 hours, 24 hours,

and 28 hours in order to obtain full aging curves of the alloy for identification of the peak aged condition. Hardness values for all alloys show promising results for an advanced aluminum alloy, with every alloy exceeding the hardness of Al-10Si-0.5Mg (100 VHN) after aging either in the as-built condition or in the solution treated condition. Hardness values of each alloy after aging in the as-built condition are shown in Table 5-2, while hardness values of each after the solution heat treated and aged condition are shown in Table 5-3. The compositions for the alloys in the table, as well as with all further discussions, utilized the measured compositions of the builds.

Table 5-2. Average Vickers hardness measurements of as-built aged samples.

Hardness of As-Built Aged Samples									
	as built	**2h**	**4h**	**8h**	**12h**	**16h**	**20h**	**24h**	**28h**
Alloy 1 (Al-4.91Cu-1.39Ag-0.20Mg)	74.99	107.11	77.21	88.88	83.13	103.00	110.25	97.28	76.14
Alloy 2 (Al-4.87Cu-2.34Ag-0.19Mg)	83.48	111.38	113.13	100.39	114.75	146.38	147.50	112.88	127.75
Alloy 3 (Al-4.44Cu-2.64Ag-0.21Mg)	101.23	78.73	84.45	106.25	113.50	114.38	85.28	91.10	87.05
Alloy 4 (Al-5.43Cu-1.48Ag-0.23Mg)	124.38	134.00	104.38	115.38	123.75	109.63	160.63	128.50	139.63
Alloy 5 (Al-5.46Cu-2.19Ag-0.19Mg)	83.05	121.13	87.09	88.15	104.08	108.63	92.96	127.63	86.90
Alloy 6 (Al-6.64Cu-3.40Ag-0.21Mg)	118.00	103.05	95.60	108.25	96.45	108.38	165.50	150.38	144.00
Alloy 7 (Al-7.74Cu-1.87Ag-0.21Mg)	111.13	113.13	110.50	115.88	156.50	121.75	119.88	107.98	101.78
Note: all alloys have about 0.2 wt% Zr and 0.3 wt% Ti.									

Table 5-3. Average Vickers Hardness measurements of solution heat treated and aged samples.

Hardness of Solution Treated and Aged Samples									
	as SHT	**2h**	**4h**	**8h**	**12h**	**16h**	**20h**	**24h**	**28h**
Alloy 1 (Al-4.91Cu-1.39Ag-0.20Mg)	101.81	111.63	132.88	155.25	165.25	166.38	172.63	159.50	115.88
Alloy 2 (Al-4.87Cu-2.34Ag-0.19Mg)	97.53	90.86	85.35	130.00	155.63	162.75	163.88	155.88	150.13
Alloy 3 (Al-4.44Cu-2.64Ag-0.21Mg)	98.41	136.25	94.66	105.75	160.13	129.38	156.38	141.75	148.13
Alloy 4 (Al-5.43Cu-1.48Ag-0.23Mg)	94.24	119.00	140.50	141.00	148.13	107.26	156.38	142.25	107.89
Alloy 5 (Al-5.46Cu-2.19Ag-0.19Mg)	119.25	121.25	126.63	142.75	143.38	173.63	177.88	147.88	118.50
Alloy 6 (Al-6.64Cu-3.40Ag-0.21Mg)	99.78	141.88	137.75	102.51	182.13	186.50	164.25	153.25	146.50
Alloy 7 (Al-7.74Cu-1.87Ag-0.21Mg)	119.38	127.75	138.75	147.50	154.25	160.25	167.63	162.50	161.50
Note: all alloys have about 0.2 wt% Zr and 0.3 wt% Ti.									

Aging curves for all alloys in the as-built aged condition are displayed in Figure 5-8. The aging curves for all alloys in the solution heat treated and aged condition are displayed in Figure 5-9. While the curves for the as-built aged samples displayed a lower peak age hardness than the solution heat treated and aged samples, all peak age values for as-built samples were seen to surpass 100 VHN. All alloys in the solution heat treated and aged condition proved to achieve peak hardnesses between 150 VHN and 180 VHN.

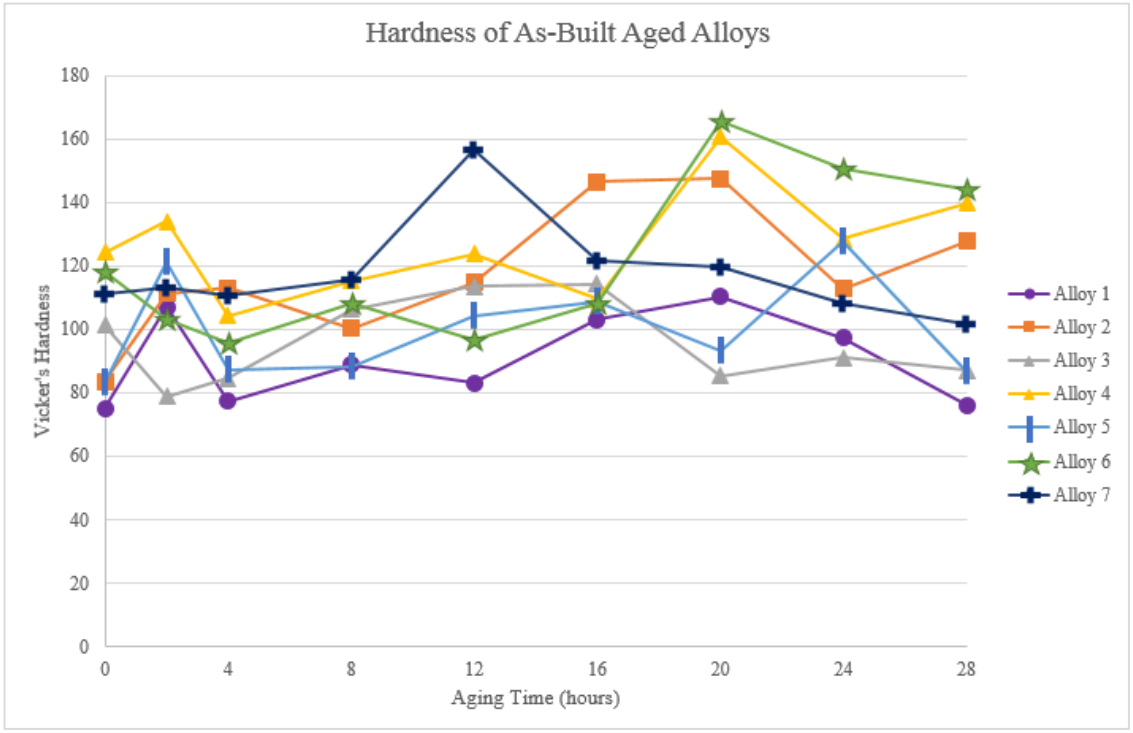

Figure 5-8. As-built aging curves for all alloys after aging at 160°C for 28 hours.

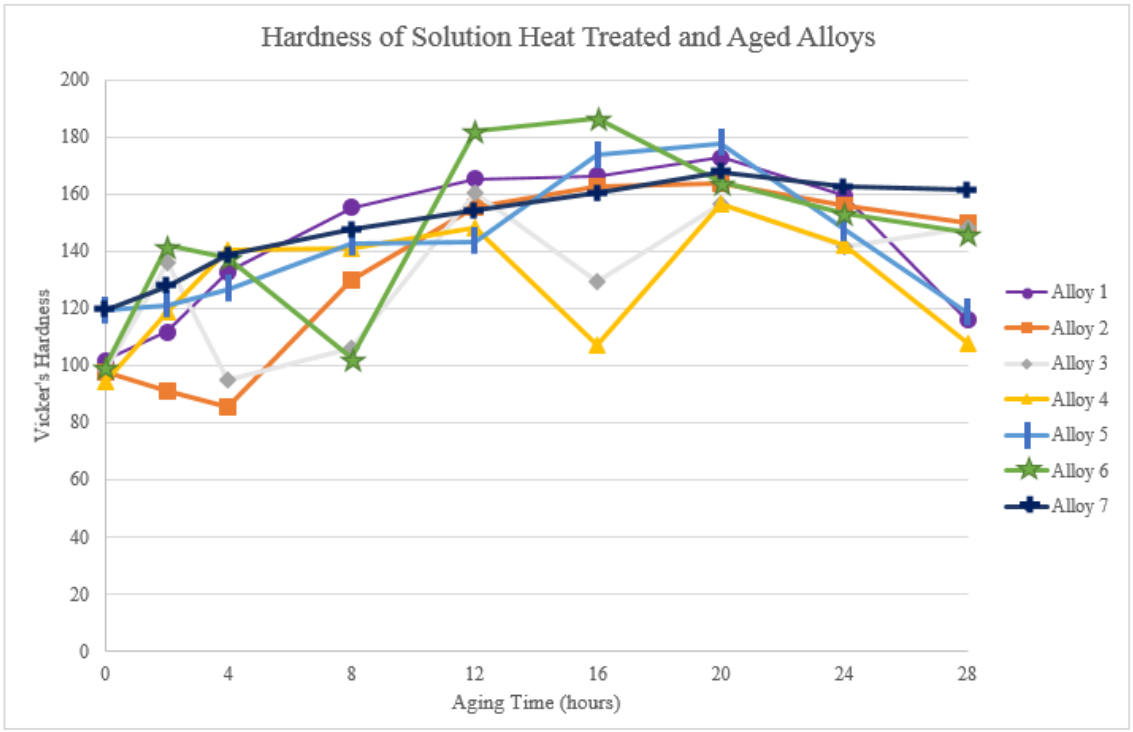

Figure 5-9. Solution heat treated aging curves for all alloys after aging at 160°C for 28 hours.

In both the as-built aged samples and the solution heat treated and aged samples, increases and decreases in hardness can be seen, which is uncharacteristic of a typical aging curve. It should be noted that these alloys were blended from elemental powder, which may have resulted in an uneven composition distribution and local concentrations. This could result in samples containing an uncharacteristic hardness measurement. Additionally, porosity below the surface of the sample could result in low hardness measurements. Aging curves for each individual alloy display error bars showing the standard deviation of each set of measurements.

Aging curves for Alloy 1 (Al-4.9Cu-1.4Ag-0.2Mg-0.2Zr-0.3Ti) proved to consistently increase in hardness until reaching the peak age condition at 20 hours for both the as-built aged condition and the solution heat treated and aged condition. The peak hardness of the solution heat treated and aged sample was 173 VHN, while the peak hardness of the as-built aged sample was 110 VHN. These aging curves are displayed in Figure 5-10. Because of the high hardness after aging and the consistent aging observed for this alloy was chosen for further characterization in the solution heat treated and peak aged condition and will be discussed in subsequent sections.

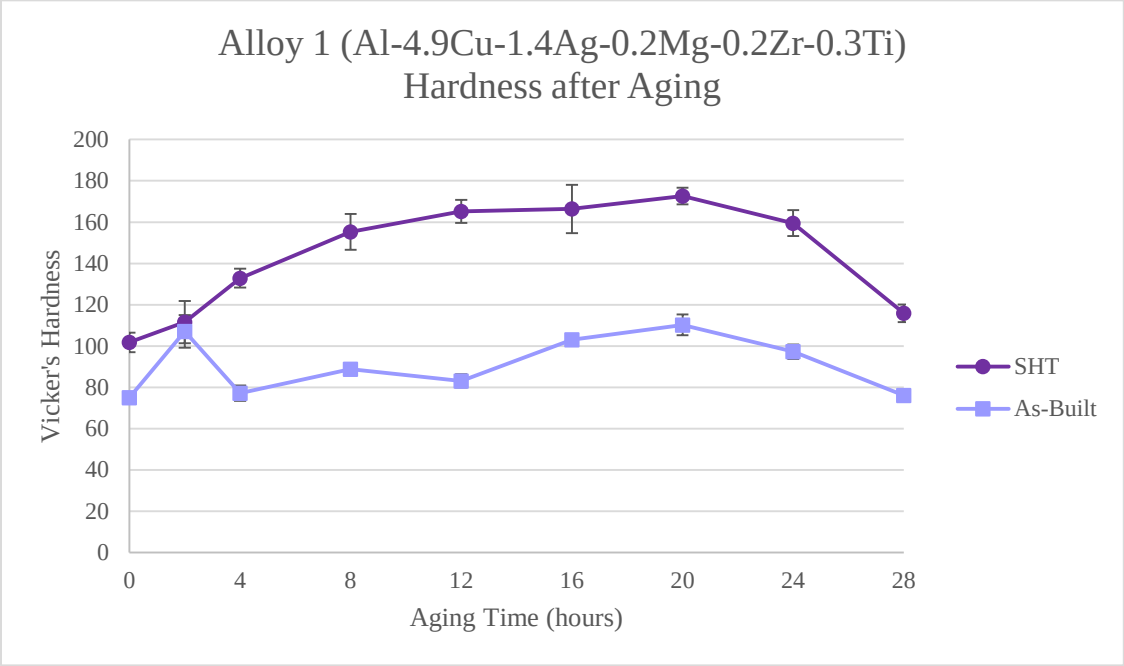

Figure 5-10. Aging curves for Alloy 1 after solution heat treatment at 510°C and aging at 160°C for 28 hours and after as-built aging at 160°C for 28 hours.

Aging curves for Alloy 2 (Al-4.9Cu-2.3Ag-0.2Mg-0.2Zr-0.3Ti) also showed promising results for aging in both the as-built condition and the solution heat treated and aged condition, with a peak age hardness value of 147 VHN and 164 VHN, respectively. The solution heat treated samples showed an initial decrease in hardness with a rapid increase, while the as-built samples exhibited a slight decrease in hardness prior to reaching the peak-aged condition, as seen in Figure 5-11. This alloy showed promising results based on hardness values; however, the deposit cracked at the baseplate interface and further broke off the baseplate completely during handling.

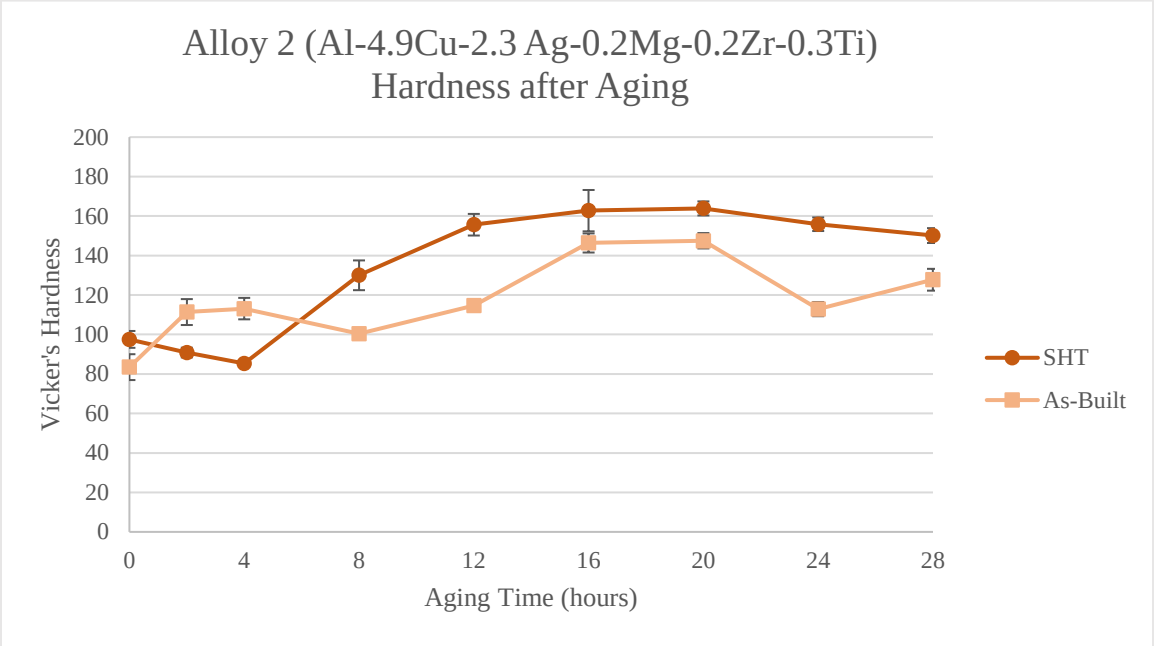

Figure 5-11. Aging curves for Alloy 2 after solution heat treatment at 510°C and aging at 160°C for 28 hours and after as-built aging at 160°C for 28 hours.

Aging curves for Alloy 3 (Al-4.4Cu-2.6Ag-0.2Mg-0.2Zr-0.3Ti) showed to be less consistent than the first two alloys in terms of displaying a smooth under-aged, peak-aged, and over-aged condition. The as-built hardness and the as-solution heat treated hardness for this alloy tested to be the same, 100 VHN. This alloy contained the lowest amount of copper out of all the alloys, with a high amount of silver. The as-built aged samples appeared to reach a peak hardness after 16 hours of aging. The solution heat treated and aged samples from this alloy show multiple peaks and troughs, with the peak age condition being unclear, but still achieving a hardness of 160 VHN after 12 and 20 hours of aging. These curves can be seen in Figure 5-12. This material also cracked at the edges of the deposit-baseplate interface and further broke off the baseplate during handling.

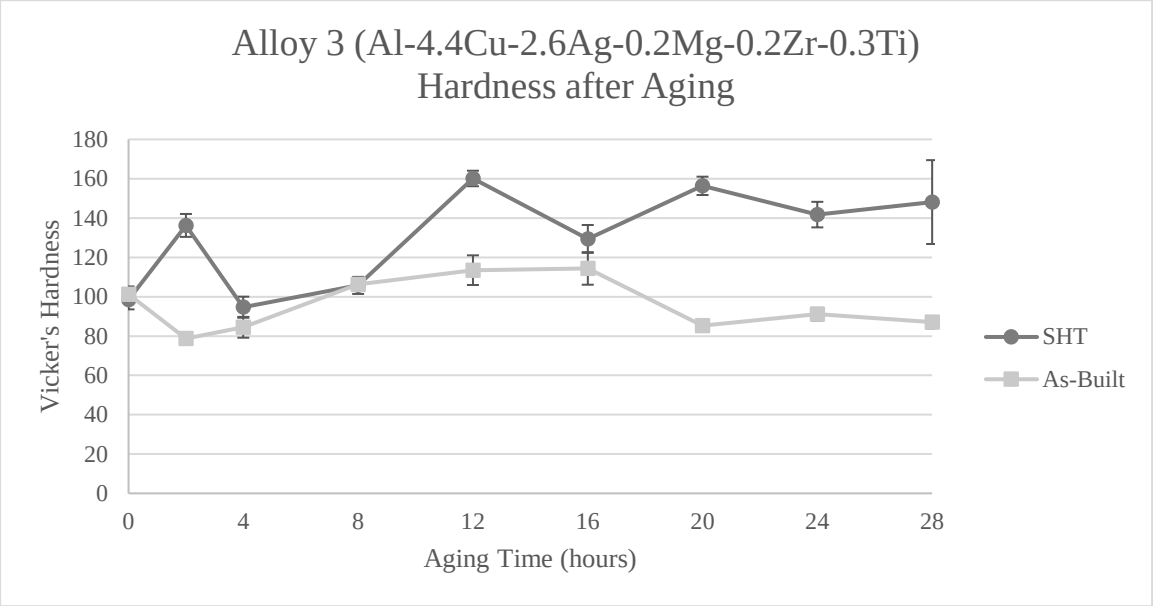

Figure 5-12. Aging curves for Alloy 3 after solution heat treatment at 510°C and aging at 160°C for 28 hours and after as-built aging at 160°C for 28 hours.

Aging curves for Alloy 4 (Al-5.4Cu-1.5Ag-0.2Mg-0.2Zr-0.3Ti) showed hardnesses to be consistently above 100 VHN, unlike the first three alloys which all contain lower amounts of copper and had initial hardnesses between 80 VHN and 100 VHN. The as-built aging curve for this alloy showed a decrease before reaching a peak hardness of 160 VHN after aging for 20 hours. The solution heat treated aging curve for this alloy showed to steadily increase to a peak hardness of 160 VHN after 20 hours, excluding the dip in hardness at 16 hours. This dip in hardness was also seen in the as-built sample. These curves are displayed in Figure 5-13. After referencing the sample designations in Table 4-10, it can be seen that these samples came from locations 11 and 12, respectively. As displayed in Figure 4-9, these samples are located at the bottom of the deposit, at the deposit-baseplate interface. It is possible that there may have been

stratification in the powder during initial layers that caused this decrease in hardness for both samples.

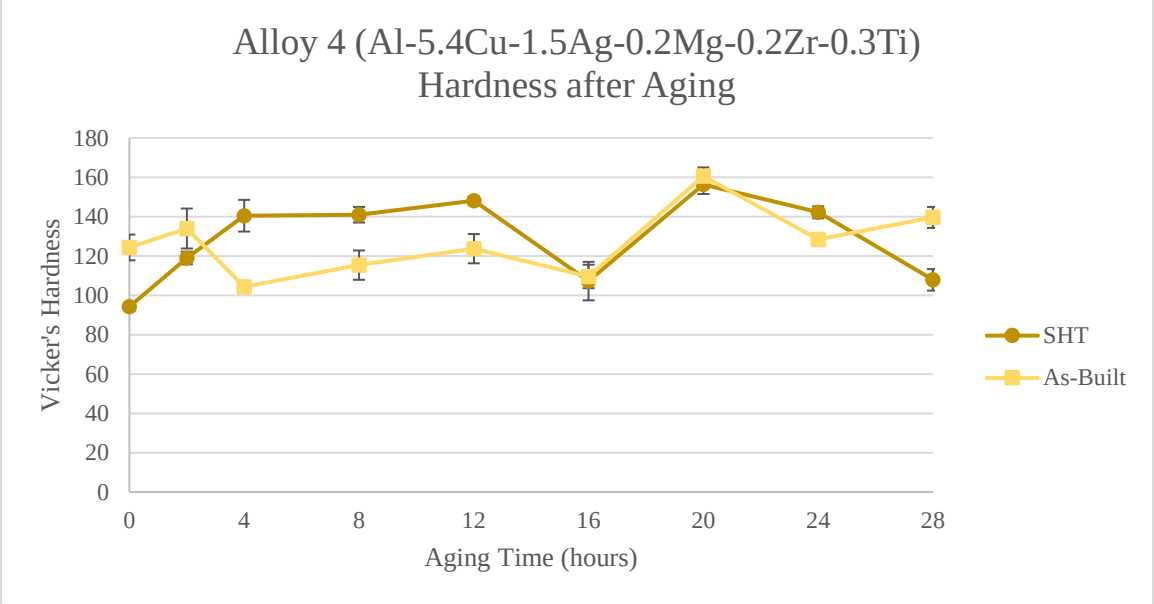

Figure 5-13. Aging curves for Alloy 4 after solution heat treatment at 510°C and aging at 160°C for 28 hours and after as-built aging at 160°C for 28 hours.

Aging curves for Alloy 5 (Al-5.5Cu-2.2Ag-0.2Mg-0.2Zr-0.3Ti) showed a steadily increasing hardness with aging time for solution heat treated samples, up to the peak hardness of 178 VHN after 20 hours of aging. A steadily increasing hardness with aging time was also seen in the as-built samples; however, there were peaks in hardness after 2 hours and 24 hours, and a dip in hardness at the expected peak age time of 20 hours. These curves are displayed in Figure 5-14. The aging curve for solution heat treated samples showed promising hardness values, starting off with an as-solution treated hardness of 120 VHN. This alloy would be of interest for future research.

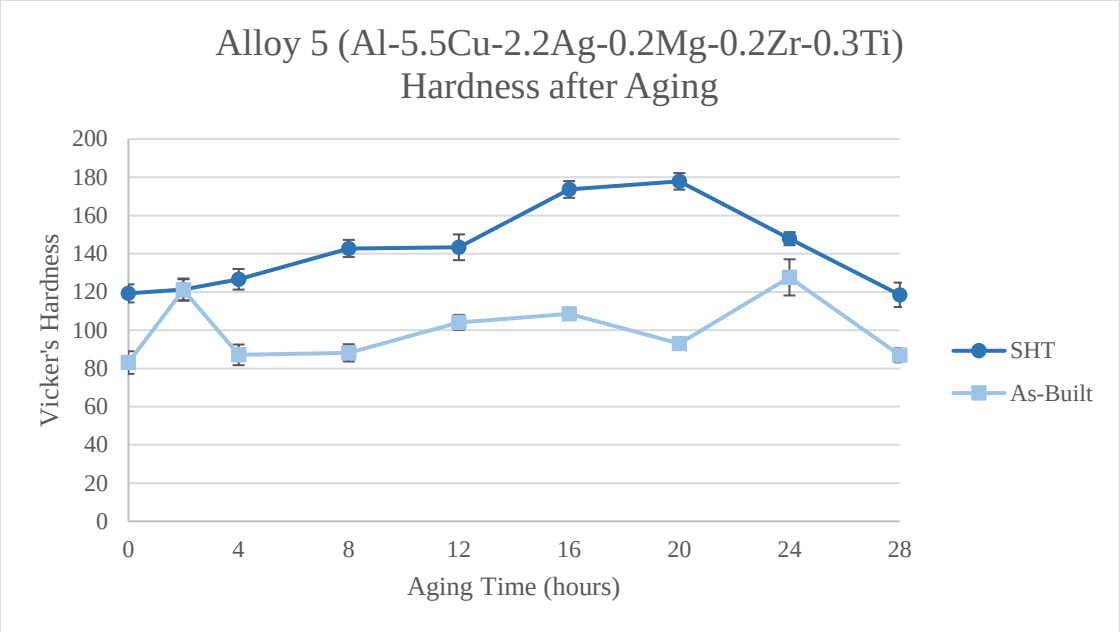

Figure 5-14. Aging curves for Alloy 5 after solution heat treatment at 510°C and aging at 160°C for 28 hours and after as-built aging at 160°C for 28 hours.

Aging curves for Alloy 6 (Al-6.6Cu-3.4Ag-0.2Mg-0.2Zr-0.3Ti) displayed a high value of peak hardness, with both the as-built and as-solution heat treated samples having hardnesses above 100 VHN. However, the as-built hardness value was shown to be higher than that of the as-solution treated sample, which can be seen in Figure 5-15. The as-built aging curve for this alloy displayed a slight drop in hardness initially, with the peak age hardness of 165 VHN being reached after 20 hours. The solution heat treated aging curve showed a significant dip in hardness after 8 hours of aging, followed by a rapid increase to the peak age condition after 16 hours, with a hardness of 187 VHN. This was the highest hardness value recorded over the duration of the experiment. This alloy contained more copper than all alloys previously discussed. Additionally, this alloy

contains the highest amount of silver out of all the alloys. This alloy may be of interest for future research.

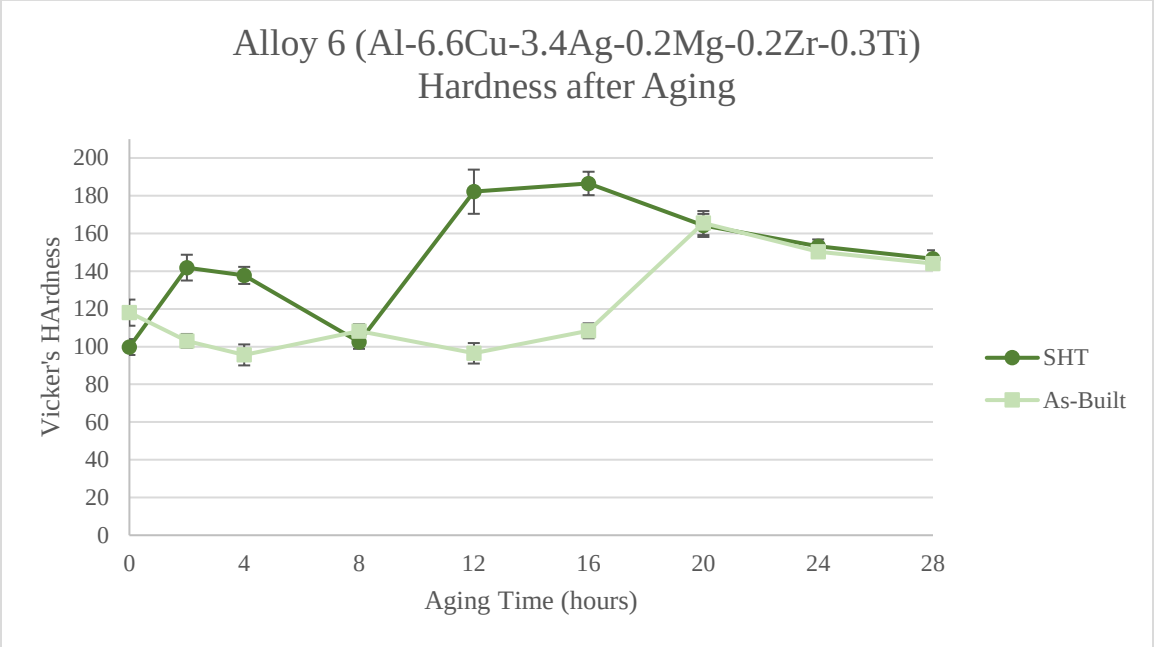

Figure 5-15. Aging curves for Alloy 6 after solution heat treatment at 510°C and aging at 160°C for 28 hours and after as-built aging at 160°C for 28 hours.

Aging curves for Alloy 7 (Al-7.7Cu-1.9Ag-0.2Mg-0.2Zr-0.3Ti) showed the highest initial hardness values for both the as-built and as- solution heat treated conditions, with both samples having a hardness above 110 VHN. The aging curve of the as-built condition proved to be fairly steady, with no significant peak age condition, but a sharp increase in hardness after 12 hours of aging. The aging curve of the solution heat treated condition showed a slow and steady increase in hardness to 168 VHN after 20 hours of aging, followed by a very minimal decrease in hardness after 20 hours. These curves are shown in Figure 5-16. This alloy exhibited a consistent aging curve in the solution heat treated condition, while also offering a good surface finish and fusion at the

deposit-baseplate interface as discussed in the previous section. This material may also be a good candidate for future research.

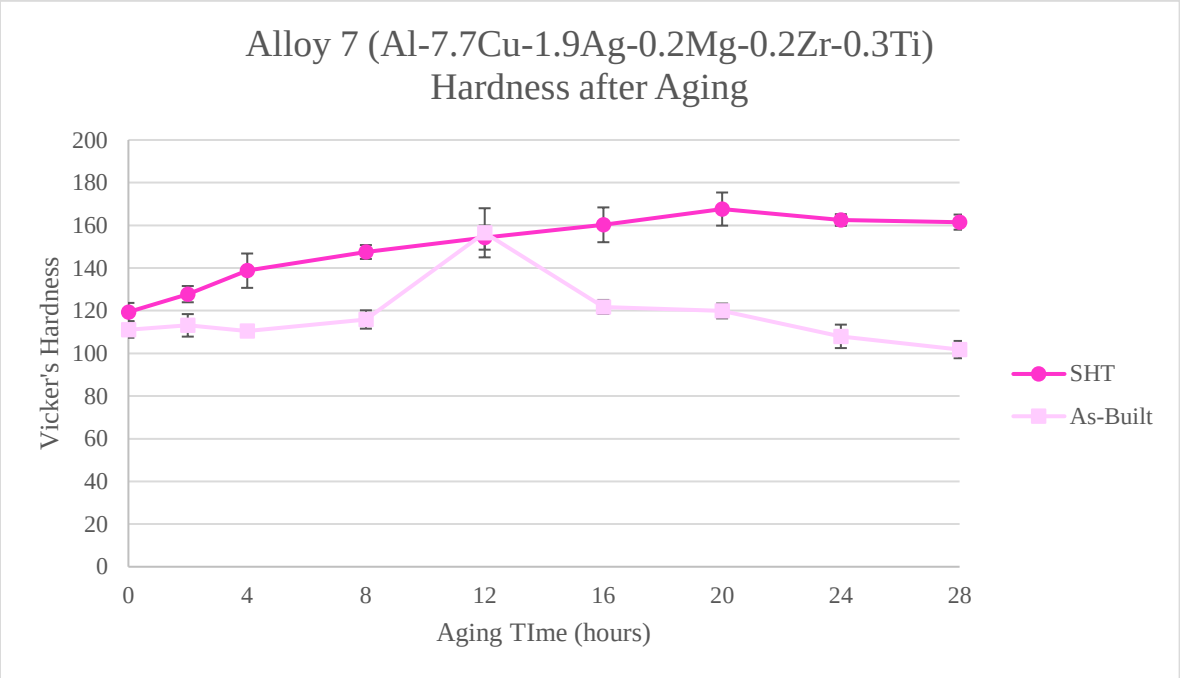

Figure 5-16. Aging curves for Alloy 7 after solution heat treatment at 510°C and aging at 160°C for 28 hours and after as-built aging at 160°C for 28 hours.

Aging curves for all the alloys which demonstrated promising hardness values with a consistent aging response in the solution heat treated condition, Alloys 1, 5, 6, and 7, are shown in Figure 5-17. Aside from the dip in hardness for Alloy 6 after 8 hours, these aging curves demonstrate clear under-aged, peak-aged, and over-aged regions. In Alloys 1, 5, and 7, the peak age was reached after 20 hours, while Alloy 6 reached the peak age condition after 16 hours. Alloys 1, 5, and 7 all had lower amounts of silver,1.39 wt% Ag, 2.19 wt% Ag, and 1.87 wt% Ag, respectively, while Alloy 6 contained the highest amount of silver out of all the alloys, at 3.40 wt% Ag. This may contribute to the

high hardness and shorter time to the peak-aged condition. In Alloy 1, Alloy 5, and Alloy 6, the effects of increasing copper content along with increasing silver content can be seen. Alloy 1 contains 4.91 wt% Cu and 1.39 wt% Ag, Alloy 5 contains 5.46 wt% Cu and 2.19 wt% Ag, and Alloy 6 contains 6.64 wt% Cu and 3.40 wt% Cu. The peak hardness for these alloys was shown to be 173 VHN for Alloy 1, 178 VHN for Alloy 5, and 186 VHN for Alloy 6, indicating an increase in hardness with the increase in the amount of copper and silver alloying elements. This is not surprising since additions directly contribute to the precipitation strengthening mechanisms in aluminum.

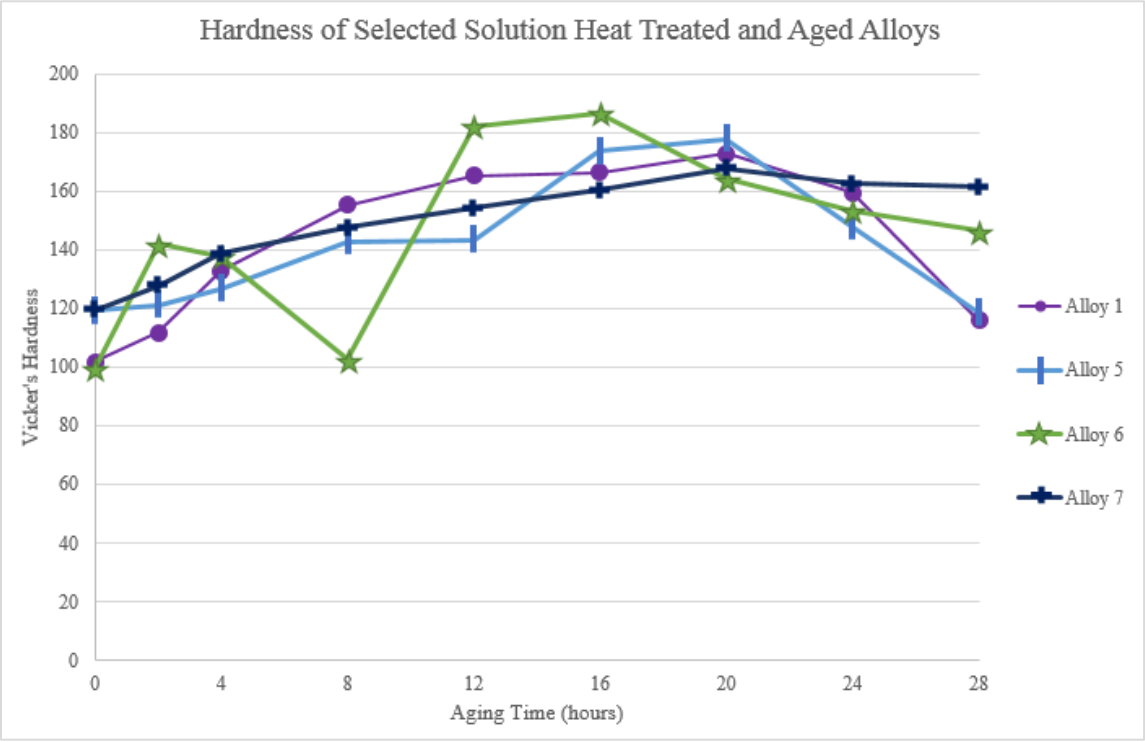

Figure 5-17. Aging curves for Alloys 1, 5, 6, and 7 after solution heat treatment at 510°C and aging at 160°C for 28 hour.

Based on the results of this research in terms of the aging curves and hardness measurements, increasing Cu content increased alloy hardness when subjected to the solution treatment and aging. Statistical modeling by Al-Obaisi showed that the optimal process variables for Al-Cu-Ag-Mg alloys were 5 wt% Cu, 0.6 wt% Ag, and 1 wt% Mg, with aging for 22.73 hours at 160°C, achieving a hardness of 178 VHN.[43] Their material was processed using chill casting and hot rolling, so the effect of solidification cracking was not considered and higher amounts of magnesium were acceptable. Similar hardness results were achieved with experimental Alloys 1, 5, 6, and 7, all of which contained a magnesium content below 0.25 wt% Mg, and a silver content above 1.0 wt% Ag. Additionally, experimental Alloys 1, 5, 6, and 7 all possessed an initial hardness at or greater than 100 VHN, the maximum hardness of the commercial Al-10Si-0.5Mg alloy. It was also shown that alloys having the highest levels of Ag (Alloy 2, 3, and 6) exhibited the highest peak-aged hardness for aging in the as-built condition, without solution heat treatment.

A comparison of peak-age hardness after solution treatment and aging for experimental Alloys 1, 5, and 6 to hardness values of selected commercial aerospace and additive manufacturing alloys is illustrated in Figure 5-18. Alloy 1 and 5 attained peak hardnesses of 173 VHN and 178 VHN, respectively, after aging for 20 hours at 160°C, while alloy 6 attained a peak hardness of 186 VHN after aging for 16 hours at 160°C. Al-10Si-0.5Mg is reported to attain a hardness of about 100 VHN after being stress-relieved at 300°C for 2 hours, or 123 VHN if left in the as-built condition.[17] Alloy 7017 (Al-Zn-Mg) is reported to attain a peak hardness of 153 VHN after aging for 25 hours at

120°C,[91] Alloy 6061 (Al-Si-Mg) is reported to attain a peak hardness of 122 HVN after aging at 175°C for 10 hours,[92] Alloy 2024 (Al-Cu) is reported to attain a peak hardness of 150 VHN after aging at 170°C for 80 hours,[93] and Alloy 7075-T6 is reported to achieve a peak hardness of 175 VHN after aging at 120°C for 24 hours.[94]

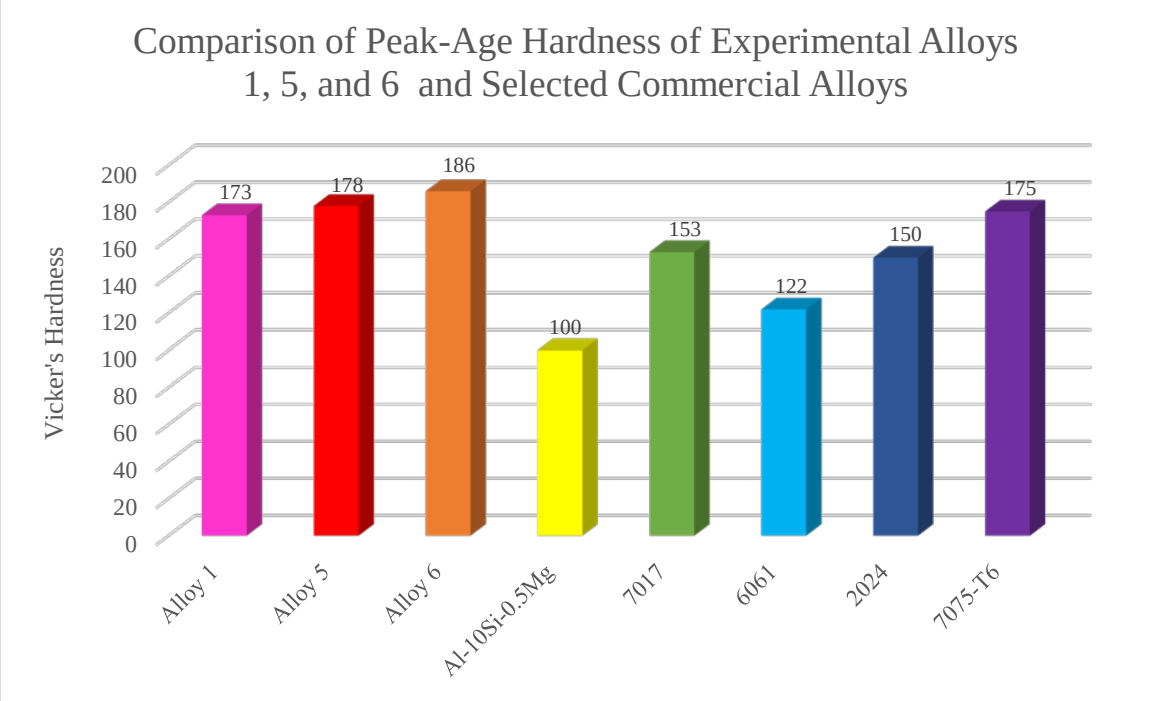

Figure 5-18. Comparison of hardness of experimental alloys with commercial alloys at peak-age condition.[91],[92],[93],[94]

5.2.2 Tensile Strength

Tensile bars were machined from Alloy 1 after solution heat treatment and aging for 20 hours to attain peak-age condition. Three specimens were obtained in the build direction (z-direction) and three specimens were obtained along the direction of the wall length (x-direction) and were tested. Results are displayed in Table 5-4.

Table 5-4. Mechanical properties of Alloy 1 after solution heat treatment at 510°C and aging for 20 hours at 160°C, compared with mechanical properties of Al-10Si-0.5Mg.

Alloy 1 (Al-4.9Cu-1.4Ag-0.2Mg-0.2Zr-0.3Ti)				
		Ultimate Tensile Strength (MPa)	Yield Strength (MPa)	Elongation (%)
x-direction	Sample 1	374	322	1.1
	Sample 2	-	-	-
	Sample 3	412	310	7.5
Average x-direction		393	316	4.3
z-direction	Sample 1	299	286	2.5
	Sample 2	306	278	1.8
	Sample 3	300	268	2.7
Average z-direction		302	277	2.3
Al-10Si-0.5Mg[17],[18]		350	230	11

Tensile and yield strength of Alloy 1 showed to be moderate. While these values were not as high as anticipated based off of the hardness results, x-direction samples still out preform Al-10Si-0.5Mg, which possesses a tensile strength of 350MPa and a yield strength of 230MPa. The very low elongation values may indicate that porosity effected the fracture of the specimens; however, even with this disadvantage the material still performed exceptionally.

5.3 Microstructures

5.3.1 Optical Microscopy

Optical micrographs of Alloy 1, after being solution heat treated at 510°C and aged for 20 hours at 160°C to obtain the peak-age condition, were taken after grinding, polishing, and etching with Keller's reagent. The location of the specimen was in the region close to the z-direction tensile specimens. Images were taken to show perspectives in both the x-direction and the z-direction, shown in Figures 5-19 and 5-20, respectively. Strengthening precipitates were not expected to be seen at these magnifications; however, black/dark purple and grey second phases were visible, as pointed out in red. In the z-direction, grain boundaries were visible at 500x and appeared to show a fine cellular structure. In order to identify these phases, samples were further characterized on the SEM.

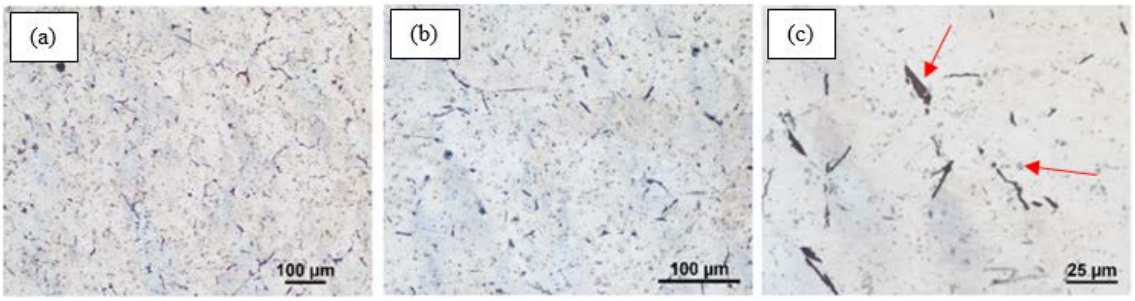

Figure 5-19. Optical micrographs of Alloy 1 in the x-direction after being solution heat treated at 510°C and aged at 160°C for 20h (a) 100x. (b) 200x. (c) 500x.

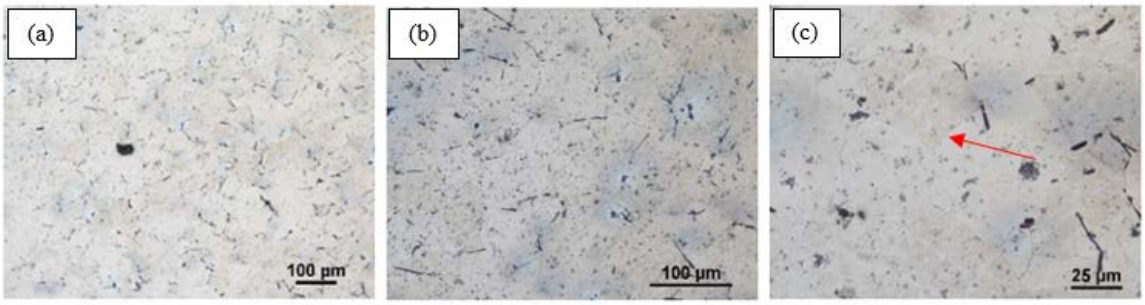

Figure 5-20. Optical micrographs of Alloy 1 in the z-direction after solution heat treated at 510°C and aged at 160°C for 20h (a) 100x. (b) 200x. (c) 500x.

5.3.2 Scanning Electron Microscopy

A sample of Alloy 1, after being solution heat treated at 510°C and aged for 20 hours at 160°C to the peak-age condition, was also characterized under the SEM. Energy-dispersive X-ray spectroscopy (EDS) was utilized to identify the large precipitates that were seen under optical microscopy. In Figure 5-21, secondary electrons are utilized to form an image with topological contrast. A complimentary image taken in the same location, shown in Figure 5-22, utilized backscattered electrons to achieve an image which displays mass contrast, with heavier elements appearing brighter and lighter atoms appearing darker. The large faceted constituents that were seen under optical microscopy appeared white under the SEM and are pointed out by the long red arrow. In the secondary electron image, many tinted areas and circle shaped outlines were observed and are believed to be due to bleeding of etchant from precipitates. Grain boundaries were also visible in the secondary electron image. In the backscattered electron image, contrast is seen between the lightweight aluminum matrix (appearing dark) and the constituents containing heavier elements, which could include Ti, Fe, Cu, Zr, and Ag

(appearing light). In order to obtain a more precise identification of the compositions of the constituents, EDS was conducted.

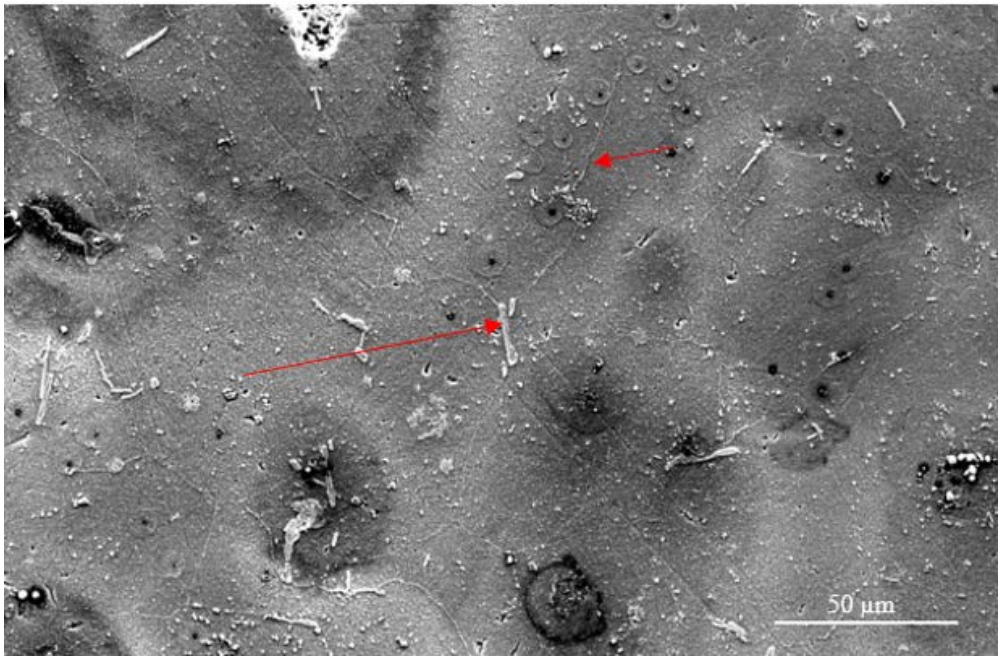

Figure 5-21. SEM secondary electron image of experimental Alloy 1 in the peak-age condition.

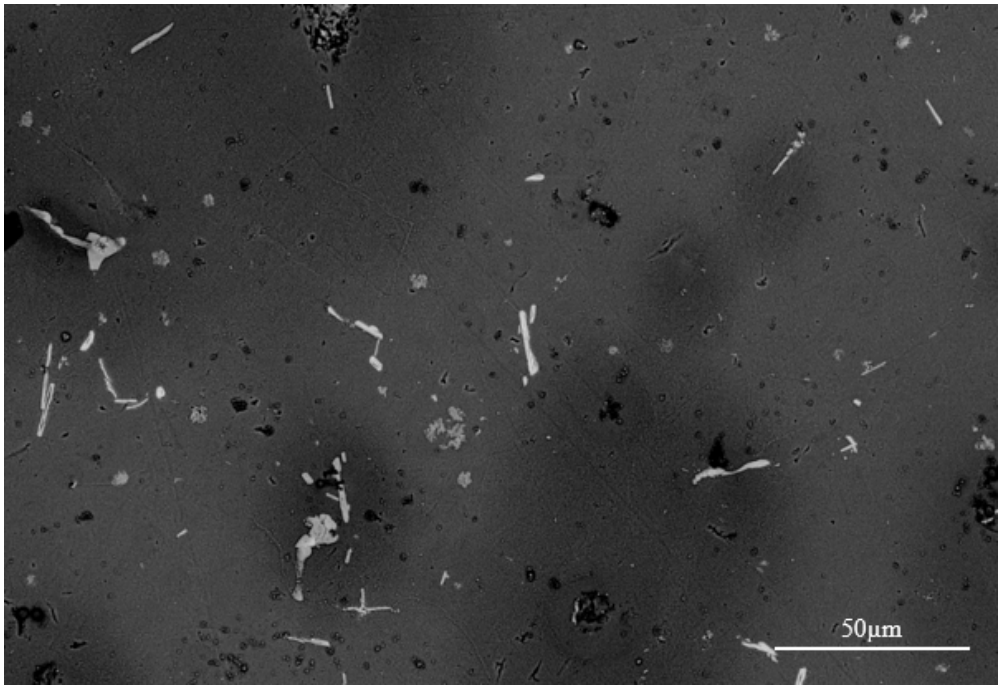

Figure 5-22. SEM backscattered electron image of experimental Alloy 1 in the peak-age condition.

EDS mapping was used to obtain an image identifying the chemistry of the selected area. Additionally, EDS point measurements were taken to identify the composition of the constituents more precisely. Figure 5-23 displays elemental maps of the area of interest. Figure 5-23 (a) shows the electron image of the area that was mapped, (b) shows the aluminum map, (c) shows the silver map, (d) shows the copper map, (e) shows the iron map, and (f) shows the titanium map.

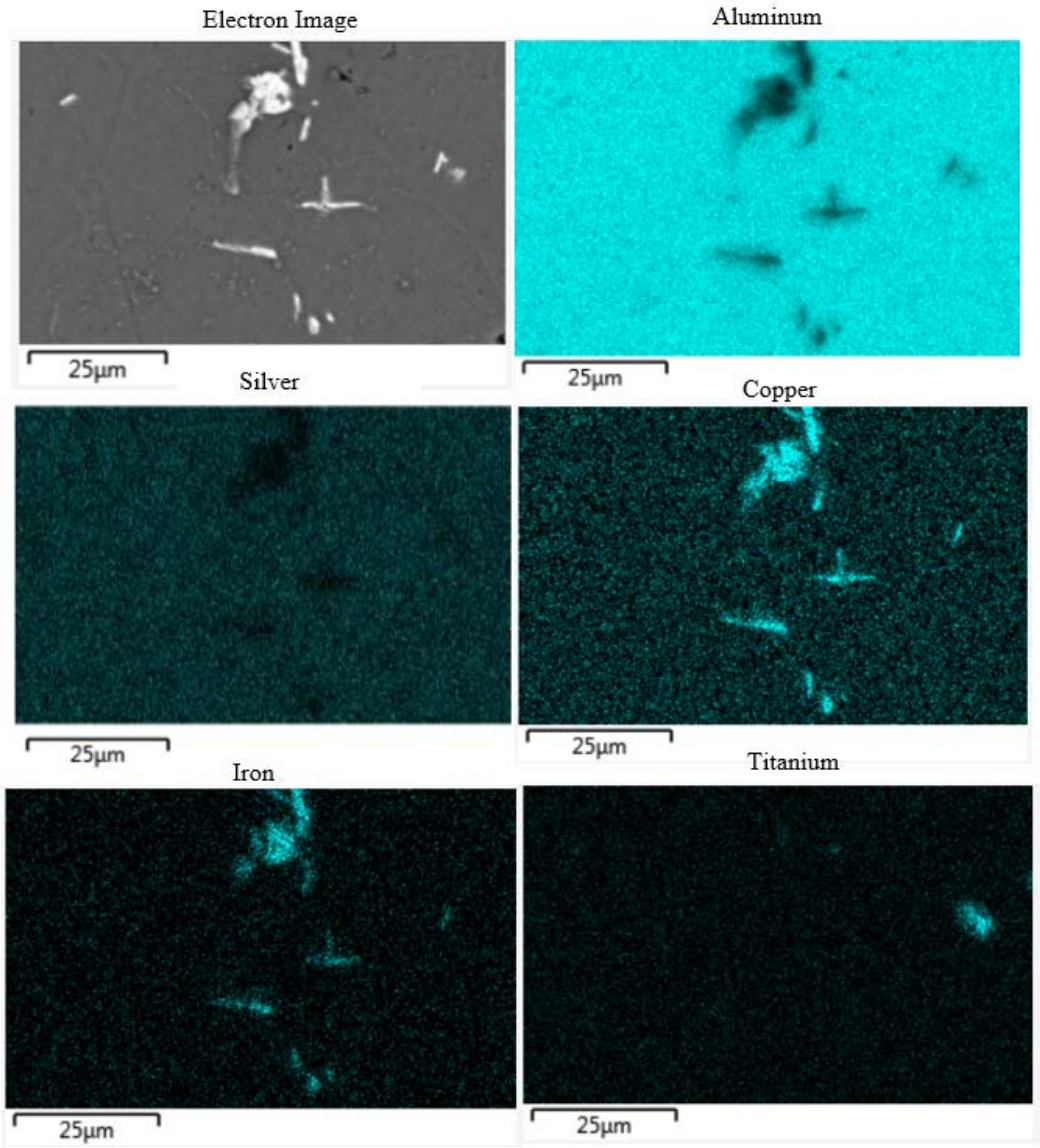

Figure 5-23. (a) SEM images of mapping area. (b) EDS map of aluminum. (c) EDS map of silver. (d) EDS map of copper. (e) EDS map of iron. (f) EDS map of titanium.

From these maps, it was seen that the matrix material contains aluminum with evenly dispersed silver, copper, iron, and titanium. The bright white precipitates was shown to contain primarily aluminum, copper, and iron, and the one lighter grey particle to the right on the electron micrograph was shown to contain titanium. Another SEM image illustrating grain boundaries, as well as intergranular constituents are shown in Figure 5-24. Point measurements were taken at areas of interest. Spectrum 6 was taken on a long, thin, white constituent on the grain boundary and can be seen in Figure 5-25, Spectrum 7 was taken on the grain boundary and can be seen in Figure 5-26, and Spectrum 8 was taken on a round constituent and can be seen in Figure 5-27.

EDS Spectrum 6 showed the long thin constituent, or segregation, at the grain boundary to contain about 77 wt% Al, 14.6 wt% Cu, 2.4 wt% Fe, and 1.3 wt% Ag. Oxygen was also identified in the spectrum, but this is probably attributed to the sample contamination. EDS Spectrum 7 showed the grain boundary to contain 91.3 wt% Al, 4.5 wt% Cu, and 2 wt% Ag representing the eutectic Al_2Cu phase. EDS Spectrum 8 showed the bright, round precipitate to contain 70 wt% Al, 20 wt% Cu, 2.9 wt% Fe, and 1.0 wt% Ag, which may represent a ternary eutectic phase of Al-Cu-Fe. It should be noted that the master alloy contained iron. These point spectrums confirm that the anticipated phases and constituents were present in the system.

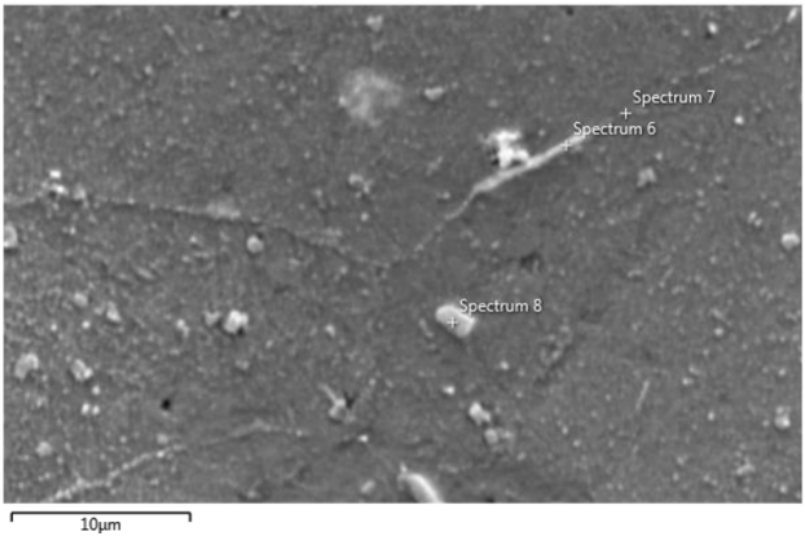

Figure 5-24. Electron image indicating locations of point EDS measurements.

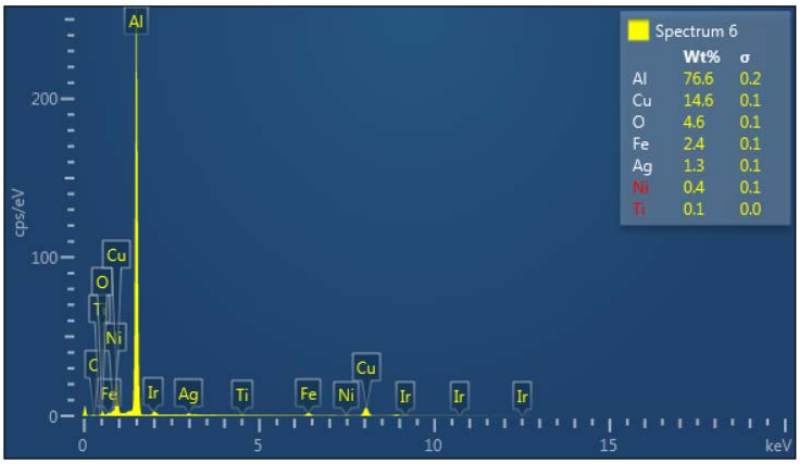

Figure 5-25. EDS Spectrum 6, long thin white constituent.

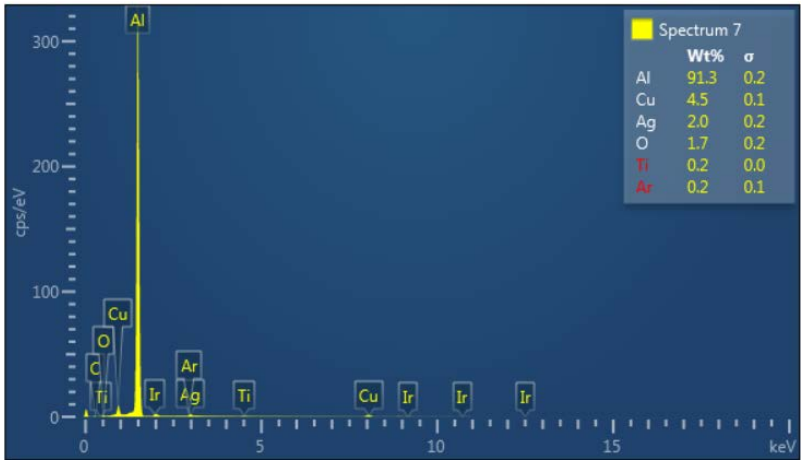

Figure 5-26. EDS Spectrum 7, grain boundary.

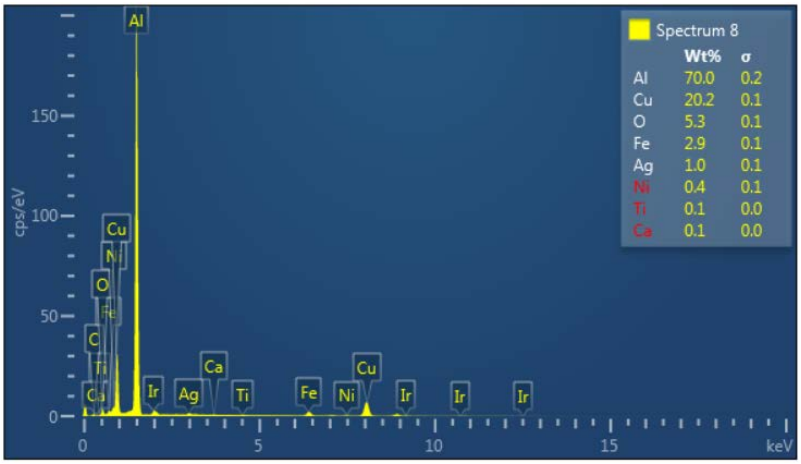

Figure 5-27. EDS Spectrum 8, round constituent.

5.3.3 Transmission Electron Microscopy

While some phases and constituents were able to be characterized using optical microscopy and scanning electron microscopy, the strengthening precipitates that are concurrently formed, θ' and Ω, are only visible under transmission electron microscopy. As discussed previously, θ' precipitates form as thin plates on the {100} planes of the aluminum matrix and Ω precipitates form as thin plates on the {111} planes of the aluminum matrix. Figure 5-28 displays images obtained from the [001] zone axis for Alloy 1 at the solution heat treated and peak-aged condition, showing small, evenly dispersed θ', which was expected in an Al-4.9Cu-1.4Ag-0.2Mg-0.2Zr-0.3Ti alloy. It can be noted that all of these precipitates are seen to form at 90° angles with each other, indicating two variants of θ' that display the edges of the plate precipitates on the {100}

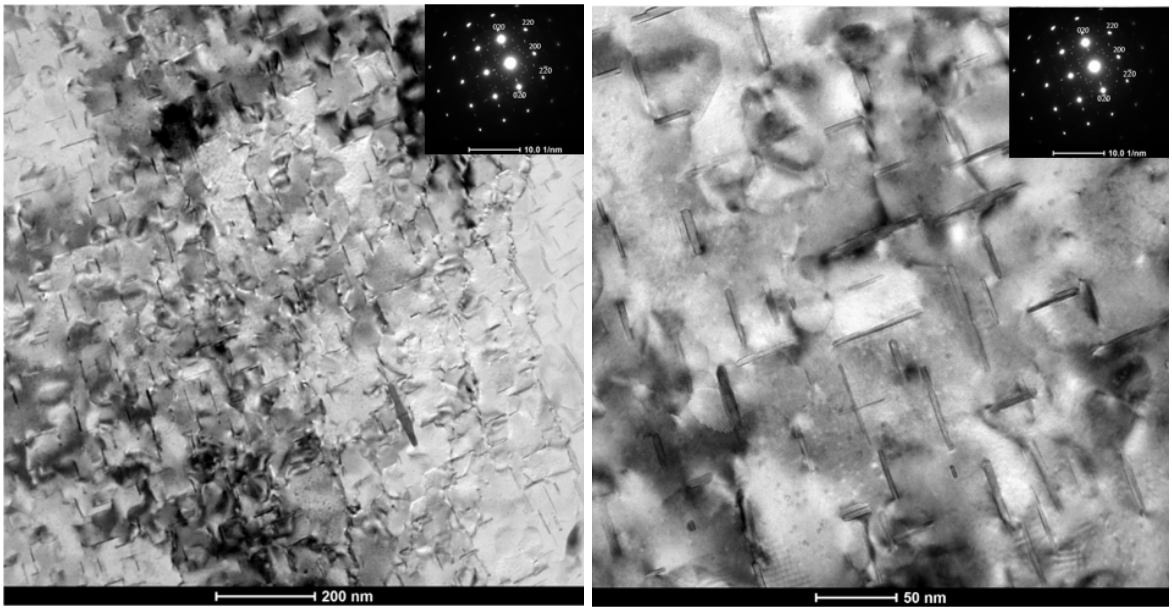

Figure 5-28. TEM images showing θ' precipitates in Alloy 1 in the peak-aged condition, with the diffraction pattern obtained for the [001] zone axis.

Figure 5-29 displays images of the same specimen (Alloy 1) obtained from a near [111] zone axis. Again, small finely dispersed plates were observed; however, these precipitates appear to be Ω. The diffraction pattern in this area had dim points on the top and bottom of the diffraction, indicating weak diffraction and suggesting the material may be slightly off the [111] zone axis. This can be confirmed when observing the plates in Figure 5-29 (a). Prior research has confirmed the presence of at least four variants of Ω observable along the $<111>_{\alpha}$ direction.[41],[67],[74] Figure 5-29, obtained near the [111] displays at least three variants.

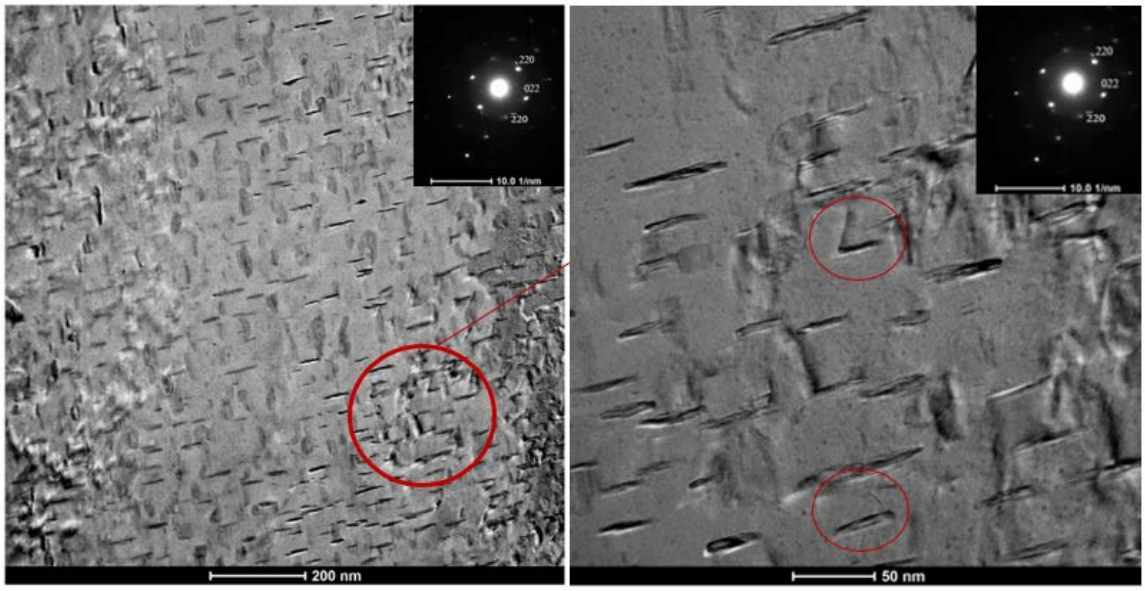

Figure 5-29. TEM images showing Ω precipitates in Alloy 1 in the peak-aged condition, with the diffraction pattern obtained for the [111] zone axis.

Chapter 6

SUMMARY AND CONCLUSION

Research was conducted to formulate compositions and determine an optimum solution and precipitation heat treatment for an aluminum alloy offering significant improvement in strength over the current Al-10Si-0.5Mg alloy used for additive manufacturing. The advanced aluminum alloy was based on the Al-Cu-Ag-Mg system, which provides the ability to respond to strengthening through multiple precipitate phases, while also appearing to have low solidification cracking tendencies. Alloys were identified and formulated through blending of an Al-0.3Mg-0.2Ti-0.3Ti powder master alloy and pure Cu and Ag powder. Specimens representing the candidate alloys were produced using a laser-based directed energy deposition system and subsequently characterized based on chemistry, microstructure, hardness, and tensile strength. Conclusions that may be drawn from this research are detailed below.

1. Utilizing the Al-0.3Mg-0.2Ti-0.3Ti master alloy blended with pure Cu and Ag powders did not achieve the exact compositions that were desired, believe to be due to non-uniform mixing; however, the compositions of the alloys that were produced were sufficient for identifying candidate alloys of interest.

2. Some cracking was observed during the build process and was believed to be due to alloys containing lower amounts of Cu or higher levels of Mg.

3. Alloys representing the moderate Cu and Ag levels, such as Alloy 1 representing Al-5.0Cu-1.4Ag-0.2Mg-0.2Zr-0.3Ti, produced hardness and mechanical properties that well exceeded current capabilities with aluminum alloys used for additive manufacturing, with hardness after solution heat treatment and peak aging being consistently above 170 VHN.

4. Alloys having relatively high Ag levels also responded to post-process aging only (without the solution heat treatment) and also produced high hardness.

5. Alloy 1 (Al-5.0Cu-1.4Ag-0.2Mg-0.2Zr-0.3Ti) was shown to exhibit very fine precipitates representing the θ'and Ω phases, with the θ' forming on the {100} planes of the aluminum matrix and the Ω forming on the {111} planes of the aluminum matrix.

6. Limited mechanical properties of Alloy 1 (Al-5.0Cu-1.4Ag-0.2Mg-0.2Zr-0.3Ti) provided an average tensile strength of 301 MPa in the z-direction and 396 MPa in the x-direction and an average yield strength of 275MPa in the z-direction and 313 MPa in the x-direction, outperforming Al-10Si-0.5Mg. Porosity may have been responsible for lower than expected results, indicated by low elongation.

References

[1] Martukanitz, R. P., Aluminum alloys for additive manufacturing, Provisional U.S. Patent Docket 059516-0225 (2017).

[2] Material Data Sheet: EOS Aluminum AlSi10Mg (2014). EOS GmbH.

[3] Aluminum 7075-T651. *Metals Handbook, Vol. 2 – Properties and Selection: Nonferrous Alloys and Special Purpose Materials*, ASM International 10th Ed. 1990.

[4] Gibson, I., Rosen, D., & Stucker, B. (2015). *Additive Manufacturing Technologies*: *3D Printing, Rapid Prototyping, and Direct Digital Manufacturing.* New York, NY: Springer-Verlag.

[5] Herzog, D., Seyda, V., Wycisk, E., & Emmelmann, C. (2016). Additive Manufacturing of Metals. *Acta Materialia, 117,* 371-392.

[6] Sun, S., Brandt, M., and Easton, M. (2017). Powder bed fusion process: an overview. *Woodhead Publishing Series in Electronic and Optical Materials: Laser Additive Manufacturing,* 55-77.

[7] Steen, W.M. (2010). *Laser Material Processing.* London: Springer.

[8] Frazier, W.E., Metal Additive Manufacturing: A Review. *J. Mater. Eng. Perform.* 23 (6) (2014) 1917-1928.

[9] Yan, M., & Yu, P. (2015) An overview of densification, microstructure and mechanical property of additively manufactured Ti-6Al-4V: Comparison among selective laser melting, electron beam melting, laser metal deposition and selective laser sintering, and with conventional powder metallurgy, In: A. Lakshmanan (Ed.), *Sintering Techniques of Materials* (77-106) London: Intech

[10] Sames, W.J., List, F.A., Pannala, S., Dehoff, R.R., & Babu, S.S. (2016). The metallurgy and processing science of metal additive manufacturing. *International Materials Reviews*

[11] Gu, D., Ma, C., Xia, M., Dai, D., and Shi, Q. (2017). A Multiscale Understanding of the Thermodynamic and Kinetic Mechanisms of Laser Additive Manufacturing. *Engineering, 3 [5],* 675-684.

[12] Martin, J.H., Yahata, B.D., Hundley, J.M. Mayer, J.A., Schaedler, T.A., & Pollock, T.M. (2017). 3D printing of high-strength aluminum alloys. *Nature, 549,* 365-369.

[13] Ghoniya, M. *Weldability.* Retrieved from https://www.slideshare.net/mubassir007/weldability-61231726.

[14] Ding, Y., Muñiz-Lerma, J.A., Trask, M., Chou, S., & Brochu, M., (2016) Microstructure and mechanical property considerations in additive manufacturing of aluminum alloys. *MRS Bulletin, 41 (10),* 745-751.

[15] Martin, J.H., Yahata, B.D., Hundley, J.M., Mayer, J.A. Schaedler, T.A., & Pollock, T.M. (2017). 3D printing of high-strength aluminum alloys. *Nature, 549,* 365-369.

[16] Lewandowski, J.J. & Seifi, M. (2016). Metal additive manufacturing: A review of mechanical properties. *Annu. Rev. Mater. Res., 46,* 151-186.

[17] Material Data Sheet: AlSi10Mg-0403 powder for additive manufacturing (2018). Stress relieved at 300 °C ±10 °C for 2 hr, air cooled. Renishaw.

[18] Material Data Sheet: EOS Aluminum AlSi10Mg (2014). EOS GmbH.

[19] Material Data Sheet: EOS Titanium Ti64 (2014). EOS GmbH.

[20] Material Data Sheet: Ti6Al4V powder for additive manufacturing (2018). Hardness after HIP. Renishaw plc.

[21] Material Data Sheet: CoCr-0404 powder for additive manufacturing (2018). Solution treated conditions: 1. Heat to 650 °C ±10 °C, hold for 15 min; 2. Heat to 1000 °C ±10 °C hold for 5 min; 3. Heat to 1050 °C ±10 °C hold for 2 hr; 4. Fast cool to < 60 °C ±10 °C using 2 bar argon quench. Renishaw plc.

[22] Material Data Sheet: In718-0405 powder for additive manufacturing. (2018). Heat treated conditions: 1. Solution treated at 980 °C ± 10 °C for 1 hr 2. Aged at 720 °C ± 10 °C for 8 hr, and further aged at 620 °C ± 10 °C for 8 hr. Renishaw plc.

[23] Material Data Sheet: Stainless Steel 316L. (2014). EOS GmbH.

[24] Steel Hardness Conversion Table: HRB to VHN. (2018). *Steel Express*.

[25] Nafsin, N., and Rashed, H.M.M.A. (2013). Effects of Copper and Magnesium on Microstructure and Hardness of Al-Cu-Mg Alloys. *International Journal of Engineering and Advanced Technology (IJEAT), 2 (5),* 533-536.

[26] Pfeifer, M. *Mechanisms for Strengthening Aluminum* [pdf document]. Retrieved from online course Aluminum Metallurgy. Industrial Metallurgists, LLC.

[27] Davis, J.R. (Ed.) (1993). *Aluminum and Aluminum Alloys.* Materials Park, OH: ASM International

[28] Gedeon, M. (2010). Solid Solution Hardening and Strength. *Brush Wellman Alloy Products Technical Tidbits, 16*.

[29] Pelleg, J.,(2013). *Mechanical Properties of Materials.* New York: Springer. Pp. 236-239.

[30] Awan, I.Z., Khan, A.Q. (2017). Precipitation from Solid Solutions. *Journal of the Chemical Society of Pakistan, 39 (3),* 319-336.

[31] Warren, A. (1997). Phase Diagrams. Retreived from: University of Southampton Engineering Materials. https://www.southampton.ac.uk/~pasr1/index.htm

[32] Callister, W. (2010). *Materials Science and Engineering: An Introduction 8e.* Danvers, MA: John Wiley & Soncs, Inc.

[33] Precipitation Hardening of Aluminum Alloys (2010). *Total Materia.*

[34] Gerold, V. (1979). *Precipitation Hardening: Dislocations in Solids, Vol. 4*. New York, NY: North-Holland Publishing.

[35] Kaufmann, N *et al.* Influence of process parameters on the quality of aluminum alloy EN AW 7075 using selective laser melting (SLM). *Phys. Procedia 83,* 918-926.

[36] Kurz, W. & Fisher, D.J. (1989) *Fundamentals of Solidification.* Trans Tech: Switzerland.

[37] Coniglio, N. & Cross, C.E. (2013). Initiation and growth mechanisms for weld solidification cracking. *International Materials Reviews, 58,* 375-397.

[38] Cross, C., Olsen, D., and Liu, S. (2003) Handbook of Aluminum: Welding Aluminum (2003), Marcel Dekker, Inc. (utilizing data from W. Pumphrey and D. Moore, Cracking during and after solidification in some aluminum-copper-magnesium alloys, J. Inst. Metals,1948).

[39] S. Kou. (2003) *Welding Metallurgy.* Wiley-Interscience: Hoboken, N.J.

[40] Taminger, K., Hafley, R.A. (2002). *13th Solid Freeform Fabrication Symposium.* Austin, TX

[41] Zhang, H., Zhu, H., Qi, T., Zhiheng, H., Zeng, X., (2016). Selective laser melting of high strength Al-Cu-Mg alloys: Processing, microstructure and mechanical properties. *Materials Science and Engineering A, 565,* 47-54

[42] Malek Ghaini, F., Sheikhi, M., Torkamany, M.J., and Sabbaghzadeh, J., (2009). The relation between liquation and solidification cracks in pulsed laser welding of 2024 aluminum alloy. *Materials Science and Engineering A, 519,* 167-171.

[43] Al-Obaisi, A.M., El-Danaf, E.A., Ragab, A.E., & Soliman, M.S. (2016) Precipitation Hardening and Statistical Modeling of the Aging Parameters and Alloy Compositions in Al-Cu-Mg-Ag Alloys. *Journal of Materials Engineering and Performance, 25(6),* 2432-2444.

[44] Hu, S.Y, Baskes, M.I., Stan, M., Chen, L.Q. (2006). Atomistic calculations of interfacial energies, nucleus shape and size of θ' precipitates in Al-Cu alloys. *Acta Materialia, 54,* 4699-4707.

[45] Sha, G., Marceau, R.K.W., and Ringer, S.P., (2011). Precipitation and solute clustering in aluminum: advanced characterization techniques. In R. Lumley (Ed.) *Fundamentals of Aluminum Metallurgy: Production, Processing, and Application.* (345-353). Elsevier Science & Technology.

[46] Jacobs, M.H. (1999). *Precipitation Hardening* [PDF Document] TALAT Lecture 1204, European Aluminum Association.

[47] Smallman, R.E. and Ngan, A.H.W. (2007). Chapter 7: Mechanical Properties II – Strengthening and toughening. *Physical Metallurgy and Advanced Material, 7th Edition.* Elsevier Science & Technology, pp 385-446.

[48] Gladman, T. (1999). Precipitation Hardening in Metals. *Materials Science and Technology, 15,* 30-36.

[49] Polmear, I.J. (2006). *Light Alloys: Metallurgy of the Light Metals, 4th Ed*. Melbourne: Elsevier's Science and Technology

[50] Xiao, D.H., Wang, J.N., Ding, D.Y., & Chen, S.P. (2002) Effect of Cu Content on the Mechanical Properties of an Al-Cu-Mg-Ag Alloy. *Journal of Alloys and Compounds, 343,* 77-81

[51] Mordike, B.L., and Ebert, T. (2001). Magnesium: Properties – appplications – potential. *Materials Science and Engineering: A, 302 (1),* 37-45.

[52] Rana, R.S., Purohit, R., Das, S. (2012) Reviews on the Influences of Alloying Elements on the Microstructure and Mechanical Properties of Aluminum Alloys and

Aluminum Alloy Composites. *International Journal of Scientific and Research Publications, 2 (6),* 1-7.

[53] Girisha, H.N., and Sharma, K.V. (2012). Effect of magnesium on strength and microstructure of Aluminum Copper Magnesium Alloys. *International Journal of Scientific & Engineering Research, 3(2),* 1-4.

[54] Wang, S.C., Starnik, M.J., and Gao, N. (2006). Precipitation hardening in Al-Cu-Mg alloys revisited. *Scripta Materialia, 54 (2),* 287-291.

[55] Silcock, J.M. (1961). The structural aging characteristics of Al-Cu-Mg alloys with Cu:Mg ratios of 7:1 and 2.2:1. *Journal of the Institute of Metals, 89,* 203-210.

[56] Styles, M.J., Marceau, R.K.W., Bastow, T.J., Brand, H.E.A., Gibson, M.A., and Hutchinson, C.R. (2015) The competition between metastable and equilibrium S (Al_2CuMg) phase during the decomposition of Al-Cu-Mg alloys. *Acta Materialia, 98,* 64-80.

[57] Griffiths, W.D., and Raiszadeh. (2009). Hydrogen, porosity, and oxide film defects in liquid Al. *Journal of Materials Science, 44(13),* 3402-3407.

[58] Liu, X.Y., Wang, Z.P., Fu, B.G., Long, L., Zhang, X.L., and Cui, H.X. (2016). Effects of Mg content on the mechanical properties and corrosion resistance of Al-Cu-Mg-Ag alloy. *Journal of Alloys and Compounds, 685,* 209-215.

[59] Deaf, G.H., Youssef, S.B., and Mahmoud, M.A. (1996). Effect of γ' and γ (Ag_2Al) Precipitates on the Steady State Creep of Al-16wt% Ag Alloys with and without Zr Additions. *Phys. Stat. Sol. (a) 158.*

[60] Rosalie, J., Bourgeois, L., and Muddle, B.C. (2012). Precipitate assemblies formed on dislocation loops in aluminum-silver alloys. *Philosophical Magazine A, 89(15).*

[61] Vietz, J.T. & Polmear, I.J.(1966). The influence of small additions of silver on the aging of aluminum alloys: observations on Al-Cu-Mg alloys. *Journal of the Institute of Metals, 94,* 410-419.

[62] Xiao, D.H., Wang, J.N., and Ding, D.Y. (2004). Effect of titanium additions on mechanical properties of Al-Cu-Mg-Ag alloy. *Materials Science and Technology, 20,* 1199-1204.

[63] Elgallad, E.M., Samuel, A.M., Samuel, F.H., and Doty, H.W. (2010). Effects of additives on the microstructure and tensile properties of a new Al-Cu based alloy intended for automotive castings. *AFS Transactions.*

[64] Song, M., Chen, K. and Huang, L. (2007). Effects of Ce and Ti on the microstructures and mechanical properties of an Al-Cu-Mg-Ag alloy. *Rare Metals, 26 (1).* 28-32.

[65] Macchi, C., Somoza, A., Ferragut, R., Dupasquier, A., and Polmear, I.J., (2009). Aging Processes in Al-Cu-Mg Alloys with Different Cu/Mg Ratios. *Physica Status Solidi, 6 (11),* 2322-2325.

[66] Gable, B.M., Zhu, A.W., Shiflet, G.J., and Starke Jr., E.A. (2008). Assessment of the aluminum-rich corner of the Al-Cu-Mg-(Ag) phase diagram. *Computer Coupling of Phase Diagrams and Thermochemistry, 32.* 256-267.

[67] Gazizov, M & Kaibyshev, R. (2017). Precipitation structure and strengthening mechanisms in an Al-Cu-Mg-Ag alloy. *Material Science and Engineering A, 702*, 29-40.

[68] Carl Cross, David Olsen, and Stephen Liu, Handbook of Aluminum: Welding Aluminum (2003), Marcel Dekker, Inc. (utilizing data from W. Pumphrey and D. Moore, Cracking during and after solidification in some aluminum-copper-magnesium alloys, J. Inst. Metals, 1948).

[69] Polmear, I.J. (1964) The effects of small additions of silver on the aging of some aluminum alloys. *Transactions of the Metallurgical Society of AIME, 230*

[70] Teleshov, V.V., Kaputkin, E.Y., Golovleva, Kosmacheva, N.P. (2005). Temperature Ranges of Phase Transformations and Mechanical Properties of Alloys of the Al-Cu-Mg-Ag System with Various Cu/Mg Ratios. *Metal Science and Heat Treatment, 47 (4).* 18-23.

[71] Chester, R.J. & Polmear, I.J. (1980). *Micron, 11*, 311-312.

[72] Castillo, L.D., and Lavernia, E.J. (2000). Microstructure and Mechanical Behavior of Spray-Deposited Al-Cu-Mg(-Ag-Mn) Alloys. *Metallurgical and Materials Transactions A, 31.*2287-2289.

[73] Li, Y., Liu, Z., Xia, Q., Bai, S., and Chen, X. (2011). Effects of Aging Temperature on the Precipitation Behavior of Ω Phase in an Al-Cu-Mg-Ag Alloy. *Met. Mater. Int, 17(1).* 1-6.

[74] Muddle, B.C. & Polmear, I.J. (1989). The Precipitate Ω Phase in Al-Cu-Mg-Ag Alloys, *Acta Metallurgica,* 37 (3), 777-789.

[75] Macchi, C., Tolley, A., Giovachini, R., Polmear, I.J., and Somoza, A. (2015). Influence of a microalloying addition of Ag on the precipitation kinetics of an Al-Cu-Mg alloy with high Mg:Cu ratio. *Acta Materialia, 98.* 275-287.

[76] Hutchinson, C.R., and Ringer, S.P. (2000). Precipitation Processes in Al-Cu-Mg Alloys Microalloyed with Si. *Metallurgical and Materials Transactions A, 3,* 2721-2733.

[77] Hono, K., Sakurai, T., and Polmear, I.J., (1995). Pre-Precipitate Clustering in Aged Aluminum Alloys. *Materials Science Forum, Vols 189-190,* 249-254.

[78] Ringer, S.P., Sakurai, T., and Polmear, I.J., (1996). Origins of Hardening in Aged Al-Cu-Mg-(Ag) Alloys. *Acta Materialia, 45 (9).* 3731-3744.

[79] Reich, L., Murayama, M., and Hono, K. (1998). Evolution of Ω phase in an Al-Cu-Mg-Ag alloy – a three-dimensional atom probe study. *Acta Materialia, 46 (17),* 6053-6062.

[80] Bai, S., Zhou, X., Liu, Z., Xia, P., Liu, M., & Zeng, S. (2014) Effects of Ag variations on the microstructures and mechanical properties of Al-Cu-Mg alloys at elevated temperatures. *Material Science and Engineering A, 611,* 69-76

[81] Ringer, P., Yeung, W., Muddle, B.C., Polmear, I.J., (1994). Precipitate stability in Al-Cu-Mg-Ag alloys aged at high temperatures. *Acta Metall. Meter, 42 (5)* 1715-1725.

[82] DeGeuser, F., Bley, F., and Deschamps, A. (2010). Early stages of Ω phase precipitation in Al-Cu-Mg-Ag observed in situ with and without applied stress by small angle x-ray scattering. *Proceesings of the 12th International Conference on Aluminum Alloys, Yokohama, Japan.* 475-480.

[83] Garg, A., Chang, Y.C., & Howe, J.M. (1990). *Scr. Mater, 24,* 677-680.

[84] Huang, B-P., & Zheng, Z-Q. (1998). Independent and Combined Roles of Trace Mg and Ag Additions in Properties Precipitation Process and Precipitation Kinetics of Al-Cu-Li-(Mg)-(Ag)-Zr-Ti Alloy. *Acta Materialia, 46 (12),* 4381-4393.

[85] Zhou, X., Liu, Z., Bai, S., Liu, M., and Ying, P. (2013). The influence of various Ag additions on the nucleation and thermal stability of Ω phase in Al-Cu-Mg alloys. *Material Science and Engineering A, 564.* 186-191.

[86] Nikulin, I., Kipelova, A., Gazizov, M., Teleshov, V., Zakharov, V., and Kaibyshev, R., (2010). Novel Al-Cu-Mg-Ag alloy for high temperature applications. *Proceedings of the 12th International Conference on Aluminum Alloys,* Japan.

[87] Cahoon, J.R., Broughton, W.H., & Kutzak, A.R. (1971). The determination of yield strength from hardness measurements, *Metallurgical Transactions, 2,* 1979-1983.

[88] Hatch, J.E. (1984). Typical properties of 25mm thick plate, Aluminum: Properties and Physical Metallurgy. Metal Parks, OH, ASM International.

[89] Material Data Sheet: Scalmalloy (2017). Typical properties after solution heat treatment and aging. AIRBUS APWORKS GmbH.

[90] Material Data Sheet: EOS Aluminum AlSi10Mg (2014). Typical properties after stress relief at 300°C for 2h. EOS GmbH.

[91] Rout, P.K, Ghosh, M.M., and Ghosh, K.S. (2015). Influence of Aging Treatments on Alterations of Microstructural Features and Stress Corrosion Cracking Behavior of an Al-Zn-Mg Alloy. *Journal of Materials Engineering and Performance, 24(7),* 2792-2805.

[92] Tan, C.F. and Said, M.R. (2009). Effect of Hardness Test on Precipitation Hardening Aluminum Alloy 6061-T6. *Chiang Mai Journal of Science, 36 (3).* 276-286.

[93] Sha, G., Marceau, R.K.W., Gao, X., Muddle, B.C., & Ringer, S.P. (2011). Nanostructure of aluminum alloy 2024: Segregation, clustering and precipitation processes. *Acta Materialia, 59 (4),* 1659-1670.

[94] Park, J.K., & Ardell, A.J. (1957). Microstructure of the Commercial 7075 Al alloy in the T651 and T7 Tempers. *Metallurgical and Material Transactions A, 14.*

[95] Zuiko, I., & Kaibyshev, R. (2018). Aging behavior of an Al-Cu-Mg alloy. *Journal of Alloys and Compounds, 759.* 108-119.

[96] Cross, C.E. (2005). On the Origin of Weld Solidification Cracking. In Böllinghaus T., Herold H. (eds) Hot Cracking Phenomena in Welds. Springer, Berlin, Heidelberg.